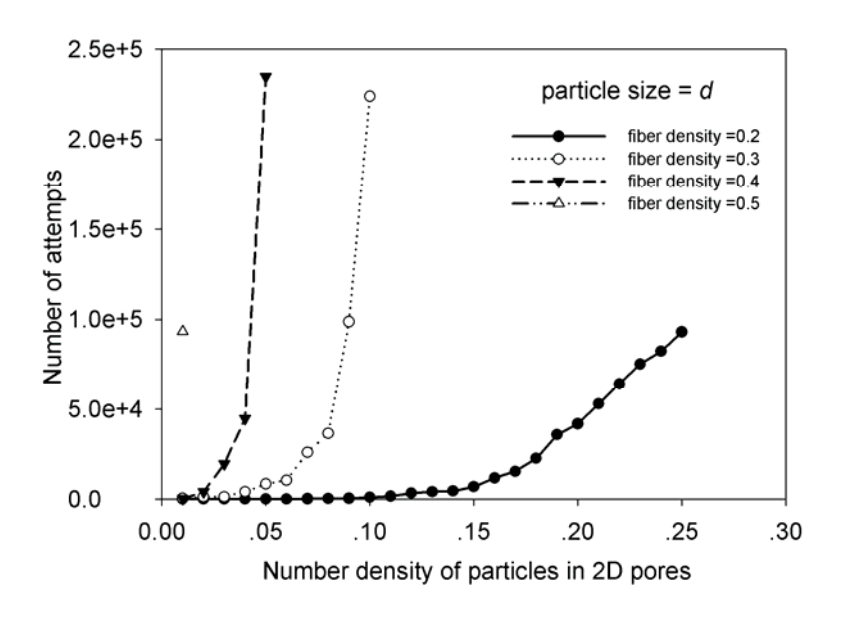
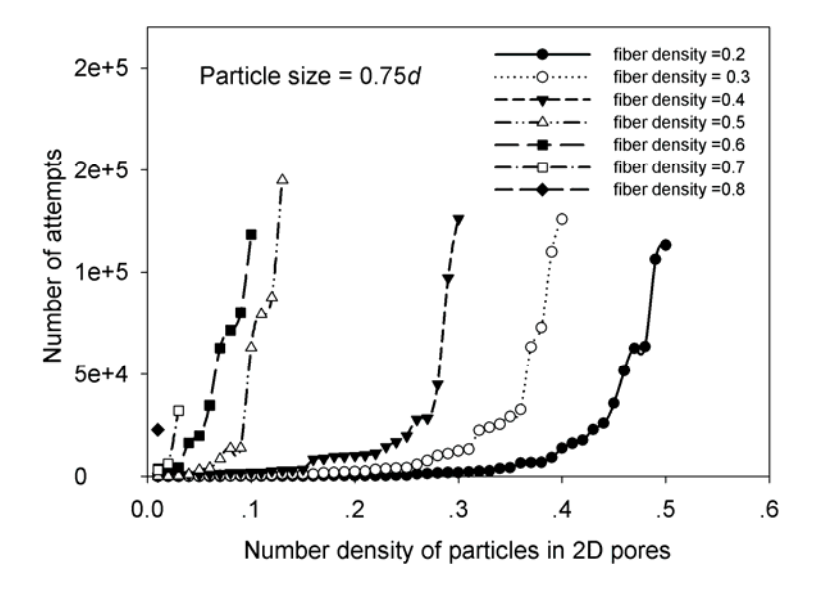
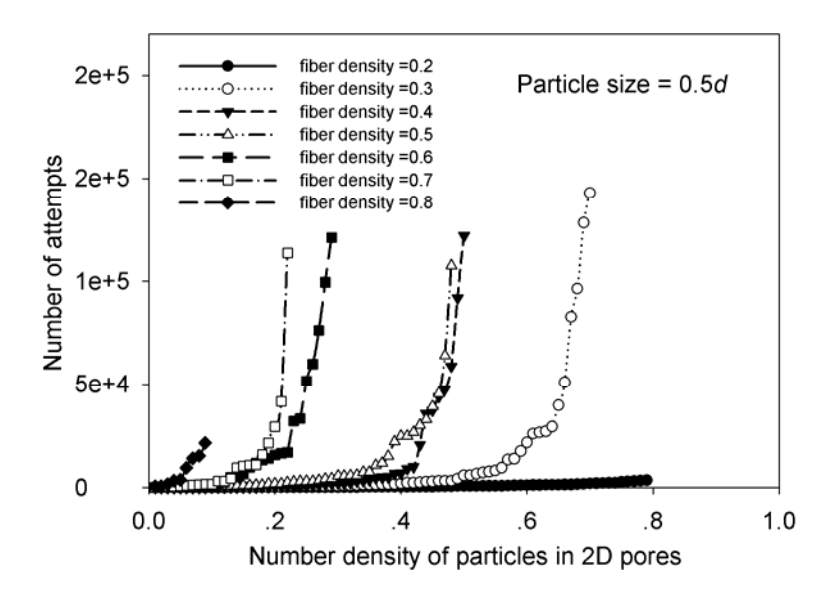
ผลการทดลองเมื่อใช้โครงสร้างเส้นใยที่มีขนาดเส้นใยเท่ากันหมดคือ 0.075d และอนุภาค มีขนาดเท่ากันหมดคือ d, 0.75d, 0.50d โดยเติมลงไปที่ความหนาแน่นของเส้นใยต่างๆ กันแสดงใน รูปที่ 4.52 – 4.54 ตามลำดับ



รูปที่ 4.52 แสดงความพยายามที่จะเติมอนุภาคขนาด d ลงไปในรูพรุนสองมิติ

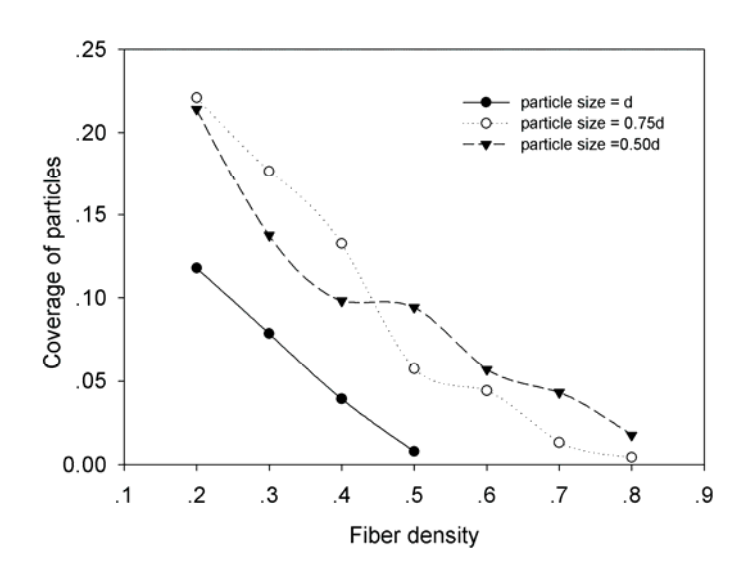


รูปที่ 4.53 แสดงความพยายามที่จะเติมอนุภาคขนาด 0.75d ลงไปในรูพรุนสองมิติ



รูปที่ 4.54 แสดงความพยายามที่จะเติมอนุภาคขนาด 0.50d ลงไปในรูพรุนสองมิติ

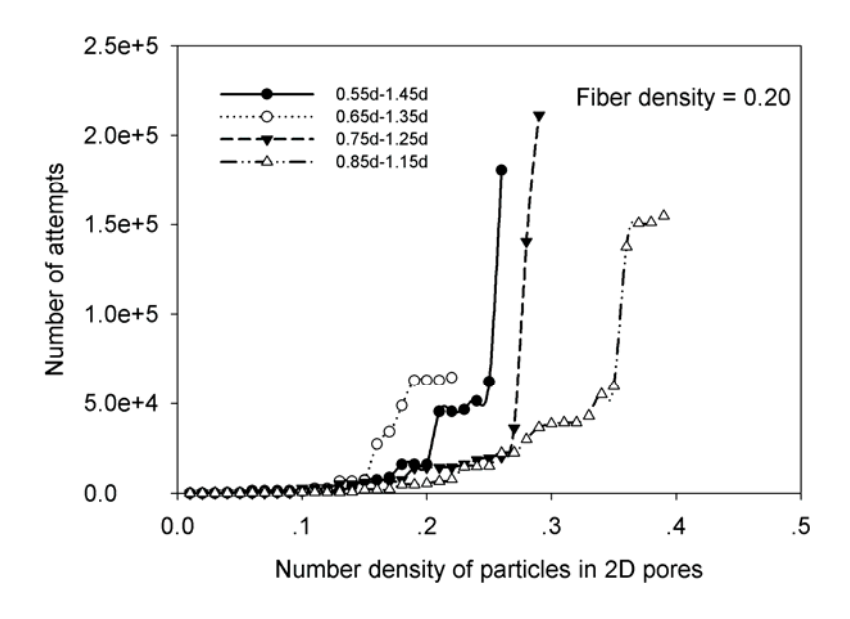
เมื่อพิจารณาเปรียบเทียบกันทั้งสามรูป จะเห็นว่าหากเติมอนุภาคที่มีขนาดใหญ่ที่สุดใน ที่นี้คือ d จะเติมลงไปในโครงสร้างที่ความหนาแน่นสูงสุดได้เพียง 0.5 เท่านั้น ในขณะที่เมื่ออนุภาค เล็กลงเป็น 0.75d และ 0.50d จะสามารถเติมลงไปในรูพรุนของเส้นในความหนาแน่นได้ถึง 0.8 เมื่อ พิจารณาในรูปใด ๆ ที่ขนาดของอนุภาคเท่ากัน จะเห็นว่าที่ความหนาแน่นของเส้นใยสูงขึ้น นั่นคือ จำนวนของรูพรุนขนาดเล็กจะมีมากขึ้นในขณะที่รูพรุนขนาดใหญ่มีน้อยลง จึงเติมอนุภาคต่อไปไม่ได้ และเมื่ออนุภาคมีขนาดเล็กลงจำนวนของอนุภาคที่จะเติมลงไปในรูพรุนก็จะมีมากขึ้นด้วย ดังนั้นจึง สามารถเปรียบเทียบพื้นที่ปกคลุมของอนุภาคในรูพรุนได้ดังรูปที่ 4.55



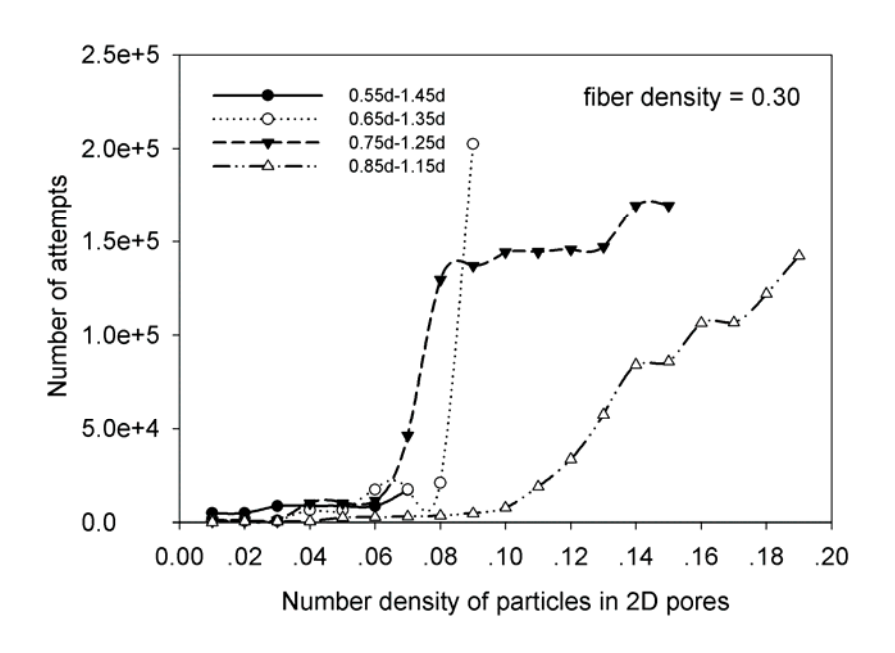
รูปที่ 4.55 พื้นที่ปกคลุมของอนุภาคต่างขนาดในรูพรุนจากโครงสร้างเส้นใยนาโน

เห็นได้อย่างชัดเจนจากรูปที่ 4.55 ว่าหากความหนาแน่นของเส้นใยมากขึ้น พื้นที่ปกคลุม ของอนุภาคในรูพรุนจะลดลงจนเป็นศูนย์ในที่สุดนั่นคือไม่มีรูพรุนที่มีขนาดเล็กพอที่จะยอมให้อนุภาค ที่มีขนาดที่กำหนดนี้ผ่านเข้าไปได้ การตกของอนุภาคหลังจากนั้นก็จะทำให้ติดอยู่กับเส้นใยทั้งหมด ดังนั้นหากพอทราบขนาดของอนุภาคที่จะกรอง อาจจะสามารถจำลองการตกทับของเส้นใย จนกระทั่งได้ความหนาแน่นที่ไม่สามารถปล่อยให้อนุภาคหลุดเข้าไปได้ และนำมาเปรียบเทียบกับ การทดลองจริงว่า หากจะให้ได้ความหนาแน่นเส้นใยขนาดนั้นจำเป็นต้องสบินนานเท่าใด หรือทำให้ มีน้ำหนักของของแข็งบนพื้นที่ประมาณเท่าใด (หรือสัดส่วนปริมาตรของแข็งของเส้นใยที่เรียกกว่า solid volume fraction หรือ SVF) และในรูปที่ 17 จะเห็นว่าหากลดขนาดของอนุภาคลง กราฟจะ เขยิบไปทางด้านขวามากขึ้น และจะเข้าใกล้กันในที่สุด

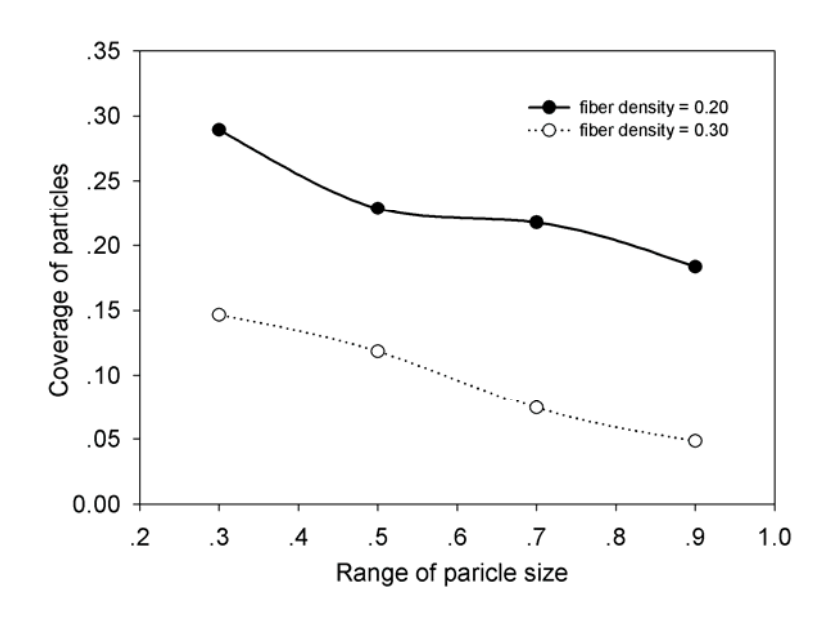
รูปที่ 4.55 สามารถนำมาใช้ในการประมาณความจุของรูพรุนได้ หากพอทราบขนาดของ อนุภาคที่นำมาใช้ นอกจากนี้ยังได้ทดลองโดยเส้นใยที่มีขนาดเท่าเดิมที่ความหนาแน่นแตกต่างกัน สองค่าคือ 0.2 และ 0.3 แต่อนุภาคในการตกในรูพรุนมีขนาดแปรเปลี่ยนไปหรือเป็น polydisperse โดยให้มีการกระจายขนาดคล้ายคลึงกับการกระจายขนาดของเส้นใยที่ใช้มาก่อน คือ 0.55d-1.45d, 0.65d-1.35d, 0.75d-1.25d, และ 0.85d-1.15d โดยทั้งหมดจะมีขนาดเฉลี่ยใกล้เคียงกับ d นั่นเอง ผลการทดลองปรากฏในรูปที่ 4.56 และ 4.57



รูปที่ 4.56 แสดงความพยายามในการเติมอนุภาคต่างขนาดในรูพรุนจากเส้นใยนาโน ที่ความหนาแน่น 0.20



รูปที่ 4.57 แสดงความพยายามในการเติมอนุภาคต่างขนาดในรูพรุนจากเส้นใยนาโน ที่ความหนาแน่น 0.30



รูปที่ 4.58 แสดงพื้นที่ปกคลุมของอนุภาคต่างขนาดในรูพรุน โดยความต่างขนาดถูกแสดงในรูปของ พิสัยซึ่งก็คือความแตกต่างของขนาดอนุภาคใหญ่ที่สุดและเล็กที่สุด

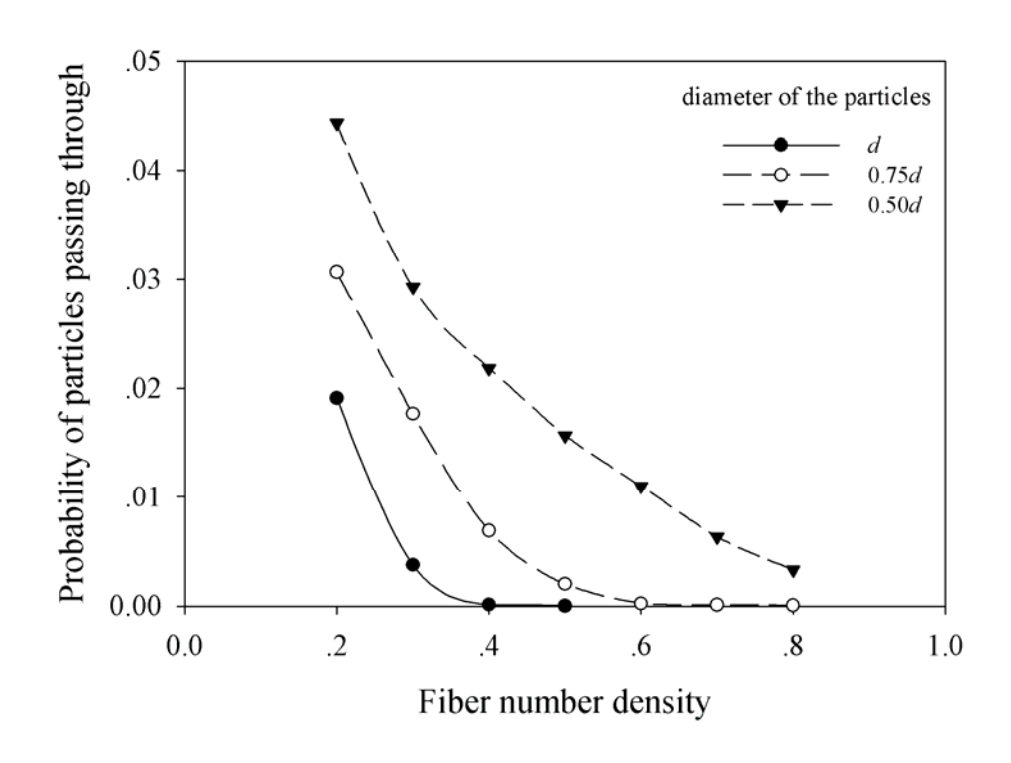
ทั้งรูป 4.56 และ 4.57 แสดงแนวโน้มที่คล้ายกันคือหากอนุภาคมีการกระจายขนาดแบบ แคบใกล้เคียง d จะทำให้สามารถตกลงไปในรูพรุนได้ด้วยความหนาแน่นที่มากกว่ากรณีที่อนุภาคมี การกระจายขนาดแบบกว้างเพราะในการสุ่มนั้นขนาดของอนุภาคทุกขนาดมีความน่าจะเป็นเท่ากัน ทั้งหมด ผลดังกล่าวมองเห็นได้ชัดเจนจากรูปที่ 4.58 ที่ทั้งสองความหนาแน่นของเส้นใย จะพบว่า พื้นที่ปกคลุมของอนุภาคต่างขนาดที่มีค่าพิสัยน้อยจะมีค่ามากกว่าอนุภาคที่มีค่าพิสัยมาก จึงเป็น การบอกเป็นนัยว่า หากอนุภาคมีความต่างขนาดกันมาก (แต่ขนาดเฉลี่ยใกล้เคียงกัน) ในการกรอง จะผ่านเข้าไปในรูพรุนได้ยากกว่า ดังนั้นจึงน่าจะเกาะติดที่ผิวของเส้นใยได้มากกว่า

ผลการทดลองการตกของอนุภาคในรูพรุนของเส้นใยนาโนในงานวิจัยนั้นแสดงให้เห็นว่า ความพยายาม (Attempts) ในการเติมอนุภาคเข้าไปในโครงสร้างรูพรุนนั้นจะยิ่งยากขึ้นอย่างมาก หากมีพื้นที่ของรูพรุนลดน้อยลง ซึ่งเป็นผลมาจากการตกทับของเส้นใยจำนวนมากยิ่งขึ้น นอกจากนี้ ยังเห็นได้อย่างชัดเจนว่า หากอนุภาคยังคงค้างอยู่ในรูพรุน การเติมอนุภาคเข้าไปอีกโดยไม่ทับซ้อน กับอนุภาคเดิมในสองมิตินั้นจะยิ่งทำได้ยากมากขึ้นเรื่อยๆ เมื่อการเติมต่อเนื่องกันไปเช่นนี้ ซึ่งเมื่อ ถึงจุดหนึ่งก็จะทำให้ไม่สามารถเติมอนุภาคต่อไปได้อีก หรือทำให้ตัวกรองนั้นเกิดการอุดตันโดย สมบูรณ์นั้นเอง นอกจากนี้ในการศึกษานั้นยังได้พบอีกว่า หากลดขนาดของอนุภาคที่เติมในรูพรุนทำ ให้การเติมนั้นง่ายยิ่งขึ้น ดังนั้นการเติมอนุภาคเข้าไปในรูพรุนของโครงสร้างนั้นจึงขึ้นกับขนาด สมพัทธ์ของรูพรุนและอนุภาค

หากพิจารณาการเติมอนุภาคตัวแรกเข้าไปในโครงสร้างรูพรุนของเส้นใยนาโนที่จำลองใน สองมิตินี้ จะพบว่าความยากง่ายในการเติมสำเร็จนั้นจะเป็นพารามิเตอร์บอกให้ทราบว่า การ เคลื่อนที่ของอนุภาคทะลุผ่านตัวกรองนั้นเป็นไปได้มากหรือน้อยเพียงใด ดังนั้นจำนวนครั้งที่ใช้ใน การเติมอนุภาคจนกระทั่งอนุภาคไปตกในรูพรุนได้สำเร็จนั้น (Number of attempts) จึงเป็นการบอก ถึงความน่าจะเป็นที่จะกรองอนุภาคไว้ได้หรือไม่ ดังนั้นจึงนิยามความน่าจะเป็นได้ดังนี้

และ

ผลการศึกษานี้แสดงในรูปที่ 4.59

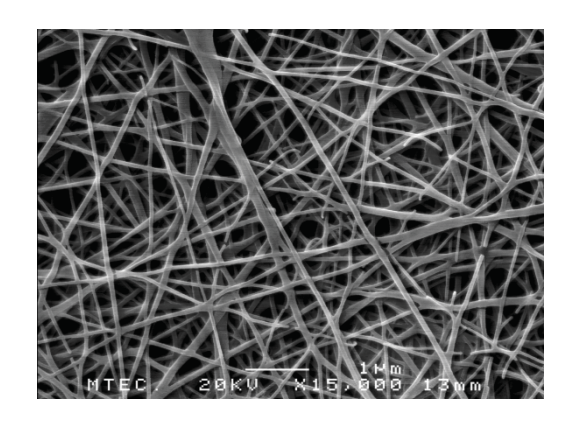


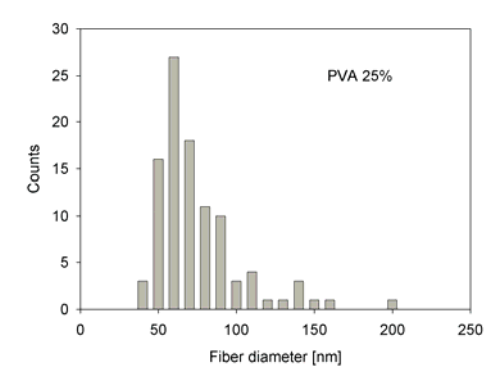
รูปที่ 4.59 ความน่าจะเป็นของการที่อนุภาคลอดผ่านช่องในรูพรุนของโครงสร้างเส้นใยนาโนได้

จากรูปจะเห็นว่า ความน่าจะเป็นที่อนุภาคจะผ่านโครงสร้างไปได้จะลดน้อยลง หรือความ น่าจะเป็นในการดักจับอนุภาคไว้ได้จะมีมากยิ่งขึ้นเมื่อมีปริมาณเส้นใยมากขึ้น อย่างไรก็ตามที่ ปริมาณเส้นใยน้อยที่สุดที่ตรวจสอบนั่นคือที่ 0.2 พบว่า ความน่าจะเป็นในการผ่านลอดไปของ อนุภาคที่เล็กที่สุดที่ตรวจสอบ (เมื่อมีรัศมีเท่ากับ 0.5d) มีค่าเพียง 0.045 เท่านั้น หรือในจำนวน อนุภาค 1000 อนุภาค จะมีอนุภาคที่หลุดลอดไปได้จำนวน 45 อนุภาค และแน่นอนที่เมื่ออนุภาคมี ขนาดเล็กลงความน่าจะเป็นที่ลอดผ่านได้จะเพิ่มสูงขึ้น

4.3.7 การพิจารณาผลการจำลองเปรียบเทียบกับผลการทดลองจริง

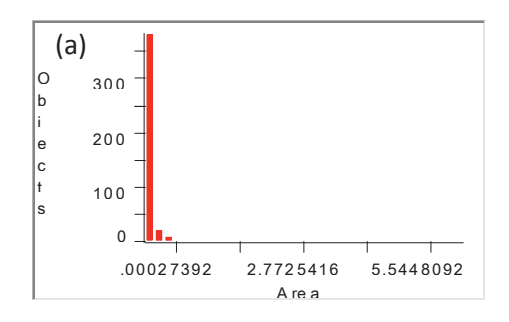
หากพิจารณาโครงสร้างเส้นใยนาโนของพอลิไวนิลแอลกอฮอล์ที่ผลิตได้ด้วยเทคนิคอิเล็ก โตรสปินนิงพบว่ามีโครงสร้างดังแสดงในรูปที่ 4.60, 4.62, และ 4.64 เมื่อเปลี่ยนความเข้มข้นของ สารละลายตั้งแต่ 25%, 30% และ 35% ตามลำดับ

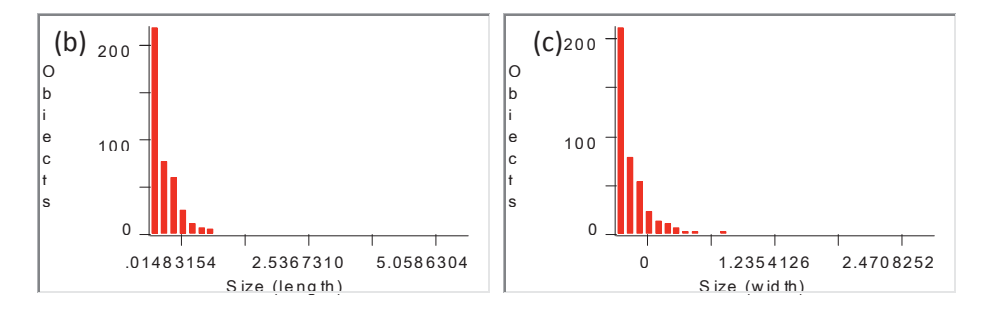




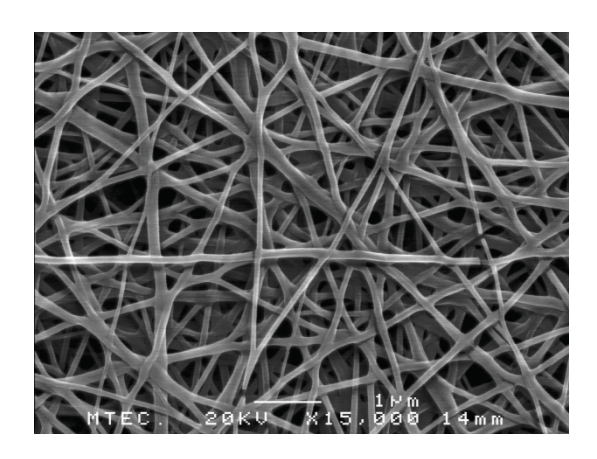
รูปที่ 4.60 ภาพถ่าย SEM และการวิเคราะห์ขนาดของเส้นใยจากสารละลาย PVA 25%

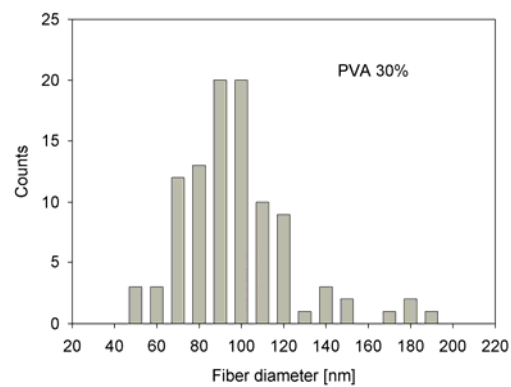
เมื่อวิเคราะห์ลักษณะของเส้นใยที่ปรากฏในภาพ SEM จะได้ผลดังรูปที่ 4.60 ด้านขวา ซึ่งแสดงการกระจายตัวของเส้นใยที่มีขนาดต่างๆ กัน และเมื่อนำภาพ SEM มาวิเคราะห์รูพรุนใน สองมิติจะได้ผลดังแสดงในรูปที่ 4.61 (a) เป็นการกระจายของพื้นที่ รูปที่ 4.63 (b) และ 4.63 (c) เป็นการกระจายของขนาดรูพรุนโดยบอกเป็นความยาวและความกว้าง ตามลำดับ





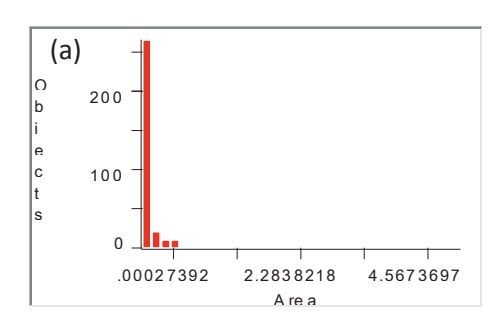
รูปที่ 4.61 การวิเคราะห์รูพรุนของภาพ SEM (รูปที่ 4.60) ขนาดของความยาวในหน่วยไมครอนและ ขนาดของพื้นที่ในหน่วยตารางไมครอน

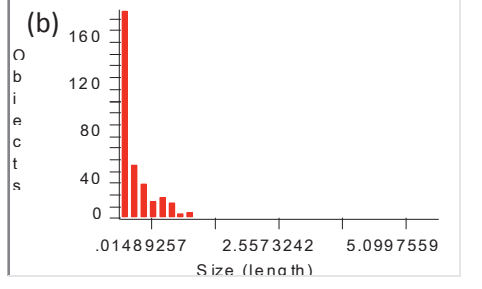


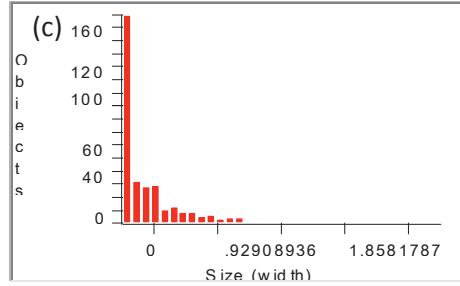


รูปที่ 4.62 ภาพถ่าย SEM และการวิเคราะห์ขนาดของเส้นใยจากสารละลาย PVA 30%

เมื่อวิเคราะห์ลักษณะของรูพรุนจะได้ผลดังรูปที่ 4.63 (a) เป็นการกระจายของพื้นที่ รูปที่ 4.63 (b) และ 4.63 (c) เป็นการกระจายของขนาดรูพรุนโดยบอกเป็นความยาวและความกว้าง ตามลำดับ

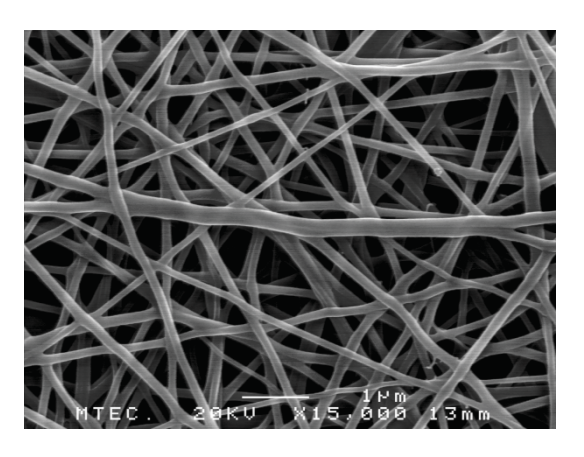


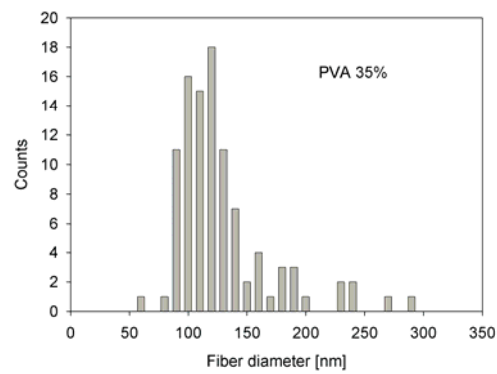




รูปที่ 4.63 การวิเคราะห์รูพรุนของภาพ SEM (รูปที่ 4.62) ขนาดของความยาวในหน่วยไมครอนและ ขนาดของพื้นที่ในหน่วยตารางไมครอน

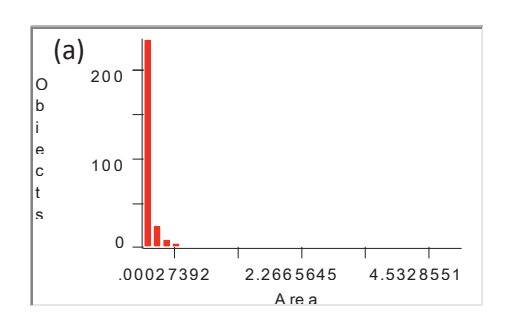
ภาพถ่าย SEM ของเส้นใยนาโนจากสารละลาย PVA ความเข้มข้น 35% แสดงในรูปที่ 4.64

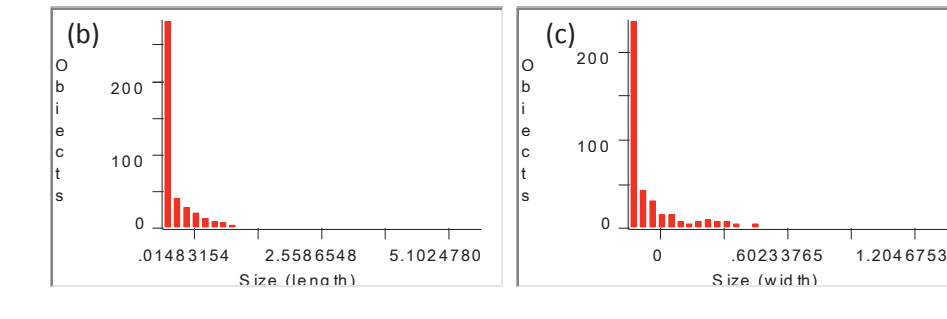




รูปที่ 4.64 ภาพถ่าย SEM และการวิเคราะห์ขนาดของเส้นใยจากสารละลาย PVA 35%

เมื่อวิเคราะห์ลักษณะของรูพรุนจะได้ผลดังรูปที่ 4.65 (a) เป็นการกระจายของพื้นที่ รูปที่ 4.65 (b) และ 4.65 (c) เป็นการกระจายของขนาดรูพรุนโดยบอกเป็นความยาวและความกว้าง ตามลำดับ

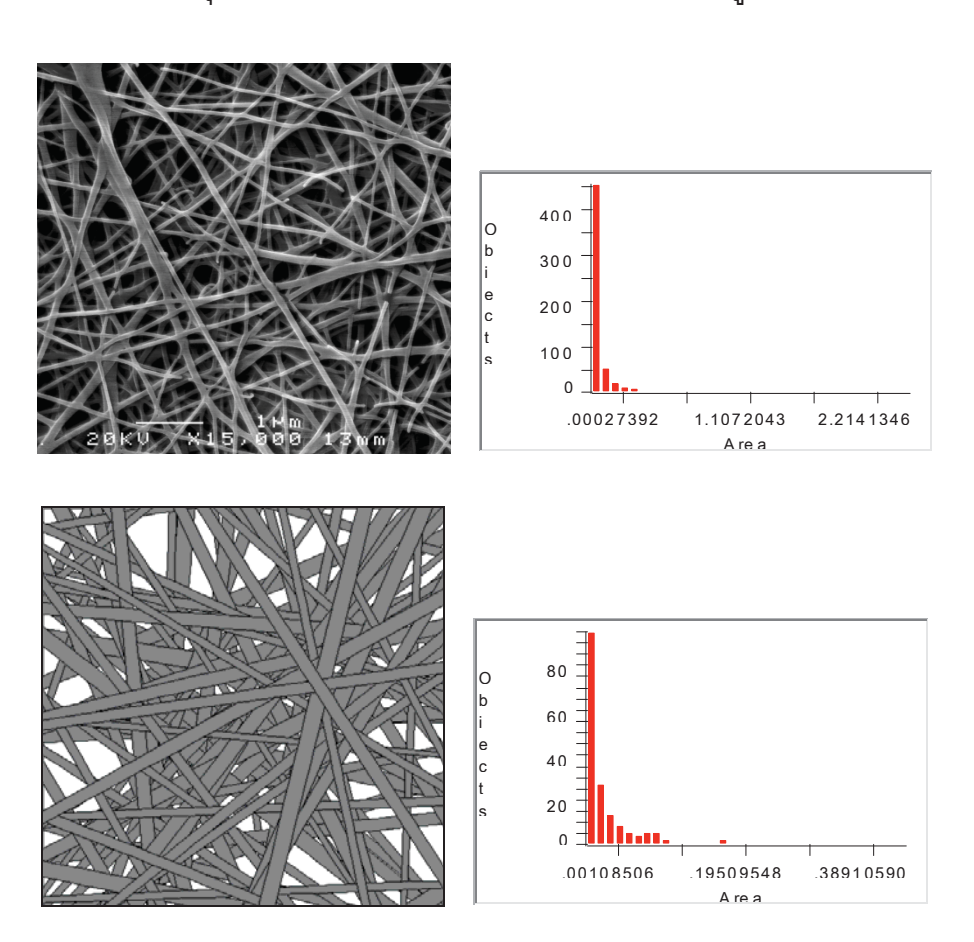




รูปที่ 4.65 การวิเคราะห์รูพรุนของรูป SEM (รูปที่ 4.64) ขนาดของความยาวในหน่วยไมครอนและ ขนาดของพื้นที่ในหน่วยตารางไมครอน

จะเห็นได้ว่าเส้นใยของ PVA ที่เตรียมได้ จะมีขนาดใหญ่ขึ้นเมื่อความเข้มข้นเพิ่มขึ้น จาก การศึกษาที่ผ่านๆ มาพบว่าความหนืดที่เพิ่มขึ้นอันเป็นผลจากความเข้มข้นที่เพิ่มขึ้นเป็นสาเหตุทำ ให้เส้นใยมีขนาดใหญ่ขึ้น จากที่ความเข้มขัน 25% ได้เส้นใยขนาด 40 - 160 nm มีขนาดเฉลี่ย ประมาณ 80 nm ที่ความเข้มขัน 30% ได้เส้นใยขนาด 30 - 190 nm มีขนาดเฉลี่ยประมาณ 100 nm และที่ความเข้มขัน 35% ได้เส้นใยที่มีขนาด 60 - 290 nm มีขนาดเฉลี่ยประมาณ 130 nm และจาก การหาสถิติของรูพรุนอันเกิดจากโครงสร้างนาโน และเมื่อพิจารณาการวิเคราะห์ขนาดของรูพรุนที่ เกิดขึ้นจากโครงสร้างซ้อนทับของเส้นใยนาโนพบว่า มีรูพรุนขนาดเล็กน้อยลงเมื่อขนาดของเส้นใย ใหญ่ขึ้น เมื่อดูจากขนาด (ความยาว) เห็นว่ามีรูพรุนมีขนาดเล็กลง ซึ่งสอดคล้องกับการจำลอง อย่างไรก็ตาม ในการจำลองนี้เปรียบเทียบที่ความหนาแน่นเชิงเส้นเท่ากัน มิได้เปรียบเทียบที่ ปริมาณของของแข็งเท่ากัน

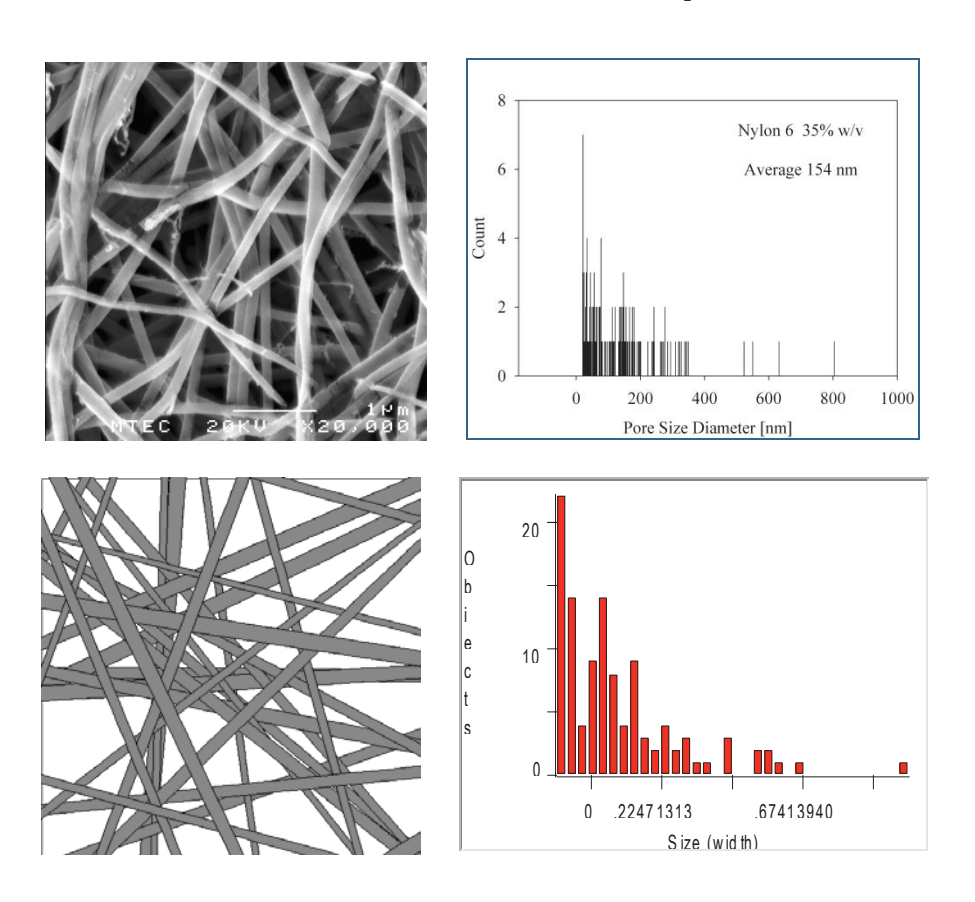
เป็นเรื่องน่าสนใจหากจะเปรียบเทียบการจำลองระบบกับผลการทดลองจริง จะเห็นได้ว่า ลักษณะการกระจายของเส้นใยจริงมีความคล้ายคลึงกับการจำลองระบบเมื่อความหนาแน่นของเส้น ใยสูงถึง 0.8 อย่างไรก็ตาม ในการวิเคราะห์ด้วยโปรแกรม image analyzer ของผลการทดลองจริง นั้นทำได้ลำบากกว่าจากการจำลองระบบเนื่องจากสีของภาพ SEM มีระดับของความลึกเข้ามา เกี่ยวข้องด้วย ดังนั้นจึงได้ทดลองปรับรูป equalization โดยโปรแกรมให้สีใกล้เคียงกันดีที่สุด และ หากจะพิจารณาคร่าวๆ เมื่อเปรียบเทียบระหว่าง PVA ที่ความเข้มข้น 25% กับการจำลองระบบที่มี การกระจายขนาดกว้างที่สุดคือ 0.55d_r-1.45d_r ดังแสดงให้เห็นอีกครั้งในรูปที่ 4.66



รูปที่ 4.66 แสดงการเปรียบเทียบรูปโครงสร้างเส้นใยจากการทดลองและการจำลองระบบ

จากรูปที่ 4.66 จะเห็นความคล้ายคลึงของสองรูป หากต้องการให้การจำลองระบบเป็น ตัวแทนของผลการทดลองจริงได้ จำเป็นต้องใช้การสเกลระบบ ภาพจากการทดลองมีเส้นใยที่มี ขนาดระหว่าง 40 - 160 nm และมีขนาดเฉลี่ยประมาณ 80 nm ส่วนรูปจากการจำลองระบบมีเส้นใย อยู่ระหว่าง 82 - 218 nm และมีขนาดเฉลี่ยประมาณ 150 nm จึงเห็นว่าเส้นใยมีขนาดประมาณสอง เท่าของขนาดของจริง (แต่พิสัย (range) มีความแตกต่างอยู่บ้างทางด้านของขนาดใหญ่) เมื่อ พิจารณาขนาดของรูพรุน หากเส้นใยมีขนาดเป็นสองเท่ารูพรุนน่าจะมีขนาดพื้นที่ scale เพิ่มขึ้นเป็น 4 เท่า (2 มิติ) เมื่อพิจารณาจากการกระจายขนาดของรูพรุน จะเห็นว่าการจำลองมีขนาดเป็นสี่เท่า ของของจริง ดังนั้น เราสามารถ scale ใหม่ได้ จากเดิมที่ให้ 0.075d = 150 nm ก็ให้เท่ากับ 75 nm แทนก็จะได้ขนาดใกล้เคียงกับความเป็นจริงมากยิ่งขึ้น อย่างไรก็ตามหากใช้การกระจายขนาดของ เส้นใยตามที่เป็นจริงพอดี น่าจะทำให้ได้การจำลองระบบที่เหมือนการทดลองยิ่งขึ้น

สำหรับการขึ้นรูปเส้นใยในลอนก็สามารถเปรียบเทียบการกระจายขนาดของรูพรุนที่ ตรวจสอบจากภาพ SEM ของเส้นใยจริงกับการจำลองเส้นใยดังแสดงในรูปที่ 4.67



รูปที่ 4.67 เปรียบเทียบตัวอย่างโครงสร้างเส้นใยนาโนของไนลอน 6 กับโครงสร้างที่จำลอง โดยคอมพิวเตอร์ พร้อมการกระจายขนาดของรูพรุน

จากรูปที่ 4.67 เมื่อพิจารณาจากค่าการกระจายขนาดของเส้นใยในการทดลองจริงซึ่งมีค่า อยู่ระหว่าง 70 ถึง 225 นาโนเมตร และมีค่าเฉลี่ยขนาดเส้นใยประมาณ 144 นาโนเมตร จะเห็นว่ามี ค่าใกล้เคียงกับการจำลองระบบในงานวิจัยนี้เมื่อให้ขนาดเฉลี่ยของเส้นใย d_f = 0.075d หรือประมาณ 150 นาโนเมตร และมีการกระจายขนาดอยู่ในช่วง 0.55df-1.45d_f

นอกจากนี้ขนาดของรูพรุนจากการทดลองซึ่งมีค่าเฉลี่ยประมาณ 154 นาโนเมตร เมื่อ นำไปเปรียบเทียบกับหาความหนาแน่นเชิงจำนวนของเส้นใยในโครงสร้างที่จำลองที่มีค่าเฉลี่ยของ ขนาดรูพรุนใกล้เคียงกันพบว่า ความหนาแน่นมีค่าเท่ากับ 0.3 และขนาดเฉลี่ยของรูพรุนมี ค่าประมาณ 163 นาโนเมตร ดังนั้นจึงได้นำรูปโครงสร้างเส้นใยนาโนที่ความหนาแน่นเชิงเส้น 0.3 มาเปรียบเทียบกับผลการทดลองจริง และพบว่ามีความคล้ายคลึงกัน การศึกษานี้นับเป็น ความสำเร็จขั้นหนึ่งที่โยงการจำลองระบบเข้ากับผลการทดลองจริง เพื่อให้ทราบว่าในสถานการณ์ การผลิตเส้นใยนาโนที่ต้องการนั้น ควรจะมีสภาวะในการจำลองระบบเป็นเช่นไร เพื่อให้ได้โครงสร้าง ที่ใกล้เคียงกับผลการทดลองจริงมากที่สุด

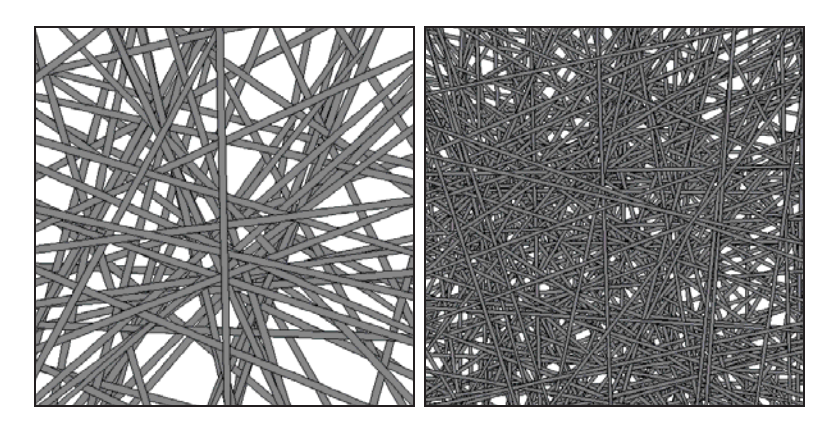
และจากผลการทดลองการกรองด้วยเส้นใยในลอนในหัวข้อ 4.1 ที่ผ่านมานั้น พบว่า โครงสร้างของเส้นใยนาโนที่มีขนาดของเส้นใยขนาดใหญ่จะเกิดรูพรุนขนาดใหญ่ด้วย การตรวจสอบ ในเรื่องนี้สามารถทำได้ด้วยการจำลองระบบเช่นกัน ในการทดลองการผลิตนั้นพบว่าโครงสร้างเส้น ใยนาโนมีความพรุน (porosity) ไม่แตกต่างกันมากนัก ถึงแม้จะมีขนาดของเส้นใยแตกต่างกัน จึง หมายถึงว่าหากเราควบคุมน้ำหนักของแผ่นเส้นใยให้ใกล้เคียงกัน เส้นใยจะมี SVF ที่ใกล้เคียงกัน นั่นเอง หากพิจารณาเส้นใยที่มีขนาดแตกต่างกัน d_1 และ d_2 เส้นใยทั้งสองนี้จะมีมวลแตกต่างกัน หากความยาวเท่ากัน และมวลทั้งหมดของเส้นใยจะขึ้นกับจำนวนเส้นใยบนแผ่นรองรับด้วย หาก กำหนดพื้นที่แผ่นรองรับเท่ากัน จะพบว่า

$$d_1^2/d_2^2 = n_2/n_1$$
 (4.3)

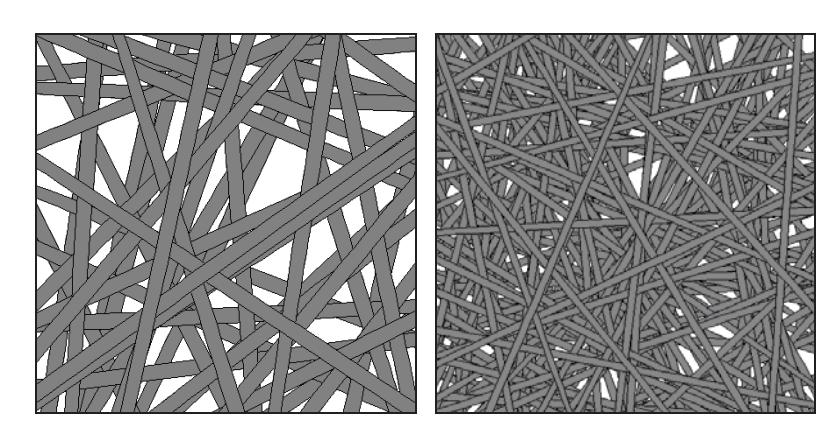
การจำลองได้เปรียบเทียบเมื่อให้ SVF ของสองระบบเท่ากัน โดย

ในกรณีที่หนึ่งเมื่อขนาดของเส้นใย d_f = 100 นาโนเมตร เปรียบเทียบกับเมื่อขนาดของเส้นใยเท่ากับ 50 นาโนเมตร จะเห็นว่าระบบแรกต้องมีความหนาแน่นเชิงจำนวน (สัมพันธ์กับ n₁) = 0.6 หาก ระบบที่สองมีความหนาแน่นเชิงจำนวนเท่ากับ 2.4 โครงสร้างทั้งสองเปรียบเทียบกันในรูปที่ 4.68

ส่วนกรณีที่สองนั้น เมื่อขนาดของเส้นใย d_f = 200 นาโนเมตร เปรียบเทียบกับเมื่อขนาดของเส้นใย เท่ากับ 100 นาโนเมตร จะเห็นว่าระบบแรกต้องมีความหนาแน่นเชิงจำนวน = 0.4 หากระบบที่สอง มีความหนาแน่นเชิงจำนวนเท่ากับ 1.6 โครงสร้างทั้งสองเปรียบเทียบกันในรูปที่ 4.69



รูปที่ 4.68 เปรียบเทียบโครงสร้างที่มี SVF เท่ากันเมื่อด้านซ้ายเป็นเส้นใยขนาด 100 นาโนเมตรที่ ความหนาแน่น 0.6 และด้านขวาเป็นเส้นใยขนาด 50 นาโนเมตรที่ความหนาแน่น 2.4



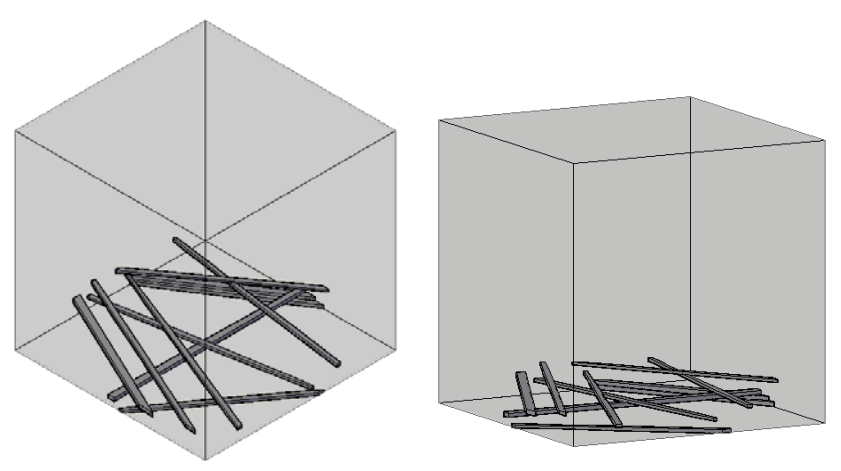
รูปที่ 4.69 เปรียบเทียบโครงสร้างที่มี SVF เท่ากันเมื่อด้านซ้ายเป็นเส้นใยขนาด 200 นาโนเมตรที่ ความหนาแน่น 0.4 และด้านขวาเป็นเส้นใยขนาด 100 นาโนเมตรที่ความหนาแน่น 1.6

จากทั้งสองรูปจะเห็นได้อย่างชัดเจนว่าเมื่อเปรียบเทียบโครงสร้างที่มี SVF เท่ากัน โครงสร้างที่มีเส้นใยใหญ่กว่าจะเกิดรูพรุนขนาดใหญ่กว่าด้วย สอดคล้องกับผลการทดลองการกรองที่ ผ่านมา

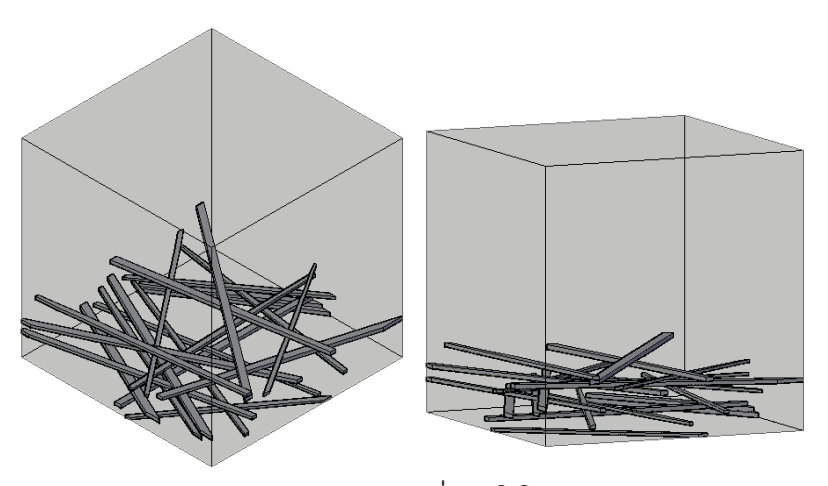
4.3.8 การจำลองเส้นใยใน **3** มิติ

ผลการทดลองสุดท้ายเป็นการจำลองเส้นใยใน 3 มิติ ซึ่งเป็นการดัดแปลงข้อมูลของเส้น ใยใน 2 มิติ โดยเพิ่มตำแหน่งของเส้นใยแต่ละเส้นในแกน z เข้าไปด้วย โดยมีสมมติฐานว่าเส้นใยแต่ ละเส้นจะอยู่ที่ตำแหน่ง z แตกต่างกัน โดยเส้นใยที่ตกมาทับทีหลังจะอยู่ในชั้นที่สูงกว่า ดังนั้นจะทำ ให้ความหนาของชั้นเส้นใยเพิ่มขึ้นเรื่อยๆ ตามจำนวนของเส้นใย ผลการจำลองระบบใน 3 มิติ แสดง ไว้ในรูปที่ 4.70 โดยแสดงถึงการเพิ่มขึ้นของจำนวนเส้นใยตามความหนาแน่นเชิงจำนวนที่สอดคล้อง

กับการทดลองใน 2 มิติ นั่นคือ ความหนาแน่นมีนิยามโดยจำนวนของเส้นใยต่อพื้นที่ที่ตกทับ (ไม่ใช่ ต่อปริมาตรตามที่นิยมใช้กันสำหรับระบบ 3 มิติ) เส้นใยที่เป็นตัวอย่างนี้มีการกระจายขนาดอยู่ ระหว่าง 0.55d_c-1.10d_f โดยที่ d_f คือขนาดเส้นใยซึ่งมีค่า 0.075d (โดย d ในที่นี้มีค่า 500 หาก ต้องการขนาดเส้นใยเท่ากับ 150 นาโนเมตร บนพื้นที่ตกทับ 5x5 ไมโครเมตร) จากรูปจะเห็นว่า โครงสร้างมีความโปร่งอันเนื่องมาจากการตกทับของเส้นใยทีละเส้นในแต่ละระดับชั้น ซึ่งในความ เป็นจริงน่าจะทึบกว่านี้เพราะเส้นใยได้รับผลจากแรงโน้มถ่วง ความโปร่งของโครงสร้างเส้นใยใน ลักษณะนี้จะให้ความเป็นรูพรุน (posrosity) ของโครงสร้างสอดคล้องกับระบบใน 2 มิติที่ความ หนาแน่นของเส้นใยต่ำๆ ดังนั้นในการนำโครงสร้าง 2 มิติไปใช้ อาจพิจารณาว่าเป็นโครงสร้างความ หนาแน่นต่ำๆ เรียงกันเป็นชั้นๆ จนเกิดเป็นโครงสร้างใน 3 มิตินั่นเอง

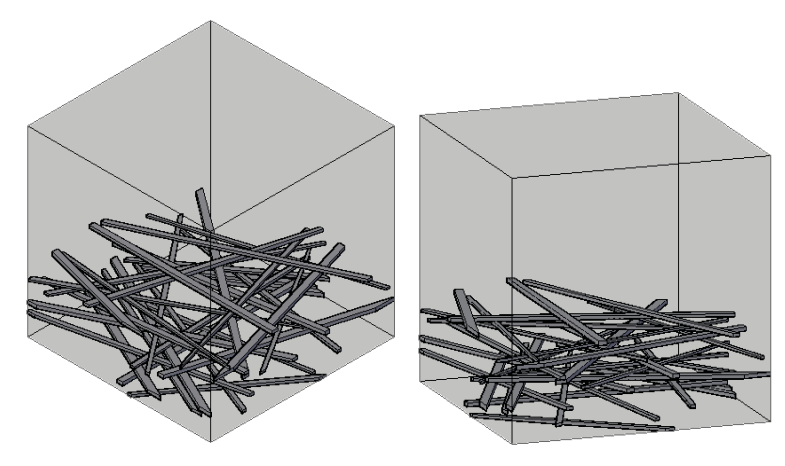


ความหนาแน่น =0.1

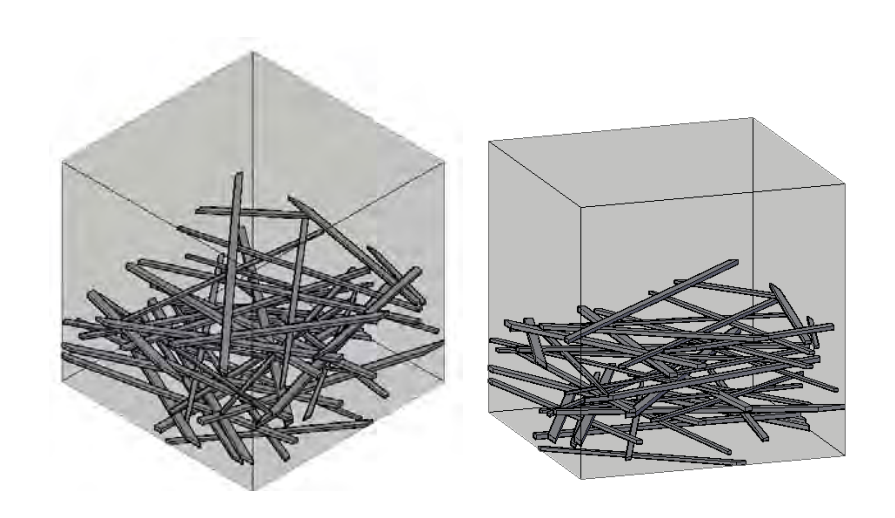


ความหนาแน่น =0.2

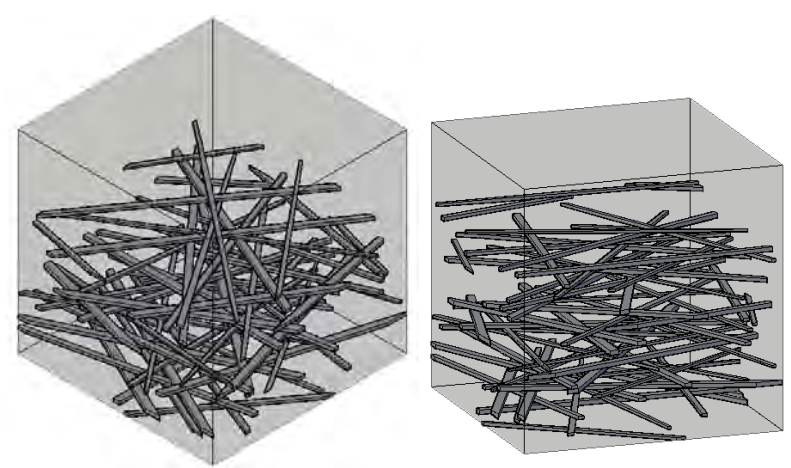
รูปที่ 4.70 แสดงโครงสร้างใน 3 มิติของเส้นใยที่เกิดการตกทับบนแผ่นรองรับ เรียงตามความ หนาแน่นตั้งแต่ 0.1, 0.2, 0.3, 0.4, 0.5, 0.6, 0.7 และ 0.8



ความหนาแน่น =0.3

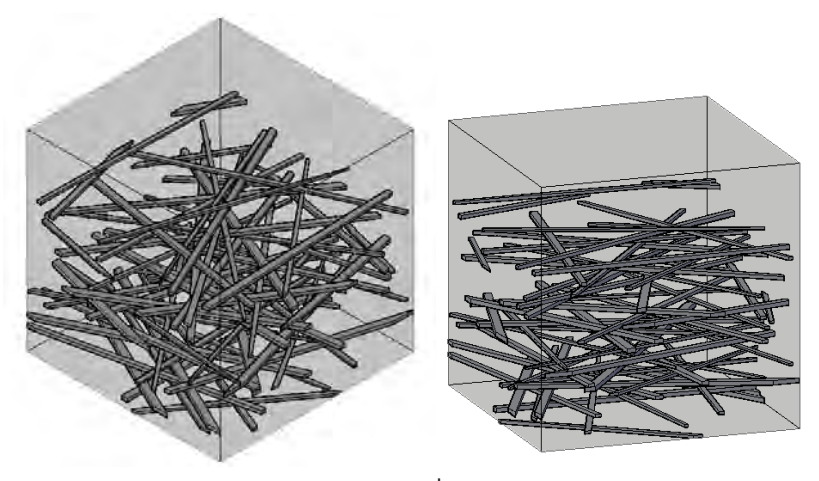


ความหนาแน่น =0.4

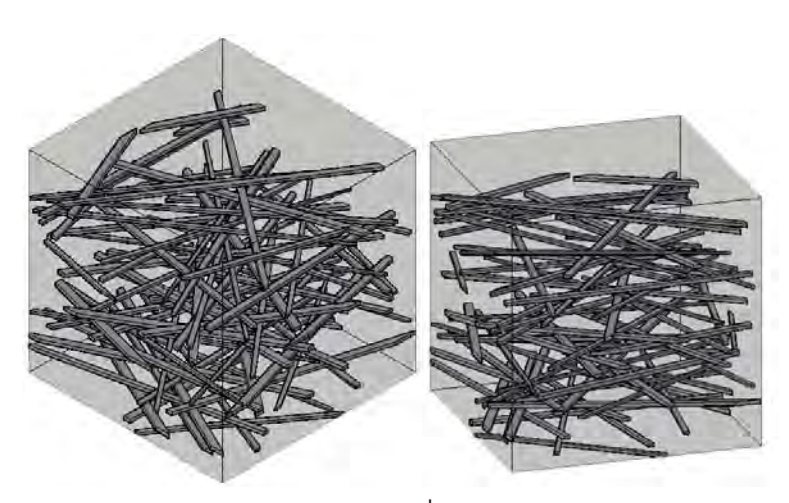


ความหนาแน่น =0.5

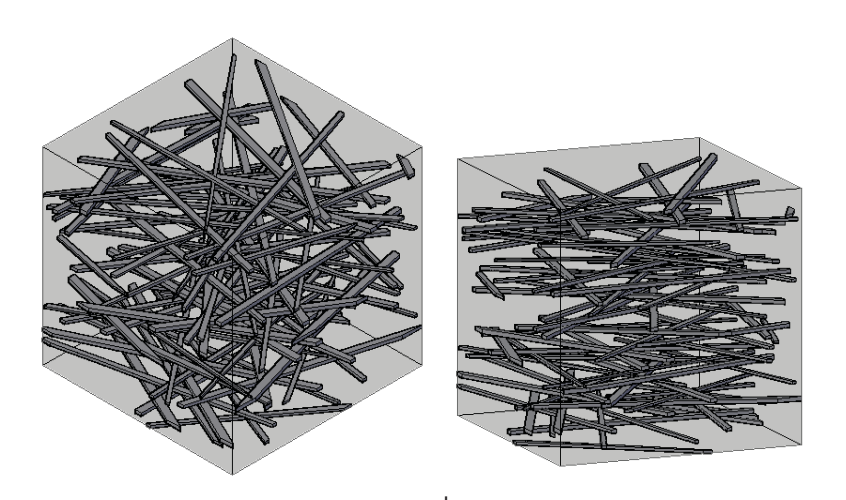
รูปที่ 4.70 (ต่อ) แสดงโครงสร้างใน 3 มิติของเส้นใยที่เกิดการตกทับบนแผ่นรองรับ เรียงตามความ หนาแน่นตั้งแต่ 0.1, 0.2, 0.3, 0.4, 0.5, 0.6, 0.7 และ 0.8



ความหนาแน่น =0.6



ความหนาแน่น =0.7



ความหนาแน่น =0.8 รูปที่ 4.70 (ต่อ) แสดงโครงสร้างใน 3 มิติของเส้นใยที่เกิดการตกทับบนแผ่นรองรับ เรียงตามความ หนาแน่นตั้งแต่ 0.1, 0.2, 0.3, 0.4, 0.5, 0.6, 0.7 และ 0.8

บทที่ 5

สรุปผลการดำเนินงานวิจัย

งานวิจัยนี้ศึกษาโครงสร้างเส้นใยนาโนที่มีความเป็นวิวิธพันธ์ โดยได้ศึกษาเส้นใยนาโนของในลอนและสารผสมระหว่างในลอนและไคโตซานเพื่อใช้เป็นวัสดุในการกรองอนุภาคและโปรตีนในน้ำ และได้ศึกษาเส้นใยนาโนของพอลิไวนิลแอลกอฮอล์ที่มีการเติมผงเขม่าดำหรือท่อนาโนของคาร์บอนเข้าไปเพื่อทำให้พื้นผิวและเนื้อเส้นใยมีการนำไฟฟ้าที่ดีขึ้น เนื่องจากตำแหน่งของสารตัวเติมกระจายทั่วถึงโครงสร้างวิวิธพันธ์นี้ และส่วนสุดท้ายคือการศึกษาการจำลองระบบในสองมิติและสามมิติเบื้องตัน เพื่อศึกษาค่าสถิติต่างๆ ที่เกี่ยวข้องกับโครงสร้าง ได้แก่ การกระจายขนาดของรูพรุน เป็นตัน การดำเนินงานในทั้งสามส่วนได้ผลสรุปดังต่อไปนี้

5.1 สรุปผลการวิจัย

จากการทดลองในส่วนแรกซึ่งเป็นเรื่องการกรองอนุภาคและโปรตีนโดยใช้เส้นใยนาโน ของในลอน 6 และในลอน 6 ผสมไคโตซาน จะพบว่าสารละลายที่ความเข้มข้นสูงขึ้นประกอบกับ หากมีสารตัวเติมอย่างไคโตซานเข้าไปเพิ่มจะทำให้ค่าความหนืดของสารละลายมีค่าสูงขึ้น โดยผล ของความหนืดที่สูงขึ้นจะมีผลแปรตามต่อกันกับขนาดของเส้นใยซึ่งจะได้เส้นใยที่มีขนาดใหญ่ขึ้น (พื้นที่ผิวสัมผัสลดลง) อีกทั้งยังส่งผลให้มีขนาดรูพรุนที่ใหญ่ ในขณะที่พื้นที่ผิวของรูพรุนจะลดลง แม้ว่าในการทดลองเส้นใยที่มีการผสมไคโตซานมากถึง 2% ของน้ำหนักในลอน 6 จะมีความหนืด สูงสุด แต่จากการเกิดกลุ่มเส้นใยขนาดเล็กขึ้นทั่วรูพรุนจึงทำให้ได้เส้นใยและขนาดรูพรุนที่เล็กลงกว่า ปกติ ทั้งนี้จากผลที่ได้ในการทดสอบการกรองวัฏภาคของเหลวด้วยปริมาตรสารกรอง 5 มิลลิลิตร และที่อัตราการไหล 8 ไมโครลิตรต่อวินาที พบว่า เมื่อนำไปกรองอนุภาคพอลิสไตรีน ขนาดนาโนที่ ขนาดต่างๆ คือ 410 นาโนเมตร 200 นาโนเมตร และ90 นาโนเมตร ก็มีประสิทธิภาพสูงพอที่จะ สามารถกรองสารเหล่านี้ได้ทั้งหมด เมื่อเทียบกับการกรองด้วยผ้าในลอนชนิดต่างๆ และกระดาษ กรองที่กรองได้เพียงแค่บางส่วน แต่จากผลการทดลองจะสังเกตได้ว่าอนุภาคพอลิสไตรีนนาโนขนาด เล็กสุด (90 นาโนเมตร) จะเกิดการจับกลุ่มรวมกันอย่างหนาแน่น จึงทำให้ผลการกรองของผ้า ในลอนและกระดาษกรองสามารถกรองได้อย่างมีประสิทธิภาพมากขึ้น เมื่อเทียบกับการกรอง อนุภาคพอลิสไตรีนขนาดที่ใหญ่กว่า อย่างไรก็ดีในการกรองโปรตีน BSA นั้นผลจากการเติมไคโต ซานลงไปจะสามารถช่วยเพิ่มประสิทธิภาพในการกรองได้ดียิ่งขึ้น เมื่อเทียบกับเส้นใยนาโนไลอน 6 แบบที่ไม่ได้เติมไคโตซาน

จากการทดลองในส่วนที่สองซึ่งเป็นเรื่อง การตรวจวัดไอระเหยของสารไอโซโพรพิล แอลกอฮอล์โดยเส้นใยพอลิไวนิลแอลกอฮอล์ที่เติมผงเขม่าดำและท่อนาโนของคาร์บอน พบว่าการ พัฒนาเพื่อพัฒนาอุปกรณ์ดักจับไอระเหยอินทรีย์สารตัวเติมที่เหมาะสมที่จะนำมาขึ้นรูปในเชิง คุณภาพกับโพลิไวนิลแอลกอฮอล์ก็คือท่อนาโนคาร์บอนที่มีการปรับปรุงการกระจายตัว เนื่องจาก ให้ผลของค่าความต้านทานที่ต่ำและมีความไวในการดูดจับที่ดีกว่าสารตัวเติมที่เป็น ผงเขม่าดำ ผง เขม่าดำที่มีการกระจายตัว และท่อนาโนคาร์บอน และเมื่อเติมสารตัวเติมเพิ่มขึ้นถึง 8% สามารถลด ค่าความต้านทานไฟฟ้าของเส้นใยนาโนได้ และพบว่าการปรับสภาพผิวสารตัวเติมจะช่วยให้ความ ต้านทานไฟฟ้าลดลงตามแนวโน้มของการเพิ่มปริมาณสารตัวเติมได้เป็นอย่างดี เมื่อนำโครงสร้างไป ตรวจวัดไอระเหยของไอโซโพรพิลแอลกอฮอล์ที่ความเข้มข้น 1-8 ppm พบว่า ค่าความต้านทาน ไฟฟ้าของเส้นใยนาโนทุกชนิดแสดงค่าความต้านทานที่ลดต่ำลงเชิงเส้นตรงเมื่อความเข้มข้นของไอ ระเหยเพิ่มขึ้น ซึ่งเป็นคุณลักษณะของเซนเซอร์ตรวจวัดไอระเหย แต่การที่จะนำเส้นใยที่ผสม ระหว่างโพลิไวนิลแอลกอฮอล์และท่อนาโนคาร์บอนที่มีการปรับปรุงการกระจายตัวมาขึ้นรูปนั้นมี ราคาที่ค่อนข้างสูงเนื่องจากราคาของท่อนาโนคาร์บอนนั้นมีราคาที่แพงทำให้อาจจะไม่เหมาะสมใน ในการผลิตในอุตสาหกรรมจริง ซึ่งเส้นใยที่เหมาะสมกว่าที่จะไปทำการผลิตในงานวิจัยนี้คือ ผงเขม่า ดำที่มีการปรับปรุงการกระจายตัว เนื่องจากให้คุณสมบัติที่คล้ายกับเส้นใยที่มีสารตัวเติมเป็นท่อนา โนคาร์บอนที่มีการปรับปรุงการกระจายตัว แต่จะให้ค่าความต้านทานของเส้นใยและความไวในการ ดูดจับที่มีประสิทธิภาพที่ด้อยกว่าเส้นใยที่มีสารตัวเติมเป็นท่อนาโนคาร์บอนที่ไม่ได้ผ่านการปรับ สภาพผิวเล็กน้อย

จากผลการทดลองทั้งสองส่วนจะเห็นผลของพื้นผิววิวิธพันธ์ในการประยุกด์ใช้ต่างๆ กัน ได้แก่ ในการกรองอนุภาคนั้น ขนาดของเส้นใยขนาดเล็กที่ปรากฏในกลุ่มของเส้นใยขนาดใหญ่ส่งผล ให้การกรองอนุภาคขนาดเล็กถึง 90 นาโมเมตรเกิดขึ้นได้ดี อีกทั้งการเติมไคโตซานส่งผลต่อความ เป็นประจุบวกของเส้นใยในบางตำแหน่งทำให้ดูดซับโปรตีนได้ดีกว่าเส้นใยในลอน 6 แต่เพียงอย่าง เดียว พื้นผิววิวิธพันธ์อันเกิดจากการผสมผงเขม่าดำหรือท่อนาโนของคาร์บอนกับพอลิไวนิล แอลกอฮอล์แล้วทำให้อนุภาคสารตัวเติมกระจายได้ดีขึ้นด้วยการปรับสภาพผิวนั้น ก็เป็นอีกหนึ่ง ตัวอย่างของการทำให้พื้นผิวมีสมบัติการนำไฟฟ้าที่ดีขึ้น โดยเกิดการเชื่อมโยงของอนุภาคที่นำ ไฟฟ้าทั่วถึงทั้งพื้นผิวและเนื้อภายในของเส้นใย อนึ่งโครงสร้างเส้นใยนาโนดังกล่าวต่างเกิดรูพรุน ภายในโครงสร้างอันเกิดจากการตกทับซ้อนแบบสุ่มตำแหน่งบนพื้นผิวรองรับ ซึ่งพบว่ามีการ กระจายขนาดของรูพรุนแตกต่างกันไป เนื่องจากเป็นโครงสร้างที่ไม่ได้ถักทอ (non-woven) แตกต่าง จากผ้ากรองไนลอนซึ่งเกิดจากการถักทอทำให้มีขนาดของรูพรุนเท่ากันทั้งหมด ดังนั้นพื้นผิวที่ ของเหลวในการกรองไหลตั้งฉากจึงมีรูพรุนปรากฏที่แตกต่างกันไปจึงเสมือนเป็นพื้นผิววิวิธพันธ์ที่มี ลักษณะการเกิดรูพรุนขึ้นกับจำนวนการตกทับของเส้นใย และขนาดและการกระจายขนาดของเส้น ใย

ในส่วนสุดท้ายจึงเป็นการจำลองการตกทับของเส้นใยนาโนบนแผ่นรองรับ เพื่อพิจารณา ลักษณะของรูพรุนที่เกิดขึ้นเมื่อมีการปรับเปลี่ยนขนาดของเส้นใยและปริมาณการตกทับของเส้นใย ในโครงสร้างสองมิติ จากการจำลองจะพบว่า หากขนาดของเส้นใยมีการกระจายขนาดแตกต่างกัน คือทั้งแคบและกว้าง แต่มีขนาดเฉลี่ยเท่ากัน จะทำให้สัดส่วนพื้นที่ตกทับของอนุภาคใกล้เคียงกัน สิ่ง ที่แตกต่างคือการกระจายขนาดของรูพรุนที่เคลื่อนไปทางขนาดเล็กมากขึ้น ส่งผลให้มีการเกิดรูพรุน ที่มีขนาดเล็กลงมากยิ่งขึ้นตามไปด้วย และเมื่อเปลี่ยนการกระจายขนาดของเส้นใยให้เคลื่อนที่ไปทางด้านขนาดใหญ่มากขึ้น ให้ผลในทำนอง เดียวกัน คือเมื่อเส้นใยมีขนาดใหญ่ขึ้นจะทำให้จำนวนรูพรุนที่เห็นในสองมิติลดน้อยลง และมีขนาด ของรูพรุนมีขนาดเล็กลง อย่างไรก็ตามการเปรียบเทียบที่แท้จริงควรเปรียบเทียบตัวอย่างที่มีปริมาณ สัดส่วนของแข็งเท่ากัน ซึ่งจะพบว่าเมื่อเส้นใยมีขนาดใหญ่ขึ้นจะทำให้ช่องว่างมีขนาดใหญ่ขึ้นด้วย ซึ่งสอดคล้องกับการทดลอง และเมื่อเปรียบเทียบขนาดของการทดลองกับการจำลองระบบจะเห็นว่า การจำลองสามารถสร้างเส้นใยนาโนได้ค่อนข้างใกล้เคียงกับความเป็นจริงเมื่อพิจารณาถึงขนาดของ จูพรุนและการกระจายขนาดของรูพรุน การจำลองระบบในโครงสร้าง 3 มิติ ยังไม่สามารถเลียนแบบ ของจริงได้ เนื่องจากการตกทับยังเกิดจากเส้นใยแข็ง (rigid fiber) ซึ่งจะไม่มีการงอตัวในแต่ละชั้น ของการตกทับ จึงส่งผลให้เห็นโครงสร้างที่โปร่ง (ความเป็นรูพรุนมาก) กว่าที่ควรจะเป็น

5.2 ข้อเสนอแนะสำหรับงานวิจัยในอนาคต

5.2.1 ในด้านการทดสอบประสิทธิภาพการกรอง ในเรื่องพื้นผิววิวิธพันธ์

- 1. เนื่องจากปริมาณของไคโตซานส่งผลต่อความเป็นวิวิธพันธ์ที่เกิดขึ้นในโครงสร้าง เส้นใยนาโน ดังนั้นควรศึกษาการเติมไคโตซานในปริมาณที่มากขึ้น เพื่อศึกษาผลของไคโตซานใน ด้านการดูดซับสารที่สามารถดูดซับได้ เช่น โปรตีน ให้ชัดเจนยิ่งขึ้น
- 2. อาจจะทดสอบการกรองด้วยค่าความเข้มข้นตั้งต้นของสารกรองที่แตกต่างกัน เพื่อสังเกตดูว่าหากมีความเข้มข้นตั้งต้นในการกรองที่เพิ่มขึ้นหรือลดลงจะส่งผลอย่างไรต่อ ประสิทธิภาพการกรอง นอกจากนี้อาจจะทดลองปรับเปลี่ยนความหนาของเส้นใยที่นำมาใช้ในการ กรองเพื่อสังเกตถึงประสิทธิภาพที่เปลี่ยนไป

5.2.2 ในด้านการทดสอบการตรวจวัดไอระเหย ในเรื่องพื้นผิววิวิธพันธ์

1. ควรทำให้การกระจายตัวของสารตัวเติมในพอลิเมอร์ดียิ่งขึ้น เพื่อศึกษา ปรากฏการณ์ percolation ต่อการลดค่าการนำไฟฟ้าของเส้นใย 2. ศึกษารูปร่างของเส้นใยหลังการดูดซับไอระเหยว่าเกิดการบวมเกิดขึ้นหรือไม่ หลังจากการดูดซับโดยนำไปทดสอบกับกล้องจุลทรรศน์อิเล็กตรอนแบบส่องกราด เพื่อจะดูว่าเกิด การเสียสภาพหรือไม่

5.2.3 ในด้านการจำลองระบบเส้นใยโดยคอมพิวเตอร์

- 1. ศึกษาการเคลื่อนที่ของอนุภาคในโครงสร้างเส้นใยนาโน อันเกิดจากเส้นใยที่ต่าง ขนาดและการเกาะติดของอนุภาคในโครงสร้างภายใน โดยพิจารณาอนุภาคที่ต่างขนาดด้วย เพื่อ ศึกษาการอุดตันของโครงสร้าง
- 2. ศึกษาความคดเคี้ยวภายในโครงสร้างเส้นใยนาโน เพื่อนำมาประมาณ ประสิทธิภาพการกรองอันเกี่ยวเนื่องกับฟลักซ์ของเหลว เพราะรูพรุนที่ต่อเนื่องแต่คดเคี้ยวและมี ขนาดของเส้นทางการไหลที่แตกต่างกัน

บรรณานุกรม

ภาษาไทย

วิภาวรรณ วงศ์ดาว และคณะ. (2553). การเปรียบเทียบรูปร่างลักษณะและคุณสมบัติทางไฟฟ้า ระหว่างเส้นใยนาโนพอลิไวนิลแอลกอฮอล์เติมผงเขม่าดำ เขม่าดำที่มีการทำให้กระจายอนุภาค และ ท่อนาโนคาร์บอน. วิทยานิพนธ์ปริญญามหาบัณฑิต, มหาวิทยาลัยธรรมศาสตร์, คณะ วิศวกรรมศาสตร์, ภาควิชาวิศวกรรมเคมี, สาขาวิชาเทคโนโลยีการจัดการพลังงานและสิ่งแวดล้อม

ภาษาอังกฤษ

- Alargova, R.G., Petkov, J.T., Denkov, N.D., Petsev, D.N., Ivanov, I.B. Modification of Ultrafiltration Membranes by Deposition of Colloid Particles. Colloids and Surfaces A 134 (1998) 331-342
- Aussawasathien D., Teerawattananon C., Vongachariya. Separation of micron to submicron particles from water: Electrospun nylon-6 nanofibrous membranes as prefilters, Journal of Membrane Science 315 (2008) 11–19
- Barhate R.S., Loong C.K., Ramakrishna S., Preparation and characterization of nanofibrous filtering media. Journal of Membrane Science 283, (2006) 209–218.
- Barhate, R.S., Ramakrishna, S. Nanofibrius Filtering Media: Filtration Problems and Solutions from Tiny Materials, Journal of Membrane Science 296 (2007) 1-8
- Biswas P., Wu C.Y., Critical review: nanoparticles and the environment. Journal of the Air and Waste Management Association 55 (2005) 708–746
- Bower, C., Kleinhammes, A., Wu, Y., Zhou, O. Intercalation and partial exfoliation of single-walled carbon nanotubes by nitric acid. Chem Phys Lett 288 (1998) 481-486
- Chuangchote, S., Sirivat, A. and Supaphol, P. Mechanical and electrorheological properties of electrospun poly(vinyl alcohol) nanofibre mats filled with carbon black nanoparticles. Natotechnology (2007) 18
- Ding, B. Wang, M., Yu, J., Sun, G. Gas Sensors Based on Electrospun Nanofibers.

 Sensors 9 (2009) 1609-1624
- Danwanichakul, P., Glandt, E.D. Percolation and jamming in structures built through sequential deposition of particles. Journal of Colloid and Interface Science 283 (2005) 41–48

- Danwanichakul P, Dechojarassri D, Werathirachot R. An Approximate Model Describing Electrospinning of Nanofibers: Process Parameter Investigation. International Journal of Electrospun Nanofibers and Applications; 2008; 2(2):103-114
- Dong, W., Zhang, T., McDonald, M., Padilla, C., Epstein J., Tian, Z.R. Biocompatible

 Nanofiber Scaffolds on Metal for Coltrolled Release and Cell Colonization,

 Nanonedicine: Nanotechnology, Biology, and Medicine 2 (2006) 248-252
- Desai, K., Kit, K., Li, J., Michael, D.P., Zivanovic, S., Meyer, H. Nanofibrous chitosan non-wovens for filtration applications. Polymer 50 (2009) 3661–3669.
- Eichhorn, S.J., Sampson, W.W. Statistical Geometry of Pores and Statistics of Porous Nanofibrous Assmblies. Journal of the Royal Society Interface 2 (2005) 309-318
- Gibson, P., Schreuder-Gibson, H., Rivin, D. Transport Properties of Porous Membranes

 Based on Electrospun Nanofibers, Colloids and Surfaces A. 187-188 (2001) 469481
- Hajra, M.G., Mehta, K., Chase, G.G. Effects of humidity, temperature and nanofibers on drop coalescence in glass fiber media. Separation and Purification Technology 30 (2003) 79–88
- Ham-Pichavant, F., Sebe, G., Pardon, P., Coma, V. Fat resistance properties of chitosanbased paper packaging for food applications. Carbohydrate Polymer 61 (2005) 259-265
- Hsieh, C., Chen, W. Gaseous Adsorption of Carbon Tetrachloride onto Carbon Nanofiber Arrays Prepared by Template-Assisted Synthesis. Diamond & Related Materials 16 (2007) 1945-1949
- Huang, Z.M., Zhang, Y.Z., Kotaki, M., Ramakrishna, S. A review on polymer nanofibers by electrospinning and their applications in nanocomposites. Composite Science and Technology 63 (2003) 2223–2253
- Kim, S.K. Chitin, Chitosan, Oligosaccharides and Their Derivatives; Biological Activities and Applications. USA. CRC Press (2011)
- Li, D., Sun, G. Coloration of textiles with self-dispersible carbon black nanoparticles. Dyes and Pigment 72 (2007) 144-149
- Li, D., Xia, Y.N. Electrospinning of nanofibers: reinventing the wheel? Advanced Materials 16 (2004) 1151–1170

- Luheng, W. Tianhuai, D. Peng, W. Influence of carbon black concentration on piezoresistivity for carbon-black-filled silicone rubber composite Carbon 47 (2009) 3151-3157
- Matsumoto, H., Yako, H., Minagawa, M., Tanioka, A. Characterization of Chitosan Nanofiber Fabric by Electrospray Deposition: Electrokinetic and Adsorption Behavior. Journal of Colloid and Interface Science 310 (2007) 678-681
- Maze, B., Tafreshi, V., Wang, Q., Pourdeyhimi, B. A Simulation of Unsteady-State Filtration via Nanofiber Media at Reduced Operating Pressures. Aerosol Science 38 (2007) 550-571
- Ng, K.W., Khor, H.L., Hutmacher, D.W. In vitro characterization of natural and synthetic dermal matrices cultured with human dermal fibroblasts. Biomaterials 25 (2004) 2807-2818
- Park, H., Park, Y.O., Filtration Properties of Electrospun Ultrafine Fiber Webs, Korean J. Chem. Eng. 22 (2005) 165-172
- Poirier, N., Derenne, S., Rouzaud, J.N., Largeau, C., Mariotti, A., Balesdent, J., Maquet, J. Chemical structure and sources of the macromolecular, resistant, organic fraction isolated from a forest soil (Lacadee, south-west France). Org Geochem 31 (2000) 813-827
- Ramakrishna, S., Fujihara, K., Teo, W.E., Lim, T.C., Ma, Z., An Introduction to Electrospinning and Nanofibers. Singapore. World Scientific (2005)
- Reisner, A.H. et al., The use of Coomassie Brilliant Blue G-250 perchloric acid solution for staining in electrophoresis and isoelectric focusing on polyacrylamide gels. Anal Biochem 64 (1975) 509–516
- Rhazi, M., Desbrieres, J., Tolaimate, A., Rinaudo, M., Vottero, P., Alagui, A., Meray, M.E. Influence of the nature of the metal ions on the complexation with chitosan. European Polymer Journal 38 (2002) 1523-1530
- Rutledge, G. C., Fridrikh, S. V. Formation of Fiber by Electrospinning. Advanced Drug Delivery Review 59 (2007) 1384-1391
- Sang, Y., Gu, Q., Sun, T., Li, F., Liang, C. Filtration by a Novel Nanofiber Membrane and Alumina Adsorption to Remove Copper (II) from Groundwater. Journal of Hazardous Materials 153 (2008) 860-866
- Sedmak, J.J., Grossberg, S.E. A rapid, sensitive and versatile assay for protein using Coomassie Brilliant Blue G-250. Anal Biochem. 79 (1977) 544–552

- Shin, C., Chase, G.G., Reneker, D.H. Recycled expanded polystyrene nanofibers applied in filter media. Colloids and Surfaces A-Physicochemical and Engineering Aspects, 262 (2005) 211–215
- Wang, J., Kim, S.C., Pui, D.Y.H. Investigation of the Figure of Merit for Filters with a Single Nanofiber Layer on a Substrate. Aerosol Science 39 (2008) 323-334
- Ye, P., Xu, Z., Wu, J., Innocent, C., Seta, P. Nanofibrous Poly(acrylonitrile-co-maleic acid)

 Mmebranes Functionalized with Gelatin and Chitosan for Lipase Immobilization.

 Biomaterials 27 (2006) 4169-4176
- Yun, K.M., Hogan Jr. C. J., Matsubayashi, Y., Kawabe, M., Iskandar, F., Okuyama, K., Nanoparticle Filtration by Electrospun Polymer Fibers. Chemical Engineering Science 62 (2007) 4751-4759
- Zhang, H., Li, S., Christopher, J.B.W., Ning, X., Nie, H., Zhua, L., (2009). Studies on electrospun nylon-6/chitosan complex nanofiber interactions. Electrochimica Acta 54 (2009) 5739–5745
- Zhang, S., Shim, W.S., Kim, J. Design of ultra-fine nonwovens via electrospinning of Nylon 6: Spinning parameters and filtration efficiency. Materials and Design 30 (2009) 3659–3666

เวบไซต์

http://chemistry.about.com/od/factsstructures/ig/Chemical-Structures---P/Polycaprolactam---Nylon-6.htm

www.koppers.com.au/images/UserUploadedImages/102/Carbon Black Morphology.jpg

http://jnm.snmjournals.org/cgi/content/full/48/7/1039/FIG1

ผลลัพธ์ที่ได้รับจากโครงการวิจัย

Reprint และ Manuscript ของเอกสารเหล่านี้อยู่ในภาคผนวก

บทความนำเสนอในที่ประชุมวิชาการที่มีรายงานการประชุม

- Panu Danwanichakul, Duangkamol Danwanichakul, "Computer Simulations of Nanofibrous Structures: The Effect of Polydispersity of Fiber Sizes on the Pore Sizes", TIChE International Conference 2011, 10-11 November 2011, Hatyai, Songkhla, THAILAND
- Panu Danwanichakul, Duangkamol Danwanichakul, Natthapong Sueviriyapan, Bumrungpol Sumruan, "Nylon 6/Chitosan Nanofibrous Structures for Filtration",1st Mae Fah Luang University International Conference 2012: Future Challenges towards ASEAN Integration, 29 November – 1 December 2012, Mae Fah Luang University, Chiang Rai, THAILAND
- Panu Danwanichakul, Sillawan Aschakulporn, Totsapon Pattarapongdilok, "Electrospun Carbon-filled Poly(vinyl Alcohol) Nanofibers for Gas Sensing", ICCET 2013: International Conference on Chemical Engineering and Technology 30-31 May 2013, Tokyo, JAPAN

บทความที่ส่งพิจารณาเพื่อตีพิมพ์

- Panu Danwanichakul, Duangkamol Danwanichakul, Natthapong Sueviriyapan, Bumrungpol Sumruan, "Nylon-6 and nylon-6/chitosan nanofibrous structures for liquid phase filtration," Separation and Purification Technology (manuscript under review)
- 2. Panu Danwanichakul, Sillawan Aschakulporn, Totsapon Pattarapongdilok, "The Reduction of Electrical Resistivity of Poly(vinyl alcohol) Nanofibers by Filling with Acid-Treated-Carbon Fillers" (To be submitted to Nanotechnology)
- Panu Danwanichakul, Duangkamol Danwanichakul, "Two-Dimensional Simulation of Electrospun Nanofibrous Structures: Connection of Experimental and Simulated Results," Journal of Chemistry (Manuscript under review)

ภาคผนวก

Paper Code: pc020

Computer Simulations of Nanofibrous Structures: The Effect of Polydispersity of Fiber sizes on the Pore Sizes

Panu Danwanichakul*, Duangkamol Danwanichakul

Department of Chemical Engineering, Faculty of Engineering, Thammasat University, Klong-Luang, Pathumthani, 12120, Thailand *e-mail: dpanu@engr.tu.ac.th

Abstract - This research aims to simulate the deposition of nanofibers on a surface of a collector. The production of the nanofibers is from electrospinning technique which is easy to operate and it is wellstudied by various research groups. Since the nanofibrous structures contain many tiny pores with size ranging from nanoscale to microscale, it is of interest to utilize such structures for processes involving surface activity. These include catalysis, drug release, sensing, and filtration. Among which, the filtration has long been applied commercially. In the simulation methods, the 2- dimensional connected structures of nanofibers will be constructed by assuming a nanofiber as an ellipse with an aspect ratio of 100 via Monte Carlo algorithm. Importantly, the size of nanofiber is assumed polydisperse during the deposition process unlike other theoretical works. This was studied as a factor influencing the average size and size distribution of pores. The configurations generated via the simulations resembled the real structures of nanofibers with polydisperse diameters. The statistics showed that the variation of size polydisperse around the same average value does not make any different to the coverage of fibers deposited on the surface but show differences in porous areas for the systems at low fiber density. In addition, the pore size distribution was found different for all samples of size variations. Interestingly, the one with smaller particles could produce the nanostructures with smaller pore size which is basically important in nanoscale properties.

Keyword: nanofiber, porous membrane, fiber diameter, polydispersity, pore size, simulation

1. Introduction

Electrospinning technique is an easy method to produce fibers whose size is in submicron range or nanofibers by applying the electrical force generated by the electric fields between the end of the metal needle and the ground. The liquid source may be a polymer melt or a polymer solution. Once the electrical force is greater than the surface tension of the hanging liquid drop at the end of the needle, it is pulled out of the needle and swirled onto the ground surface. Continuous fibers are produced in this manner while the solvent evaporates and the final nonwoven nanofibrous structure is obtained. A large number of literatures discussing the production of nanofibers from various polymer systems and their applications have been continuously investigated. Still the research on nanofibers is receiving more and more attention since the benefit of large surface area to volume ratio of nanostructures has been proven to help increasing the efficiency in many aspects including the higher mechanical strength, the increase in surface activity, and the increase in adsorption capacity. nanofibers were widely studied for their uses as nanosensors, drug delivery systems, scaffolds, wound dressings, as well as filters. The study on surface characterization and pore generation of nanofibrous membrane is, thus, of great interest.

As was already known, there are factors influencing the sizes of the fibers produced via electrospinning. Those are the voltage of power supply, the distance between the needle tip and the ground, the solution flow rate, the viscosity, the conductivity and surface tension of the polymer solutions. Some of these factors were modeled by Danwanichakul et al. [1] by using the poly (vinyl alcohol) as a model polymer. However, not only the fibers but also the pores generated by the overlapping of the fibers themselves are of importance. Park and Park [2] found that the pore size distribution in nanofibrous structures was narrow or sometimes considered as monodisperse pores. The study was done experimentally and there are no explanations for that to happen. The theoretical work could then fill the gap. Eichhhorn and Sampson [3] simulated the fibers by assuming that they are of cylindrical shape whose diameter is so much smaller than the length. They found that if the mass of fibers per unit area was fixed, when the mass of the fibers increased, the average size of the pores increased. Maze et al. [4] simulated the filter using nanofibers with a diameter of 200 nm and allowed the particles with diameters between 50-500 nm to pass through the pores. They found that the pressure drop was related to the pore size as could be predicted by the fluid mechanics

To our knowledge, there have been only those two works aiming at simulating the nanofibrous structures and they assumed monodispersity of fiber size in their studies. However, in all real experiments, the fibers have all kinds of size distributions that should affect the size of the pore as well. This research work, thus, investigated the effect of fiber size distribution on the pore size of the nanofibrous membrane via the computer simulation of the overlapping fibers on the surface, i.e. 2 dimensional systems.

2. Research Methodology

The computer programming was written in Fortran in this study. The deposition of fibers on the surface was performed by Monte Carlo simulations. First, the position on the 2D system and the size of fibers was randomly sampled one by one. The "2D" fiber was modeled as an ellipse whose aspect ratio, i.e. the length ratio of the long axis to the short axis, equals to 100. The length of short axis of the reference fiber was set at 0.015d where d could be arbitrary set at 10 microns so 0.015d represents the fiber with diameter of 150 nm. The deposited area was scaled as $100a^2$, equivalent to the area of the width of 10d and the length of 10d. Not the position of the fiber center but the angle of the fiber respect to the x-axis was also sampled randomly on the surface. The size polydispersity of the fibers was varied according to the uniform size distribution to be 0.85df- $1.15d_{\rm f}$, $0.75d_{\rm f}$, $1.25d_{\rm f}$, $0.65d_{\rm f}$, $1.35d_{\rm f}$, and $0.55d_{\rm f}$, $1.45d_{\rm f}$, where $d_{\rm f}$ is the reference fiber as which is 0.015d as mentioned before.

3. Results and Discussion

3.1 The simulated configurations of nanofibrous structures with size polydispersity

All samples are compared at the same fiber number density where the number density is defined as the number of fibers on $100d^2$ area. For example, the number density of 0.8 means that there are 80 fibers on $100d^2$ area and this is the condition in all samples in Fig. 1. It could be seen that the size of fibers could be differentiated from one another more easily as the size distribution is wider.

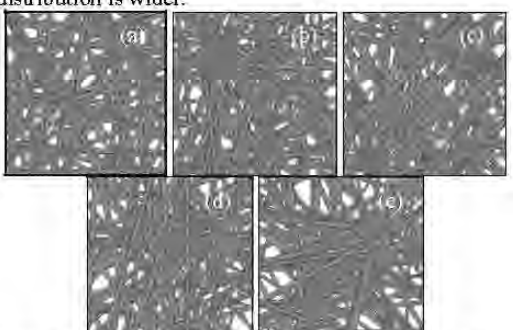


Fig. 1. Nanofibrous structures with various size polydispersity (a) monodisperse d_t (b) 0.85d_t-1.15d_t (c) 0.75d_t-1.25d_t (d) 0.65d_t-1.35d_t (e) 0.55d_t-1.45d_t

pc020-2

3.2 The coverage of fibers and the porous areas on the surface

It is of interest to compare the coverage of the fibers on the simulated area when the density of the fibers increased upon further deposition via electrospinning process. The results are displayed in Fig. 2.

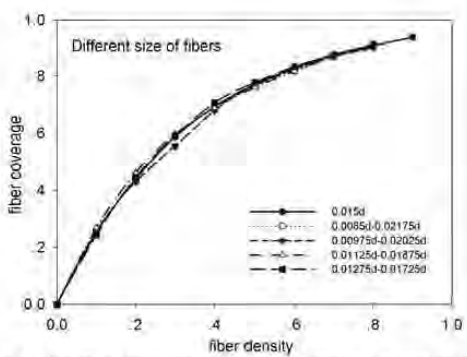


Fig 2. The surface coverage of nanofibers during the deposition on the surface. The results for different size distribution were compared.

The gray scale analysis with Photoshop was applied in this study. The differentiation between the deposited area (gray area) and the available area or porous area (white area) could be done with the program. These are monotonous results showing that all samples could have the same coverage area even though the fiber sizes could be differentiated. This happens probably because the chosen size distribution is still too close to each other and all distributions have the same average size which is $d_{\rm f}$. This may be considered as a confirmation that if the average size of nanofibers could be controlled to be equal for all samples, then the 2D coverage of the fibers could be pretty much the same,

The effect of number density on the surface coverage is also clearly seen in Fig.2. The coverage certainly increases upon increasing the number density but the increase rate is slower at higher density due to the overlapping of the fibers. However, upon adding more fibers, the pore size of the structures decreases as shown in Fig. 3.

In Fig. 3, it is obvious that an increase in fiber density could decrease the pore size of nanostructures rapidly at low fiber density. The rate of decreasing the pore size is lower when the fiber density increases due to less probability for fibers to deposit on the available areas. The transition is seen at density of 0.3. This may be considered as a crossover of the pore generation mechanism. At a low fiber density, the deposition of fibers generate new pores by separating the previous pores while at a high fiber density, the fibers deposited on the surface overlapped with one another and may not generate new pores. Therefore, there exists some density that the rate of pore generation was reduced immediately.

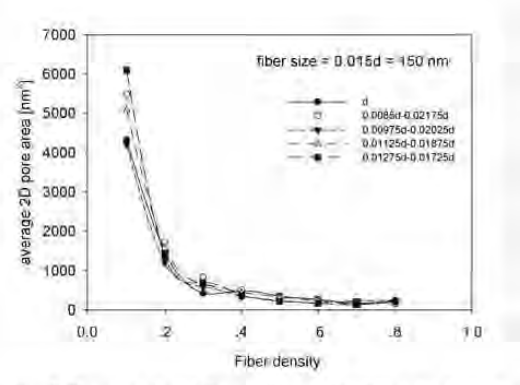


Fig. 3. The pore size of the nanofibrous structures as a function of fiber density.

As can be observed, at a high fiber density on the surface, there are lots of small pores whose size are around 1-2 times the fiber size. Fig 3 also shows the similar results of average 2D opening areas of pores when the size distribution is closely varied. The discussion was already given earlier. However, it is more interesting when the size distribution of the pores was studied since the results were different as will be discussed further.

3.3 The size distribution of pores in 2D nanostructures

Fig. 4 shows the pore size distribution of the nanofibrous structures generated from various size distributions of nanofibers. All are compared at the same density of 0.5. The area is reported in squared micron. It is seen that even though the average size of pores seems to be equivalent, the pore size distributions are apparently different.

When the size distribution skews to smaller sizes, there will be the emergence of smaller pores. This phenomenon is crucial since the expected properties of nanostructures occur when their dimensions are reduced to nano-range. Therefore, in a nanoscale investigation, determination of size distribution is necessary, apart from the average size in order to realize the nanostructures.

Fig 4(e) shows that there are a largest number of smallest pores since the size distribution covers down to $0.55d_6$ compared with other figures. Apparently, pore size distribution is not uniform and not a normal distribution. In all figures, there are very few numbers of large pores, whereas there are many small pores as expected when the density of fibers on the surface is high enough.

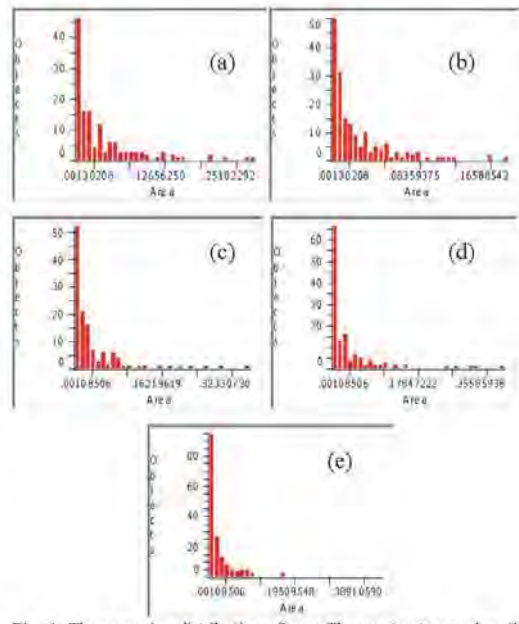


Fig. 4. The pore size distribution of nanofibrous structures when the fiber size distribution was varied. (a) monodisperse d_t (b) $0.85d_t$ $1.15d_t$ (c) $0.75d_t$ 1 $.25d_t$ (d) $0.65d_t$ 1 $.35d_t$ (e) $0.55d_t$ 1. $.45d_t$

4. Conclusions

The simulation of nanofibrous structures via Monte Carlo method in 2 dimensions was successfully performed. The results confirmed that even though there are some variations in fiber size, if the average size of fiber could be controlled, the surface coverage of fibers randomly deposited during electrospinning process could be the same. This is also true for the average pore areas of the nanofibrous structures. The difference may be seen at lower number density of fibers. The non-woven structures seemed to be equivalent for all samples when the number density is the same.

The size distribution of pores within the nanofibrous structures was determined. It was found different when the fiber distribution was different. The results show that the smaller pore size could be obtained in the case of smaller fibers were produced and deposited on the surface. Therefore, the study confirmed that production of finer fibers is crucial in generating the finer pores and this is the heart of nanotechnology.

Acknowledgements

This research was jointly funded by the Thailand Research Fund (TRF) and Thammasat University (Grant# DBG5380007). All assistances from the Faculty of Engineering are highly appreciated.

References

- P. Danwanichakul, D. Dechojarassri and R. Werathirachot An Approximate Model Describing Electrospinning of Nanofibers: Process Parameter Investigation. International Journal of Electrospun Nanofibers and Applications (2008) 2(2), 103-114
- [2] H. Park and Y.O. Park, Filtration Properties of Electrospun Ultrafine Fiber Webs, Korean J. Chem. Eng. 22 (2005) 165-172
- [3] S.J. Eichhorn and W.W. Sampson, Statistical Geometry of Pores and Statistics of Porous Nanofibrous Assemblies. *Journal of the Royal* Society Interface 2 (2005) 309-318
- [4] B. Maze, V. Tafreshi, Q. Wang, and B.A. Pourdeyhimi, Simulation of Unsteady-State Filtration via Nanofiber Media at Reduced Operating Pressures. Aerosol Science 38 (2007) 550-571



NYLON 6/CHITOSAN NANOFIBROUS STRUCTURES FOR FILTRATION

Panu Danwanichakul*, Duangkamol Danwanichakul, Natthapong Sueviriyapan, Bumrungpol Sumruan

Department of Chemical Engineering, Faculty of Engineering, Thammasat University, Klong Luang, Pathumthani, 12120, Thailand *e-mail: dpanu@engr.tu.ac.th

Abstract

This research is to investigate nanoporous electrospun structures obtained from electrospinning technique for using as filters. In the research, Nylon 6 and the blend of Nylon 6/chitosan nanostructures were fabricated from polymer solutions at various concentrations ranging from 30 to 35% w/v. The kinematic viscosity of the Nylon 6 and Nylon 6/Chitosan solutions was determined by using Cannon-Fenske (Reverse Flow) viscometer while the morphology of nanofibers was observed with Scanning Electron Microscope (SEM). The results showed that the solutions with a higher viscosity yielded fibers with larger diameters and pores. Although the solution of nylon 6/chitosan at a ratio of 50:1 (30% wt nylon) had the highest viscosity in the experiment, the formation of small sized ultrafine fiber group generated even much smaller pores. In the filtration test, the flow rate of the suspension of polystyrene particles in water was adjusted to 8 µm/s and the nanofibrous filters with the thickness in the range of 0.1±0.02 mm were used. The results showed complete removals of polystyrene particles when using nanofibrous filters for both pure Nylon 6 and Nylon 6/chitosan nanofibers, being compared with the filter paper and commercial nylon fabric with No. 80/55 and No. 150/35, which showed much lower performance, i.e. filtration efficiency of 2.71 to 14.50%.

Keywords: filtration, chitosan, nylon 6, nanofiber, electrospinning

Introduction

The electrospinning method has become a popular method for producing fibers with diameters in the range of few microns and submicron. It was invented in 1934 to produce polymer filaments by using electrostatic force. When the electric field was applied to the polymer solution, the charged liquid jet will be pulled out of the capillary tip. The jet with small diameter will undergo stretching and bending instability. After the solvent rapidly evaporates, the fibers will be left solidified on a collector (Mincheva et al. 2008). Many researchers were successful to produce the nanofibers via electrospinning technique (Huang et al. 2003; Li and Xia 2004). Since the structures contain small fibers as well as small pores, there are many applications regarding high surface area to volume ratio of the nanofibrous structures. The applications include drug releases, sensing vapor gases, wound dressing, catalysis, and filtration. The efficiency of nanofibrous filters as a filtration media were studied by many research groups. (Barhate et al. 2006; Gibson et al. 2001; Hajra et al. 2003; Shin et al. 2005).



One of the polymers usually used for filter productions is Nylon. Therefore, the electrospun Nylon 6 nanofibrous structures could certainly be employed as a membrane material for water filtration because they have high chemical and thermal resistance as well as wettability (Aussawasathien et al. 2008). Another material that has interested many groups is chitosan, which is a biopolymer having a wide range of applications. It is derived from chitin by removing the N-acetyl group on the copolymer consisting of β -(1 \rightarrow 4)-2-acetamido-2-deoxy-D-glucopyranose and β -(1 \rightarrow 4)-2-amino-2-deoxy-D-glucopyranose units. Due to its excellent properties including biocompatibility, biodegradability, and antibacterial activity, chitosan has been extensively found beneficial in many biomedical applications such as scaffolds and tissue engineering (Huang et al., 2005; Jiang et al.; 2006), and wound dressings to prevent fatal infections (Burkatovskaya et al., 2006). High-molecular-weighted chitosan can be dissolved only in an acidic condition, and it is barely soluble at pH above 6.5. Geng et al. (2005) was able to electrospin chitosan nanofibers from acetic acid solution. Others tried to blend chitosan with other electrospinnable polymers such as poly(vinyl alcohol) (Chuachamsai et al. 2008).

It was reported by Nirmala et al. (2011) that Nylon 6/chitosan composite nanofibers could be electrospun from a formic acid solution and the structures contains fibers with ultrafine web. They applied this structure for biomedical applications. However, the ultrafine fibers could be very useful in filtration as well and this has not been investigated before. Therefore, in this work, such nanofibrous structures of this polymer blend was applied in the filtration of colloidal particles from water phase.

Methodology

Material

High-molecular-weighted chitosan (%Degree of Deacetylation = 98.6) was obtained from A.N. Lab Aquatic Nutrition, Thailand. Nylon 6 was purchased from Sigma-Aldrich Co.LLC. Formic Acid was supplied from Ajax Finechem Pty Ltd. Polystyrene particles with average particle sizes of 90 nm (50-100 nm), 200 nm (200-300 nm) and 410 nm (400-600 nm) were purchased from Spherotech, Inc. All chemicals were of analytical grade and used without further purification. Commercial Nylon fabric with No. 80/55 and No. 150/35 were purchased by Synthetech Co.,Ltd.

Spinning solution preparation

Nylon 6 was dissolved in 10 ml of 90%wt formic acid to obtain the spinning solutions with Nylon 6 concentrations of 30-35 %wt/vol. Then chitosan was added in Nylon 6 solution at various amounts which are 1, 1.5 and 2% of the Nylon 6 concentration to get the weight ratios of Nylon 6 to chitosan of 100:1, 100:1.5 and 50:1, respectively. Each mixture was blended with magnetic stirrer at room temperature for 2-4 hr until the solution was homogeneous.

Electrospinning of nanofibers

The electrospinning apparatus was set up as shown in Figure 1. The spinning solution was poured into a 2 ml syringe with 0.8 mm-ID and 4.2 cm needle. The high voltage power supply (PS/MJ30PO400 Glassman) was connected to the end of the needle by a stainless steel electrode. Another electrode was connected to the stationary collector covered with 3.5 X 3.5 cm² copper plate. The electrospinning voltage was set at 21 kV and the distance between the needle tip and the collector was held constant at 9 cm. The spinning time was about for 1.5-3 hr to get the mats with 0.1 ± 0.02 mm in thickness.



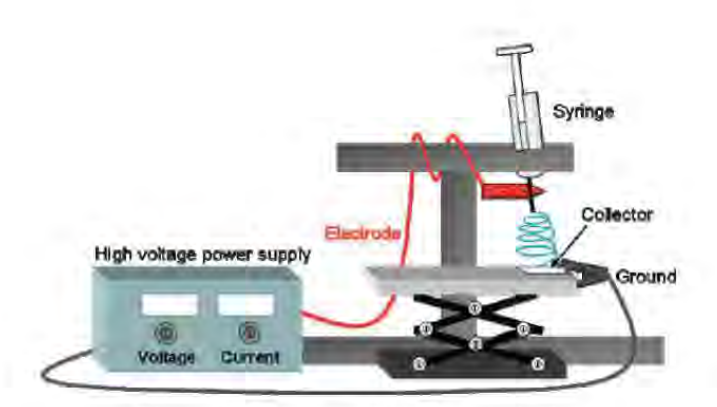


Figure 1 Apparatus of the electrospinning

Determination of kinematic viscosity

The kinematic viscosity of the Nylon 6 and Nylon 6/Chitosan solutions was determined by using Cannon-Fenske (Reverse Flow) viscometer, size 400 (U853) and size 450 (E641) from Cole Parmer at 40°C. Cannon-Fenske viscometer, size 400 was applied for Nylon 6 solution while size 450 was applied for Nylon 6/Chitosan solution.

Morphology of nanofibers

The morphology of nanofibers was observed with Scanning Electron Microscope (SEM) (JEOL JSM-6310F) after gold coating by a gold sputtering coater for 100 seconds. The average pore size diameter of fiber was obtained with an image analyzer.

Filtration of polystyrene particle by nanofiber

Firstly, the nanofiber was placed in the syringe filter holder with a diameter of 13 mm and then 5 ml of 200 ppm polystyrene particle suspension was pumped through the filter by a syringe pump at a flow rate of 8 µl/sec. The polystyrene colloidal particles were collected after filtering and the concentration of filtrate was measured. The results were compared with those for No. 1 Whatman filter paper and commercial Nylon fabrics, No. 80/55 and 150/35. The calibration curve of polystyrene particle concentration was prepared from polystyrene colloidal suspension with concentrations of 20, 40, 80, 120, 160 and 200 ppm. UV-VIS spectrophotometer was applied at a wavelength of 490 nm for measuring the concentration of the filtrate. Filtration efficiency (%) was defined by equation (1).

Filtration efficiency (%) =
$$1 - \frac{C_{\text{filtrate}}}{C_{\text{initial}}} \times 100$$
 (1)

Where C_{filtrate} and C_{initial} are polystyrene concentrations in the filtrate and in the suspension feed, respectively



Results

Kinematic viscosity of spinning solutions.

Kinematic viscosity of Nylon 6 and Nylon 6/Chitosan solutions at various concentrations was shown in Figure 2.

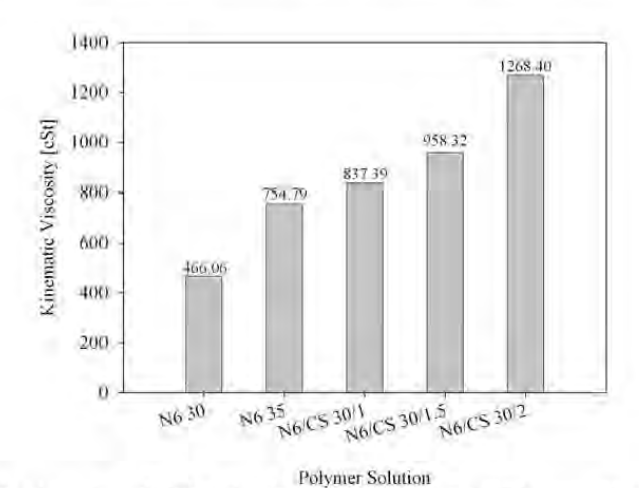


Figure 2 Kinematic viscosity of Nylon 6 solutions and Nylon 6/Chitosan solution at various concentrations

Considering Nylon 6 without adding chitosan, the kinematic viscosity was increased with increasing Nylon 6 content. When chitosan was added in Nylon 6 solution, the kinematic viscosity was also increased with increasing chitosan content. Noticeably, the kinematic viscosity of the 30%wt/vol Nylon 6 blended with 1% wt/vol chitosan was slightly higher than that of the 35% wt/vol Nylon 6 solution. Chitosan molecules seem to be very large when compared with nylon molecules.

Morphology of nanofibers.

SEM micrographs of electrospun products from solutions with different Nylon 6 concentrations with and without adding chitosan were shown in Figure 3. Evidently, when the polymer concentration increased, the nanofiber diameter increased. These SEM micrographs were then used to analyze the average diameter and average pore size as shown in Figure 4.



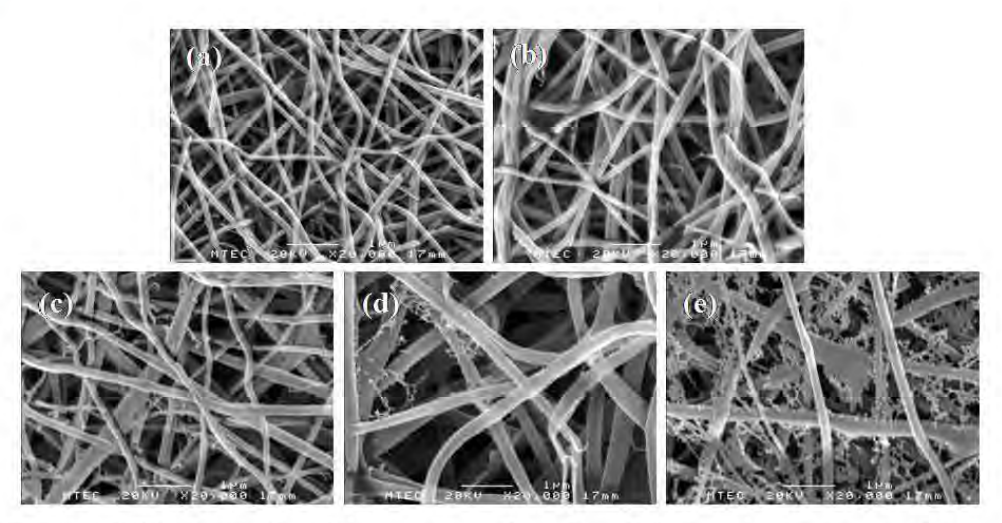


Figure 3 SEM micrographs of electrospun products from different polymer concentrations (a) 30%wt/vol Nylon 6 (b) 35%wt/vol Nylon 6 (c) 30%wt/vol Nylon 6/CS with 1.0% of Nylon 6 (d) 30%wt/vol Nylon 6/CS with 1.5% of Nylon 6 (e) 30%wt/vol Nylon 6/CS with 2.0% of Nylon 6

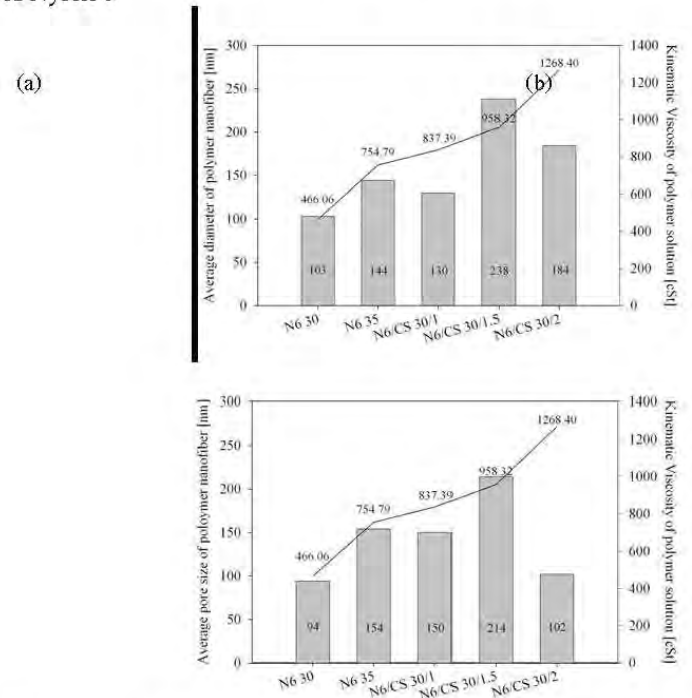


Figure 4 Kinematic viscosity of Nylon 6 and Nylon 6/Chitosan solutions at various concentrations together with (a) average diameter and (b) average pore size of nanofiber



Comparing Figure 4(a) and Figure 4(b), it was likely that the average diameter and average pore size show the same trend except in the case of 30%wt/vol Nylon 6 blended with 2%wt/vol chitosan where very small pores formed by ultrafine fibers were found leading to a much lower average pore size.

Filtration of polystyrene particle by nanofibers.

Figures 5-7 show SEM micrographs of polystyrene particles, whose size were of 410, 200 and 90 nm, which were collected by different filters. As can be seen in Figure 5(a)-5(d) and Figure 6(a)-6(d), when 410-nm- and 200-nm-polystyrene particles were filtered, a few of them stuck onto the commercial nylon fibers of both types, No. 80/55 and No. 150/35, whereas there were a large number of polystyrene particles on Nylon 6 nanofibers produced from a 30%wt/vol solution and on No.1 filter paper. Nonwoven structures seemed to collect the particles better than the woven ones. Figure 7 shows that 90-nm polystyrene particles covered thoroughly on the filter paper and nanofibers while the particles covered partly on the commercial nylon fibers. The filtration efficiency of each filter was shown in Table 1.

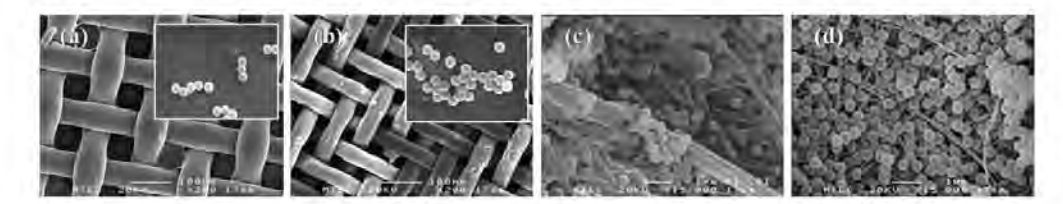


Figure 5 SEM micrographs of 410-nm polystyrene particles collected by different filters (a) Commercial Nylon fabric, No. 80/55 with 200x magnification (b) Commercial Nylon fabric, No. 150/35 with 200x magnification (c) Filter paper with 15,000x magnification (d) Nanofibers from 30%wt/vol Nylon 6 solution, with 15,000x magnification.

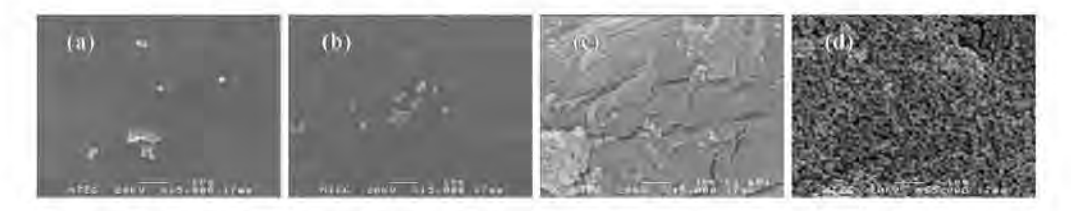


Figure 6 SEM micrographs of 200-nm polystyrene particles collected by different filters (a) Commercial Nylon fabric, No. 80/55 with 200x magnification (b) Commercial Nylon fabric, No. 150/35 with 200x magnification (c) Filter paper with 15,000x magnification (d) Nanofibers from 30%wt/vol Nylon 6 solution, with 15,000x magnification.



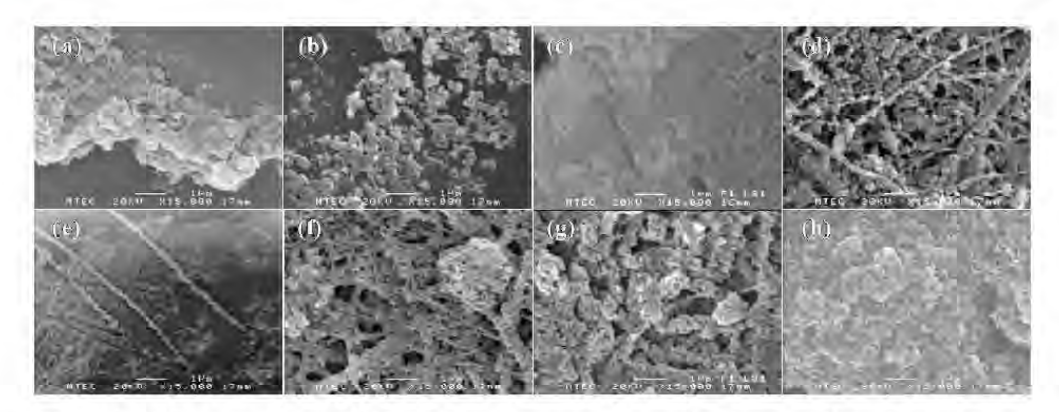


Figure 7 SEM micrographs of 90-nm polystyrene particles collected by different filters at 15,000x magnification (a) Commercial Nylon fabric, No. 80/55 (b) Commercial Nylon fabric, No. 150/35 (c) Filter paper (d) Nanofibers from 30%wt/vol Nylon 6 solution (e) Nanofibers from 35%wt/vol Nylon 6 solution (f) Nanofibers from 30%wt/vol Nylon 6 /CS 1.0% of Nylon 6 solution (g) Nanofibers from 30%wt/vol Nylon 6 /CS 1.50%of Nylon 6 solution (h) Nanofibers from 30%wt/vol Nylon 6 /CS 2.0% of Nylon 6 solution

In Table 1, it was clearly shown that the nanofibrous structures could capture polystyrene particles much better than filter paper and the commercial nylon fabrics, No. 80/55 and No. 150/35. Moreover, every sample of nanofiber filters showed 100% filtration efficiency for every particle size. For filter paper, it could remove polystyrene particles with a size of 410 nm better than that of 200 nm but less than that of 90 nm. The higher efficiency was seen when filtering much smaller particles attributable to particle self-aggregation due to high surface energy of fine particles. In addition, although the pore size of commercial nylon fabric with No. 80/55 was larger than that of No. 150/35 but it was observed that the filtration efficiency of the former was higher than the latter. This result may be because the commercial nylon fiber with No. 80/55 has also larger fiber size than that of No. 150/35 and the polystyrene particles may attach onto the fiber surface and then formed the filter layer or filter cake, thereby, increasing the efficiency.

Table 1 Filtration efficiency of different filter type when applied to filter polystyrene particles with various sizes

Filter type	Filtration efficiency (%)			
	Particle size			
	410 nm	200 nm	90 nm	
NC 80/55	7.79	4.93	14.50	
NC150/35	4.96	2.93	2.71	
Filter Paper	35.89	8.27	59.14	
N6 30	100.00	100.00	100.00	
N635	100.00	100.00	100.00	
N6/CS 30/1	100.00	100.00	100.00	
N6/CS 30/1.5	100.00	100.00	100.00	
N6/CS 30/2	100.00	100.00	100.00	



Discussion and Conclusion

In this work, Nylon 6 and Nylon 6/CS nanofibrous structures were used as filters for a removal of polystyrene particles of different size and compared with commercial nylon fabrics and filter paper. It was found that kinematic viscosity of Nylon 6 solutions and Nylon 6/Chitosan solution was increased with increasing polymer content, which in turn increased the size of the fibers as confirmed with SEM micrographs. In addition, the average fiber diameter of nanofibrous structures and their average pore size showed the same trend. Moreover, the nanofiber filters could capture polystyrene particles much better than filter paper and the commercial nylon fabrics, No. 80/55 and No. 150/35. The nanofiber filter gave 100% of filtration efficiency while filter paper and commercial nylon fiber gave 8.27% - 59.14% and 2.7% – 14.50% of filtration efficiency, respectively. Interestingly, self-aggregation of fine particles played an important role on the filtration efficiency. In conclusion, nanofibrous structures could successfully remove particles in a size range of micron and sub-micron down to 90 nanometers from the suspension.

Acknowledgements

This research was jointly funded by the Thailand Research Fund (TRF) and Thammasat University (Grant#DBG5380007). All assistances from the Faculty of Engineering are highly appreciated.

References

- Burkatovskaya M, Tegos GP, Swietlik E, Demidova TN, Castano AP, Hamblin MR (2006) Use of chitosan bandage to prevent fatal infections developing from highly contaminated wounds in mice. Biomaterials 27:4157-4164.
- Chuachamsai A, Lertviriyasawat S, Danwanichakul P (2008) Spinnability and Defect Formation of Chitosan/Poly Vinyl Alcohol Electrospun Nanofibers. Thammasat International Journal of Science and Technology (TIJSAT) 13, Special edition: 24-29
- Geng X, Kwon O, Jang J (2005) Electrospinning of chitosan dissolved in acetic acid. Biomaterials 26:5427-5432
- 4. Huang Y, Onyeri S, Siewe M, Moshfeghian A, Madihally SV (2005) In vitro characterization of chitosan-gelatin scaffolds for tissue engineering. Biomaterials 26:7616-7627.
- Huang ZM, Zhang YZ, Kotaki M, Ramakrishna S (2003) A review on polymer nanofibers by electrospinning and their applications in nanocomposites. Compos Sci Technol 63(15):2223–2253.
- Jiang T, Abdel-Fattah WI, Laurencin CT (2006) In vitro evaluation of chitosan/poly(lactic acid-glycolic acid) sintered microsphere scaffolds for bone tissue engineering. Biomaterials 27:4894-4903.
- Li D, Xia YN (2004) Electrospinning of nanofibers: reinventing the wheel? Adv Mater 16: 1151–1170.
- Mincheva R, Stoilova O, Penchev H, Ruskov T, Spirov I, Manolova N, Rashkov I (2008) Synthesis of polymer-stabilized magnetic nanoparticles and fabrication of nanocomposite fibers thereof using electrospinning. Eur Polym J 44:615-627
- Nirmala R, Navamathavan R, Kang HS, Mohamed HE, Kim HY (2010) Preparation
 of polyamide-6/chitosan composite nanofibers by a single solvent system via
 electrospinning for biomedical applications. Colloid Surface B 83:173–178.

Electrospun Carbon-Filled Poly(vinyl alcohol) Nanofibers for Gas Sensing

Panu Danwanichakul, Sillawan Aschakulporn, and Totsapon Pattarapongdilok

Abstract—A family of poly(vilnyl alcohol) (PVA) nanofibers filled with carbon black particles and carbon nanotubes were investigated for their electrical properties. Carbon fillers were found to decrease the resistivity of the fiber mats linearly when detecting IPA vapor whose concentration increased from 1 to 8 ppm, confirming the possibility to be used as a gas sensor. Surface treatment with nitric acid could decrease the filler aggregate size and disperse the fillers more uniformly in the fibers, thereby, reducing the resistivity. The self-dispersible carbon black (SDCB) particles could decrease the resistivity of the PVA nanofibers better than untreated carbon nanotubes (CNT). Both SDCB and SDCNT samples could maintain the resistivity when the temperature increased, while the resistivity of CB and CNT samples decreased with temperature. In addition, the resistivity decreased along the dynamic increase in moisture content at 45°C. However, the presence of IPA could still be detected together with moisture.

Keywords—Carbon Black, Carbon Nanotube, Nanofiber, Poly(vinyl alcohol).

I. INTRODUCTION

THE electrospinning technique has been investigated governing the morphology of the obtained nanofibers [1]. Due to its large surface area to volume ratio, the nanofibrous structure could be used in many applications related to surface activity of the fibers. For example, in catalysis lots of pores in nanofibrous structures vield higher rate of adsorption of reactants and higher reactivity due to a large number of active sites. In biomedical engineering, the nanostructures have been applied for drug release and promoting cell growth, each of which process needs large surface area to increase its rate and process continuity. Besides, gas sensing applications have also been studied since the initial steps of sensing, which are diffusion and adsorption of gas molecules into the material of fibers, required a large interfacial area between solid and liquid or gas phase. Such application is the focus of this research.

Polymers usually applied in electrospinning process should be easily fabricated from their solutions or melts. Poly(vinyl alcohol) (PVA) is one of the most used in film forming or fiber fabrication. Therefore, it has been used in all applications mentioned so far as a polymer matrix of nanofibers. The composite of PVA and other materials, which are also polymers or particulate fillers to enhance specific properties of the fibers, has been widely experimented. The mechanical properties of PVA nanofibers were enhanced by adding carbon black particles in the fibers [2]. As expected, carbon black, which has been used as reinforcing filler in rubber tyre industries for a long time, could increase tensile strength of the nanofibers as the filler loading increased from 1 to 10%wt of PVA content. Multi-walled carbon nanotubes (MWCNT) were also reported to improve tensile strength of PVA fibers [3] since it could nucleate crystallization of PVA in the composite nanofibers. The composite nanofibers mats were later crosslinked with glutaraldehyde to improve its mechanical strength as a post-treatment.

Those carbon-filled PVA nanofibers were of interest for their mechanical properties. However, carbon nanotubes (CNT) were also well known for their electrical conductivity. Recently, the composite of PVA and CNT was prepared and studied as conductive nanofibers [4]. In that work, CNTs were dispersed homogeneously in N-methyl-2-pyrrolidone and mixed with PVA solution. It was found that the conductivity could increase upon increasing the CNT loading. Since gas sensing application is closely related to the electrical conductivity of the materials, the improvement of conductivity of PVA nanofibers by incorporating carbon nanotubes have attracted many research groups, one of which blended PVA, polyaniline and CNT together and electrospun the fibers in order to make a CO sensor and their product could detect CO in the range of 100-500 ppm [5].

The success of conductivity or mechanical properties improvement of PVA nanofibers not only lies in filling the fibers with conductive carbon particles but it also depends on how well the fillers are dispersed inside nanofibers. Ultrasound was applied to suspensions four times before electrospinning the PVA solution blended with carbon black particles [3]. Bang et al. [6] have currently treated the MWCNT with acids by varying the pH of the solution and they found that a lower pH gave smaller fiber diameter, thereby, increasing mechanical properties. Li and Sun [7] have applied the method of acid treatment before to carbon black particles in order to disperse them more homogeneously in suspension as a black dye in coloration of cotton fibers.

In this work, the nitric acid treatment [7] was adopted in

P. D. is with the Chemical Engineering, Faculty of Engineering, Thammasat University, Pathumthani, 12120, Thailand (corresponding author to provide phone: 662-564-3001 ext. 3123; fax: 662-564-3024; e-mail: dpanu@engr.tu.ac.th).

S. A. was with the Chemical Engineering, Faculty of Engineering, Thammasat University, Pathumthani, 12120, Thailand.

T. P. was with the Chemical Engineering, Faculty of Engineering, Thammasat University, Pathumthani, 12120, Thailand.

order to produce self-dispersible carbon black (SDCB) particles to be filled in PVA nanofibers, which have not been reported before by other groups. The electrical properties were compared with those of carbon-black-filled-, carbon-nanotube-filled- and self-dispersible-carbon-nanotube-filled PVA nanofibers. The model gas to be detected in the study is isopropyl alcohol (IPA), which is usually used as a degreaser in electronic device productions. To test the sensitivity of nanofibrous structures, the concentration of IPA was varied lower than 8 ppm.

II. MATERIAL AND METHODOLOGY

A. Material

Polyvinyl alcohol (PVA) used in this research was purchased from Sigma Aldrich. It is a cold water soluble type with molecular weight (Mw) of 40,000-70,000 and degree of hydrolysis of 98%. Carbon black (N-330, particle size about 33 nm) was supplied by Loxley Public Co., Ltd. Multi-walled carbon nanotube with carbon content more than 95%, (O.D. x L equals 6-9 nm x 1 μm) was purchased from Sigma-Aldrich Co.LLC. Nitric acid and isopropyl alcohol (IPA) were supplied from Merck Ltd., Thailand.

B. Self-dispersible carbon black and self-dispersible carbon nanotube preparation

2 g carbon black or carbon nanotube was mixed with 150 ml. of 65%w/w nitric acid and then it was refluxed at 120°C for 2 hr. After that the mixture was heated at 130°C. To remove nitric oxide left on particle surfaces, particles were washed in water and then were precipitated by using centrifugal speed of 3000 for 15 min. The filtered precipitate was then added into distilled water and was centrifuged at the same condition again. The self-dispersible carbon black (SDCB) particles and self-dispersible carbon nanotubes (SDCNT) were received after drying the precipitate at 80°C for 24 hr. The size distributions before and after surface treatment of carbon black particles were analyzed by a centrifugal particle size analyzer (Shimadsu, model SA-CP3).

C. Spinning solution preparation

To obtain pure PVA solution, PVA powder was dissolved in distilled water to get PVA concentration of 25, 30 and 35%w/v. The spinning solution was prepared by firstly mixing 1 g of PVA with 10 ml of distilled water. After that the fillers which are CB, SDCB, CNT and SDCNT were added into PVA solution to obtain the ratio of PVA to filler of 100:4, 100:6 and 100:8.

D. Electrospinning of nanofibers

The spinning solution was poured into a 2 ml syringe with 0.8 mm-ID and 3.5 cm needle. The high voltage power supply (PS/MJ30PO400 Glassman) was connected to the end of the needle by a stainless steel electrode. Another electrode was connected to the stationary collector covered with 2 x 2 cm² copper plate. The electrospinning voltage was set at 18 kV

and the distance between the needle tip and the collector was held constant at 7 cm. The spinning time was about 25 min.

E. Morphology of nanofibers

The morphology of nanofibers was observed with scanning electron microscope (SEM) (JEOL JSM-6310F) after gold coating by a gold sputtering coater for 100 seconds. The average fiber diameter was obtained with an image analyzer.

F. Resistivity of nanofibers

The nanofiber of unknown resistance was connected in series with the known resistance. The voltage of the known resistance and that of nanofiber were measured by using a multimeter as shown in Figure 1 for the experimental setup.

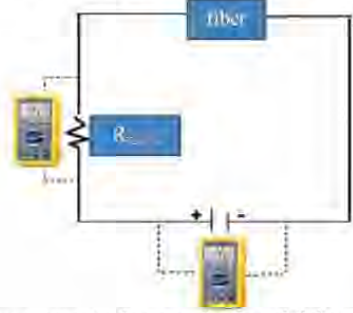


Fig. 1 The setup apparatus for measuring the resistivity of nanofibers.

The resistivity of nanofiber was calculated from (1), When R_{koown} and R_{jiber} are resistivity of known and nanofiber, respectively while V_{supply} and V_{known} are the supply voltage and voltage measured from known resistance, respectively.

$$R_{\text{fiber}} = \frac{\left(V_{\text{supply}} - V_{\text{brown}}\right)}{V_{\text{brown}}} x R_{\text{brown}} \tag{1}$$

G. The effect of IPA concentration on resistivity of fibers

The experiment was done at the condition of fixing the relative humidity at 40% and the temperature at 32°C. The concentration of IPA in the air was varied by adding liquid IPA drop by drop into the whole volume where the fibers were placed and the resistivity of the fibers was measured.

H. The effect of temperature on resistivity of fibers

The air in the closed vessel contained 67 ppm IPA. The relative humidity was fixed at 40% and the temperature was at 32°C. The whole system was heated to 40°C. The resistivity of the fibers was measured at various temperatures stepping up with an increment of 1°C.

I. The effect of relative humidity on resistivity of fibers

The experiment was done with 67 ppm IPA vapor in the air. The liquid water was placed inside this close system while maintain the constant temperature of 45°C so the relative humidity was changed from 45% to 80% upon continuing evaporation, during which time the resistivity of the fibers was measured. The results were also compared with those in the presence of only water vapor in the air.

III. RESULTS AND DISCUSSION

A. Size distribution of carbon black particles

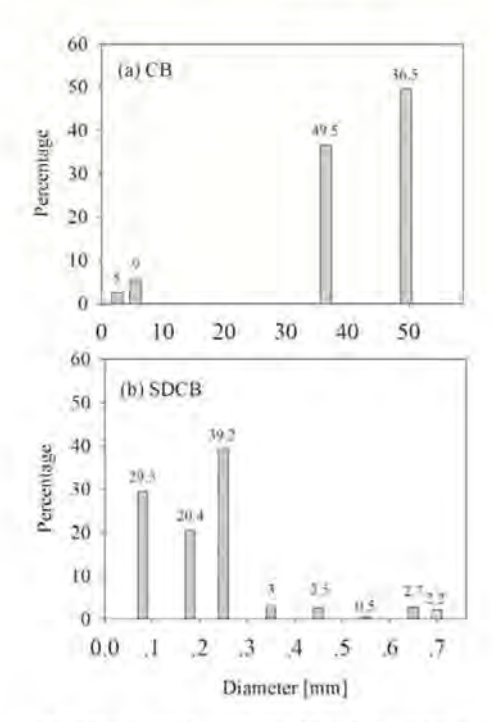


Fig. 2 Size distributions from centrifugal size analyzer of (a) carbon black particles (CB) and (b) self-dispersible carbon black particles (SDCB)

The size distributions of carbon black particles before and after surface treatment with nitric acid were shown in Figure 2. It was clearly seen that carbon black particles in suspension usually aggregated as a large particle, whose size was as large as 50 microns, whereas the self-dispersible carbon black particles were much smaller, whose size mostly fell in the range of 100 nm to 250 nm. This is due to the repulsive forces among the carboxylic groups generated upon oxidation with nitric acid on the treated particle surface that preclude the aggregation of particles [7].

B. Morphology of nanofibers

When mixing surface-treated and untreated carbon black particles into PVA solution and spinning electrically to obtain nanofibrous mats as shown in Figure 3, the structures looked similar to one another. The fibers filled with treated carbon nanotubes and untreated looked similar to other fibers as well. Nonetheless, the average size of the fibers of each sample was a little different. It seemed that adding self-dispersible fibers yielded slightly larger nanofibers. This may be attributable to more amount of fillers could be dispersed in the fibers since the particle dispersion was better, leading to a little higher viscosity, which in turn resulting in larger diameters. However, on the whole, they could be considered physically similar to one another. Therefore, incorporating each species of carbon filler of the same loading in the fibers did not affect the shape and size of fibers similar to what observed in [2].

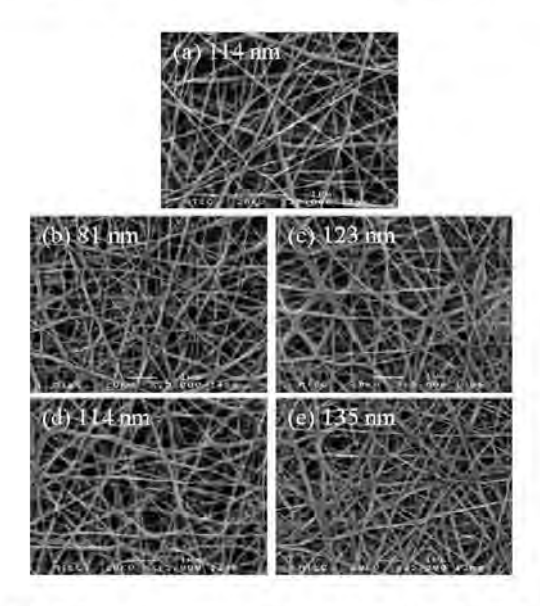


Fig. 3 SEM micrographs of (a) PVA nanofibers (b) PVA nanofibers filled with carbon black (PVA/CB) (c) PVA nanofibers filled with self-dispersible carbon black (PVA/SDCB) (d) PVA nanofibers filled with carbon nanotubes (PVA/CNT) (e) PVA nanofibers filled with self-dispersible carbon nanotubes (PVA/SDCNT)

C. Resistivity of nanofibers

The resistivity of nanofibers was shown in Figure 4. The concentration of IPA was varied in a very low range up to 8 ppm in order to observe the sensitivity of the nanofibers. It is clearly seen that for all types of fibers a decreasing trend of resistivity was seen when the IPA concentration increased because IPA is a polar substance that could conduct electricity. Therefore, these nanofibers could be applied as gas sensors for detecting polar molecules such as alcohols and quantifying their concentrations in ambient air.

When comparing all types of fibers, pure PVA nanofibers possessed highest resistivity. Embodying the fibers with carbon fillers could linearly increase the conductivity as shown. Since all samples looked similar, the surface area per unit volume of them should also be similar. Thus, the decrease in resistivity should be resulted from the conductive filler loading. It was experimented earlier by our groups that upon increasing the filler loading up to 8% wt/vol in suspension, the resistivity was decreased. Therefore, in this work, we fixed the loading at 8% wt/vol in prepared suspension. Adding more filler beyond that resulted in particle aggregation which caused poor conductivity in the solid fiber mats. Surface treatment of particles is, thus, essential. As shown in the figure, the influence of selfdispersible carbon black particles was very interesting since it could decrease resistivity of the fibers to be lower than fibers filled with carbon nanotubes which are widely known as an excellent conductor. This finding implied that aggregation of carbon nanotubes occurred during the mixing process in PVA solution. As expected, the sample filled with self-dispersible carbon nanotubes was the best conductors among all. The surface treatment of particles could benefit an increase in conductivity of nanofibers since particles could be dispersed more uniformly in each fiber, yielding better percolation throughout the structures, which is the mechanism governing electrical conductivity of the membrane.

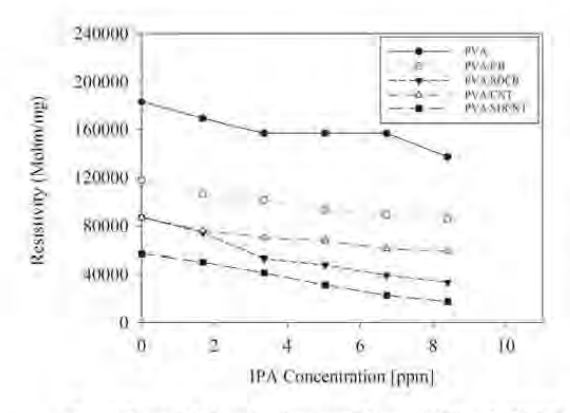


Fig. 4 The resistivity of various nanofibers at 32°C and 40%RH was shown decreasing with an increase in IPA concentration.

D. The effect of temperature on nanofiber resistivity

It is also intriguing to investigate the effect of temperature on the resistivity of nanofibers while absorbing IPA vapor which was fixed at 67 ppm. This effect is important when a sensor is applied at a temperature higher than room temperature. The results are shown in Figure 5. At first, the resistivity of PVA increased with temperature and then dropped. It is possible that when heated, PVA fibers initially relaxed and the whole nanostructures might slightly expand resulting in disconnected path of electrical conduction. However, when the temperature increased, both the diffusion rate of IPA molecules from the air to the nanofiber surface

and the diffusion rate inside the solid fibers could increase, which are favorable for an increase in electrical conduction. Therefore, these two factors were competitive and the maximum of resistivity of PVA nanofibers was observed.

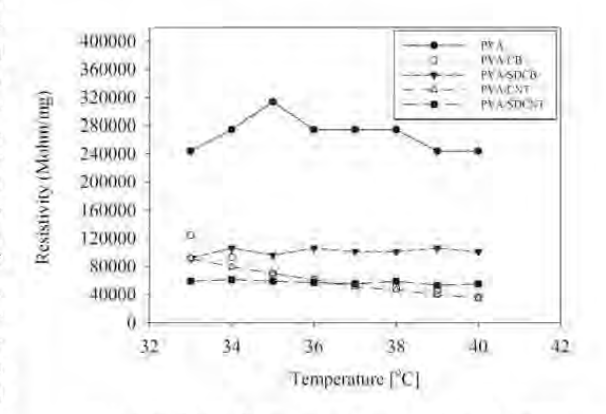


Fig. 5 The effect of temperature on resistivity of various nanofibers absorbing 67 ppm isopropyl alcohol (IPA) at 32°C and 40%RH. (a) PVA (b) PVA/CB (c) PVA/SDCB (d) PVA/CNT (e) PVA/SDCNT

For other carbon-filled nanofibers, the results could be classified into two groups. The first group represents the trend of decreasing of resistivity and the second group represents the trend of almost constant resistivity. As shown Figure 5, PVA nanofibers with untreated fillers belong to the first group while PVA nanofibers with self-dispersible fillers belong to the second group. These phenomena could also be explained with the same reason provided for pure PVA nanofibers. The carbon-filled nanofibers possessed much higher mechanical strength than pure PVA fibers [2] because PVA chains were more or less fixed in place with attractive interactions from carbon particles, which act as reinforcing filler in polymer matrix. The structures would be stronger if the filler particles were smaller and dispersed more uniformly inside each fiber, which is the case for self-dispersible carbon black particles and self-dispersible nanotubes. It is possible that the PVA/SDCB and PVA/SDCNT structures were strong enough to withstand thermal expansion so the diffusion of more IPA to the structures did not occur at higher temperatures. Unlike those two, the resistivity of PVA/CB and PVA/CNT decreased with temperature, which was likely due to a slight effect of thermal expansion of PVA matrix, which facilitated the diffusion of more IPA molecules inside the fibers. Interestingly, the change of resistivity of PVA/CB and PVA/CNT upon changing the temperatures implies that these two nanofibers could be applied as a temperature sensor while the PVA/SDCB and PVA/SDCNT could be used as a gas sensor at any temperature.

It should be noted that at lowest temperature of 33°C, the resistivity of nanofibers of the PVA was the highest, followed

by PVA/CB, PVA/CNT which was close to PVA/SDCB and then PVA/SDCNT, whereas at highest temperature of 40°C, the order was rearranged to PVA, PVA/SDCB, PVA/SDCNT, PVA/CNT and PVA/CB. The trend at a high temperature was confirmed again in a separate experiment where the temperature was set at 45°C, as shown in Figure 6, which showed the comparison of resistivity of fibers when exposed to water vapor alone and when exposed to water vapor together with IPA vapor.

E. The effect of water vapor on fiber resistivity

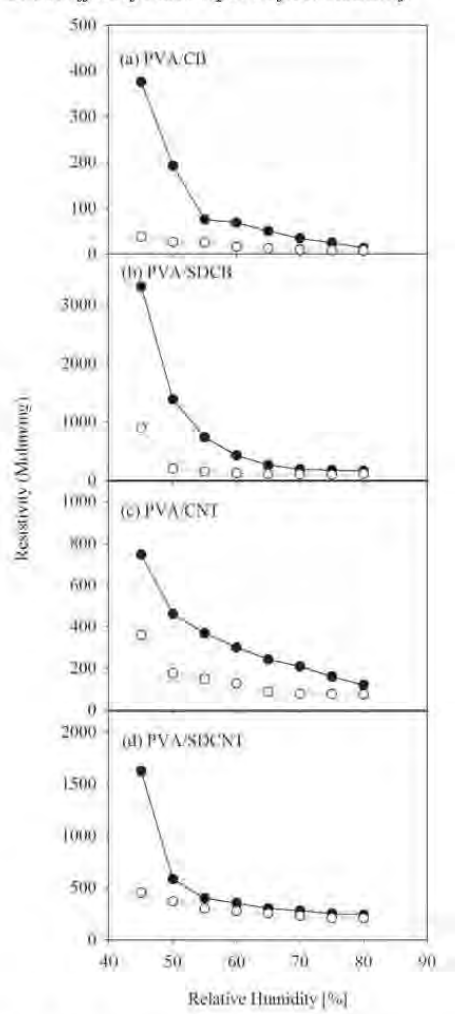


Fig. 6 The effect of relative humidity on resistivity of various fibers. The black dot refers to water vapor alone and the white dot refers to water and IPA vapors. (a) PVA (b) PVA/CB (c) PVA/SDCB (d) PVA/CNT (e) PVA/SDCNT

Because there is always water vapor in the air, the effect of humidity on the detection of IPA vapor should also be

studied. It is obvious that the PVA fibers were sensitive to water vapor in the air as they were sensitive to the IPA vapor. These fibers could be potentially applied as humidity sensors as well. As the relative humidity increased from 45% to 80% while the IPA concentration was fixed at 67 ppm in the air, the resistivity of the fibers absorbing both gasses decreased and it was closer to the resistivity of fibers absorbing water vapor alone. However, the separation between these two could be seen at a low humidity of 40% which is the ambient humidity when the experiment was done. When the differentiation between the resistivity of both systems was mainly considered, the sample PVA/SDCB shows the largest separation of the two numbers, followed by PVA/SDCNT.

IV. CONCLUSION

This research showed the possibility of applying electrospun poly (vinyl alcohol) filled with self-dispersible carbon black (SDCB) and self-dispersible carbon nanotube (SDCNT) compared with the nanofibers filled with asreceived fillers to be used as a gas sensor. The morphology of nanofibers, their electrical properties before and after the detection of isopropyl alcohol (IPA) vapor in the air, as well as the effect of moisture content in the air were investigated in this work. The results showed that adding those fillers in the nanofibers decreased the resistivity of the structures at room temperature especially with SDCB and SDCNT particles, which were dispersed better in the structures because of charges from the surface treatment. The surface treatment was proved to be the essential step during incorporation of nanosized fillers in the polymer matrix. This actually benefit in the reduction of filler usage as well as the increase in performance of the nanofibers as was seen for the case of SDCB particles which could enhance the fiber conductivity comparable to CNTs.

When nanofibers were tested for both humidity and the presence of IPA vapor in the air, the resistivity was found decreasing along the dynamic increase in moisture content at 45°C. However, the presence of IPA could still be detected together with the effect of moisture. The SDCB-filled and SDCNT-filled PVA nanofibers could differentiate the presence of IPA and water more clearly than others. In addition, a dynamic increase in temperature was found to decrease the resistivity of nanofibrous structures embodied with CB and CNT while the ones with SDCB and SDCNT showed small degree of fluctuation around a constant resistivity, implying that the latter two were more appropriate for gas sensor application. More importantly, the nanostructures could detect the low concentration limit of IPA concentration ranging from 1-8 ppm. The linear relationship between the IPA concentration and the resistivity of the sensors were clearly observed.

All the results evidently indicated that these nanocomposites, especially SDCB composites should gain more attention in the field of sensors, provided that the degree

of dispersion of carbon black particles is maximally enhanced.

ACKNOWLEDGMENT

This research was jointly funded by the Thailand Research Fund (TRF) (Grant number: DBG5380007) and Thammasat University. All assistances from the Faculty of Engineering are highly appreciated.

REFERENCES

- P. Danwanichakul, D. Dechojarassri, R. Werathirachot, "An Approximate Model Describing Electrospinning of Nanofibers: Process Parameter Investigation," International Journal of Electrospun Nanofibers and Applications, 2008. 2(2), pp. 103-114.
- Nanofibers and Applications, 2008, 2(2), pp. 103-114.
 S. Chuangchote, A. Sirivat, P. Supaphol, "Mechanical and electro-rheological properties of electrospun poly(vinyl alcohol) nanofibre mats filled with carbon black nanoparticles." Nanotechnology, 2007, 18 (14), art. no. 145705.
- M. Naebe, T. Lin, W. Tian, L. Dai, X. Wang, "Effects of MWNT nanofillers on structures and properties of PVA electrospun nanofibres," Nanotechnology, 2007, 18 (22), art. no. 225605
 O. Koysuren, "Preparation and characterization of polyvinyl
- O. Koysuren, "Preparation and characterization of polyvinyl alcohol/carbon nanotube (PVA/CNT) conductive nanofibers," Journal of Polymer Engineering, 2012, 32 (6-7), pp. 407-413
 Y. Wanna, S. Pratontep, A. Wisitsoraat, A. Tuantranont, "Development
- [5] Y. Wanna, S. Pratontep, A. Wisitsoraat, A. Tuantranont, "Development of nanofibers composite Polyaniline/CNT fabricated by Electro spinning Technique for CO Gas Sensor," Proceedings of IEEE Sensors, 2006, art. no. 4178628, pp. 342-345
- [6] H. Bang, M. Gopiraman, B.-S. Kim, S.-H. Kim, I.-S. Kim, "Effects of pH on electrospun PVA/acid-treated MWNT composite nanofibers," Colloids and Surfaces A: Physicochemical and Engineering Aspects, 2012, 409, pp. 112-117
- [7] D. Li, G. Sun, "Coloration of textiles with self-dispersible carbon black nanoparticles," Dyes and Pigments 2007, 72, pp. 144-149

Panu Danwanichakul was born in Bangkok, Thailand on June 17, 1973. He got his bachelor degree in chemical engineering at Chulalongkom University, Bangkok, Thailand in 1994. In 1997, he got his master degree in chemical engineering at University of Delaware, Newark, Delaware, USA and immediately after that, he pursued his Ph.D. in chemical Engineering at University of Pennsylvania, Philadelphia, Pennsylvania, USA and finished his degree in 2003. His thesis applied statistical thermodynamics to study the nanostructures grown by slow deposition on a solid surface.

After finishing Ph.D. he returned to Thammasat University, Thailand, and has worked as a full time lecturer in the department of chemical engineering, faculty of engineering. Now he is an associate professor in the same department and serves as a chair of the center of excellence on natural rubber technology, which is located at the faculty of engineering. His current research interests include natural rubber technology, adsorption technology and continuing theoretical work on nanostructures and applications of remotibers.

Assoc. Prof. Danwanichakul was awarded best teaching award from Thammasat University in 2006 and good research award from Thammasat University in 2010. His Ph.D. dissertation was also recognized by National Research Council of Thailand in 2008.

MANUSCRIPT submitted to Separation and Purification Technology

NYLON-6 AND NYLON-6/CHITOSAN NANOFIBROUS STRUCTURES FOR LIQUID PHASE FILTRATION

Panu Danwanichakul*, Duangkamol Danwanichakul, Natthapong Sueviriyapan, Bumrungpol Sumruan

Department of Chemical Engineering, Faculty of Engineering, Thammasat University, Klong Luang, Pathumthani, 12120, THAILAND

*corresponding author:

Department of Chemical Engineering, Faculty of Engineering, Thammasat University, 99 Moo 18, Paholyothin Rd., Klong-Nung, Klong Luang, Pathumthani, 12120, Thailand Tel. & Fax: 662-5643001 ext. 3123, email: dpanu@engr.tu.ac.th

Abstract

The nanoporous structures of electrospun nylon-6 and nylon-6/chitosan were investigated to be used as filter media. Nylon-6 nanofibers were fabricated from the solutions with concentrations of 30 and 35% wt/v while the blends were from 30% wt/v nylon-6 with chitosan contents of 1, 1.5 and 2% of nylon-6 content. The results showed that the solution with higher viscosity vielded structures with larger fiber diameters and larger pores. However, the blend solutions yielded bimodal size distribution of ultrafine fibers among large ones, resulting in smaller average fiber and pore sizes. The pore sizes determined from the SEM figures were consistent with those calculated from Hagen-Poiseuille equation. In addition, the iodine adsorption increased as the pore size decreased, implying an increase in total pore surface. In the filtration test, the flow rate of 200 ppm suspension of polystyrene particles (400, 200 and 90 nm) was adjusted to 8 μm/s and the nanofibrous filters with the thickness of 0.1±0.02 mm were used. The results showed complete removals of polystyrene particles when using nanofibrous filters. These were compared with the filter paper and commercial nylon fabric with No. 80/55 and No. 150/35, which showed much lower performance. In addition, the nanostructures could also adsorb BSA up to 53% from 10 ppm BSA solution.

Keywords: filtration, chitosan, nylon-6, nanofiber, particle

1. Introduction

Nowadays, the electrospinning method has become a popular method for producing fibers with diameters in the range of few microns and submicron in laboratory. It was invented in 1934 to produce polymer filaments by using electrostatic force. When the electric field was applied to the polymer solution, the charged liquid jet will be pulled out of the capillary tip. The jet with small diameter will undergo stretching and bending instability. After the solvent rapidly evaporates, the fibers will be left solidified on a collector. Many researchers were successful to produce nanofibers via electrospinning technique (For example, Huang et al. 2003; Li and Xia 2004). Since the structures contain small fibers as well as small pores, there are many applications regarding high surface area to volume

ratio of the nanofibrous structures. These include drug releases, wound dressing, vapor gas sensing, catalysis, and filtration, on which the latter application is focused in this work.

The efficiency of nanofibrous structures as filter media were studied by many research groups. For instance, polyvinylidene fluoride nanofibers were electrospun in to membranes and investigated for membrane separation of polystyrene particles of 1, 5 and 10 micrometers in liquid phase. With thickness of 0.3 mm and pore size ranging from 4 to 10 micrometers, the membrane could reject 90% of particles (Gopal, 2006). Another group produced electrospun polyacrylonitrile nanofibers and applied as a midlayer support in membrane for ultrafiltration to remove MgSO₄ particles in water (Yoon, 2009).

One of the polymers usually used as filter cloth is nylon. Therefore, the electrospun nylon-6 nanofibrous structures could certainly be employed as a membrane material for water filtration because they have high chemical and thermal resistance as well as wettability. In a study of separation of polystyrene particles in water whose sizes were varied to be 0.5, 1000, 6000 and 10000 micrometers by using nylon nanofibrous membrane with thickness ranging from 0.15 to 0.6 mm and with the feed concentrations of particles from 62.5 to 250 ppm, the separation factor could be up to 85 to 100% dependent on the particle size (Aussawasathien et al. 2008). In addition, nylon-6 nanofibrous membranes were also employed to remove aerosol, where the Peclet number and slip flow phenomena were investigated along with the filtration efficiency (Hung et al, 2011).

Another material that has interested many groups is chitosan, which is a biopolymer having a wide range of applications. It is derived from chitin by removing the N-acetyl group on the copolymer consisting of β -(1 \rightarrow 4)-2-acetamido-2-deoxy-D-glucopyranose and β -(1 \rightarrow 4)-2-amino-2-deoxy-D-glucopyranose units. Due to its excellent properties including biocompatibility, biodegradability, and antibacterial activity, chitosan has been extensively found beneficial in many biomedical applications such as scaffolds and tissue engineering (Huang et al., 2005; Jiang et al., 2006), and wound dressings to prevent fatal infections (Burkatovskaya et al., 2006). High-molecular-weighted chitosan can be dissolved only in an acidic condition, and it is barely soluble at pH above 6.5. Geng et al. (2005) were able to electrospin chitosan nanofibers from acetic acid solution while other groups attempted to blend chitosan with other electrospinnable polymers such as poly(vinyl alcohol) (Chuachamsai et al., 2008), poly(ethylene oxide) (Desai et al., 2009) and nylon-6.

It was reported by Nirmala et al. (2011) that nylon-6/chitosan composite nanofibers could be electrospun from a formic acid solution and the structures contained fibers with ultrafine web. They applied this structure for biomedical applications. However, the ultrafine fibers could be very useful in filtration as well and this has not been investigated before. Therefore, in this work, the nanofibrous structures of this polymer blend was mainly studied for the filtration of colloidal particles from water phase which should be physically attributable to the relative sizes of particles and pores. In addition, the chemical effect of blending chitosan was also reported for the adsorptive behavior of the membrane in capturing bovine serum albumin (BSA) in water. The detail of our investigation was focused on the relation of fiber size and pore size of the structures with

the filtration efficiency. Therefore, we applied Hagen-Poiseuille equation to determine the pore size and applied iodine number measurement in order to investigate the adsorptive surface area of these structures.

2. Material and Methods

2.1 Materials

High-molecular-weighted chitosan (%Degree of Deacetylation of 98.6) was obtained from A.N. Lab Aquatic Nutrition, Thailand. Nylon-6 and bovine serum albumin (BSA) were purchased from Sigma-Aldrich Co. LLC. Formic acid was supplied by Ajax Finechem Pty Ltd. The suspensions of polystyrene particles with average particle sizes of 90 nm (50-100 nm), 200 nm (200-300 nm) and 410 nm (400-600 nm) were purchased from Spherotech, Inc. All chemicals were of analytical grade and used without further purification. Commercial nylon fabric of No. 80/55 and No. 150/35 were purchased from Synthetech Co., Ltd.

2.2 Spinning solution preparation

Nylon-6 was dissolved in 10 ml of 90% wt formic acid to obtain the spinning solutions with concentrations of 30 and 35 % wt/vol, namely N6 30 and N6 35, respectively. Since chitosan used in our experiments were of high molecular weight, so the addition of chitosan to nylon-6 was limited by the solution viscosity. Chitosan was added in nylon-6 solution at various amounts which are 1%, 1.5% and 2% of nylon-6 content to get the weight ratios of nylon-6 to chitosan of 100:1, 100:1.5 and 50:1 so they were called N6/CS 30/1, N6/CS 30/1.5 and N6/CS 30/2, respectively. Each mixture was blended with a magnetic stirrer at room temperature for 2-4 hr until the solution was homogeneous.

2.3 Electrospinning of nanofibers

The spinning solution was poured into a 2 ml syringe with a needle with a diameter of 0.8 mm and a length of 4.2 cm. The high voltage power supply (Glassman PS/MJ30PO400) was connected to the end of the needle by a stainless steel electrode. Another electrode was connected to the stationary collector covered with 3.5 X 3.5 cm² copper plate. The electrospinning voltage was set at 21 kV and the distance between the needle tip and the collector was held constant at 9 cm. The spinning time was about 1.5-3 hr in order to obtain the nanofiber mats with 0.1±0.02 mm in thickness.

2.4 Determination of kinematic viscosity

The kinematic viscosities of nylon-6 and nylon-6/chitosan solutions were determined by using Cannon-Fenske (Reverse Flow) viscometer from Cole Parmer at 40°C. The viscometer of size 400 (U853) was applied for nylon-6 solutions while that of size 450 (E641) was applied for nylon-6/chitosan solutions.

2.5 Morphology of nanofibers

The morphology of nanofibers was observed with scanning electron microscope (SEM) (JEOL JSM-6310F) after coating by a gold sputtering coater for 100 seconds. Each SEM figure was analyzed for the average fiber size as well as the apparent average pore size of the structure.

2.6 The average pore size determination by Hagen-Poiseuille equation

In this experiment, a syringe containing 5 ml water was vertically connected to a filter holder where the filter medium would be placed inside. A 0.5 kg piece of metal was then placed at the end of the syringe, pushing the water to pass through the filter medium. The volumetric flow rate of water was measured. The flow is so slow that it could be considered a laminar flow and pores inside nanofibrous structure are usually interconnected, thus the structures resemble a bundle of tortuous tubes. To simplify the calculation, the tortuosity was neglected and the $Hagen-Poiseuille\ equation$ should be applied. In this research, the Reynolds number (Re) was $7.41 \times 10^{-5} \pm 1.05 \times 10^{-5}$ which ensures the flow to be laminar in a circular tube. Therefore, the approximate average pore diameter of nanofibrous structures can be determined by Hagen-Poiseuille equation (Johnston, 2003),

$$\frac{d^2}{32} = \frac{u\mu z}{\Delta P} \tag{1}$$

Where, d is the average pore diameter (m), u is the velocity (m/s), μ is the viscosity of water at 25 °C (Pa·s), z is the filter thickness (m) and ΔP is pressure drop (Pa).

2.7 Iodine Number Measurement

Another experiment that could yield an indirect evidence of pore size inside the filter is iodine adsorption. Iodine molecules could be adsorbed on the surface of nanofibers. Therefore, iodine adsorption capacity of the filter could reflect the total surface of the pores, which is closely related to the pore size. The experiment followed the method described in ASTM WK29867 - Revision of D1510 - 09b entitled the Standard Test Method for Carbon Black, Iodine Adsorption Number.

In the experiment, 6 mg of filter was submerged in 25 ml of 0.4728 N iodide solution and those were centrifuged at 4000 rpm for 5 min. Subsequently, 20 ml of supernatant was titrated with 0.0394 N sodium thiosulphate solution until the color changed to yellow. This was followed by adding 5 drops of 1% starch solution as an indicator and the titration was continued until the end point was reached, where the solution was colorless. The iodine adsorption number could be calculated from Eq. (2).

$$I = \frac{(B-S)}{B} x \frac{V}{W} x N x 126.91$$
 (2)

Where, I is iodine adsorption number (g/kg), B is titrant volume used for a blank sample (ml), S is titrant volume used for our sample (ml), V is an exact volume of sodium thiosulfate solution which is 25 ml, W is sample weight (g) and N is the normality of iodine solution which is set at 0.04728 (meq/ml). The value 126.91 refers to mass equivalence of iodine (mg/meq).

2.8 Filtration of polystyrene particles

Firstly, the nanofiber filter was placed in the filter holder with a diameter of 13 mm and 5 ml of 200 ppm polystyrene particle suspension was pumped through the filter by a syringe pump at a fixed flow rate of 8 µl/sec. The polystyrene (PS) colloidal particles were collected by the filter and the concentration of the filtrate was measured. The filtration results were compared with those using No. 1 Whatman filter paper and commercial nylon fabrics, No. 80/55 and 150/35. The experiments were performed for all size ranges of polystyrene particles as described in section 2.1. The concentration of polystyrene particles in the filtrate was obtained by using the calibration curve showing the linear relation between the concentration and absorbance measured with UV-VIS spectrophotometer at 490 nm. The filtration efficiency is expressed as

Filtration efficiency (%) =
$$1 - \frac{C_{\text{filtrate}}}{C_{\text{initial}}} \times 100$$
 (3)

Here, C_{initial} and C_{filtrate} are the initial concentration of PS particles in suspension and the concentration in the filtrate coming out of the filter, respectively.

2.9 Adsorptive filtration of BSA proteins by the nanofibrous structures

In another experiment, the solution of bovine serum albumin (BSA) with a concentration of 10 ppm was used to study the possibility of protein separation using different nanofiber filter medium. The calibration curve was prepared from the BSA solution with varying concentration up to $10~\mu g/ml$. The BSA solution has to be mixed with dye reagent based on Bradford method. UV-VIS spectrophotometer was applied at a wavelength of 595 nm for measuring the concentration of BSA in a filtrate. Filtration efficiency (%) was defined by equation (3).

3. Results and Discussion

3.1 Morphology of nanofibers

SEM micrographs of electrospun products from solutions of different nylon-6 concentrations with and without adding chitosan were shown in Figure 1. The image analysis of SEM figures gave the average diameters of fibers and pores of the structures shown in Figure 2(a) and 2(b), respectively, along with the corresponding kinematic viscosities of solutions. The polymer concentration is closely related to the viscosity of the spinning solution, which plays an important role in yielding nanofibers without beads. In this work, the concentration of nylon-6 was varied first and it was observed that at the spinning temperature of 30 °C, the solution with nylon-6 concentration below 30% wt/vol was not viscous enough to generate the smooth fibers and that over 35% wt/vol was too

viscous to be electrically spun. The chitosan was added later and the amount was also adjusted to be in the range of fiber spinnability. Evidently, the system of nylon-6/chitosan blend used in this work is different from those in another work (Nirmala et al, 2011).

As seen from Figures 1 and 2(a), without chitosan, the kinematic viscosity of nylon-6 solution was increased with increasing polymer concentration, thereby increasing the fiber diameter. Since chitosan has a much larger molecule than nylon-6, adding chitosan whose amount was only 1% of nylon-6 content in N6 30 solution could increase the solution viscosity to be higher than that of N6 35 solution. Upon increasing chitosan content in N6 30 solution, the kinematic viscosity is exponentially increased. It is probably from the rapid increase in the degree of polymer chain entanglement of both polymers, where the system was reported to show the hydrogen bonding between hydroxyl and amino groups of chitosan and amide group of nylon (Zhang et al, 2009). As reported in previous research works (Nirmana, 2011; Zhang et al., 2009), the structures from nylon-6/chitosan blends were composed of typical fibers as in the case of pure nylon-6 together with the ultrafine nanofibers resembling the continuous spider web. In our case, the ultrafine nanofibers could also be seen in Figure 1(c) - 1(e), whose amount was increased when the chitosan content was increased. Being compared with structures from other works, the ultrafine nanofibrous structure in Figure 1(e) did not extend continuously and thoroughly among the relatively large nanofibers. expected that the ultrafine nanofibers were also generated inside the pores throughout the structures and this could be helpful in filtration processes because it could increase probability of particle capture and the adsorption of molecules on to nanofiber surfaces. The results will be discussed next.

In Figure 2(a), because of the existing ultrafine fibers in polymer blend samples, the size distribution was bimodal. The average sizes were 103, 144, 130, 238, and 184 nm for N630, N635, N6/CS 30/1, N6/CS 30/1.5, and N6/CS 30/2, respectively. The average size would be resulted from the average of populations of large fibers and ultrafine fibers. Obviously, in the case of N6/CS 30/2, the ultrafine nanofibers have a significant weight in the average.

Of interest is the comparison between Figure 2(a) and 2(b). The similar trends of nanofiber size and pore size of the structures are clearly seen. The electrospun fibers with smaller size could generate the nonwoven mat with smaller pores inside its structure upon random deposition on the metal collector. Importantly, if the ultrafine nanofibers could be greatly generated as in the case of adding 2% chitosan, even a large number of smaller pores within a large pore could be produced. In this work, the average pore sizes are 94, 154, 150, 214, and 102 nm for N630, N635, N6/CS 30/1, N6/CS 30/1.5 and N6/CS 30/2, respectively. We expect that not only the overall viscosity of the solution is important in controlling the fiber and pore size, but the local viscosity of the solution blend is also significant. Blending two polymers in the same solution might generate the heterogeneity of viscosity at local composition attributable to the polymer chain interactions, thereby producing the fibers with bimodal distribution.

3.2 Average pore diameter measurement using Hagen-Poiseuille equation

The average pore size calculated by using Hagen-Poiseuille equation when the pressure drop of water flow was kept constant is shown in Figure 3, where all parameters involving the fiber size and pore size are displayed together for comparison. The pore sizes were 137, 159, 143, 184, and 85 nm for N6 30, N6 35, N6/CS 30/1, N6/CS 30/1.5 and N6/CS 30/2, respectively. The results were consistent with those from the image analysis of SEM micrographs, implying the applicability of Hagen-Poiseuille equation. The calculation was, however, based on the superficial velocity of the fluid through the medium, not the actual fluid velocity, both of which are related with the porosity. In addition, the tortuosity of the pores inside the filter medium might also play the important role. Thus, the equation could be modified to

$$\frac{d^2}{32} = \frac{u\mu z\tau}{\Delta P\varepsilon} \tag{4}$$

Where, ε is porosity and τ is tortuosity of the filter, which could affect the velocity of the liquid flow and the traveling distance of the flow. In woven cloth, the value of tortuosity lies between 1.0 and $1/\varepsilon$ (Johnston, 2003). The porosity of the structures may be approximated from the Blake-Kozeny equation, which was derived for describing the laminar flow in a packed column of spherical particles as

$$\frac{\Delta P}{Z} = \frac{150u\,\mu(1-\varepsilon)^2}{D_f^2\varepsilon^3} \tag{5}$$

Here, $D_{\rm f}$ is the average fiber diameter and are defined the same as in Eq. (1). Similar to the packed column, the pores inside the filter were generated from the deposition of all fibers so the equation should be applied with some acceptable errors resulted from the difference of hydraulic radii of pores generating by packed spheres and those by deposited fibers. If we assume Blake-Kozeny equation to be valid, the porosities would be 0.765, 0.735, 0.735, 0.675 and 0.565 for N6 30, N6 35, N6/CS 30/1, N6/CS 30/1.5 and N6/CS 30/2, respectively. If the tortuosity for each sample was assumed to be unity, the average pore sizes would be approximated to be 157, 185, 167, 224 and 113 nm for N6 30, N6 35, N6/CS 30/1, N6/CS 30/1.5 and N6/CS 30/2, respectively, which could predict better results for some samples. This is worth investigating more in detail in the future.

3.3 Iodine number measurement

The standard method of iodine adsorption on surface of carbon black particles was adopted here to measure the total surface area of the fibers. This could imply the pore size inside each filter. The iodine numbers were also shown in Figure 3.

The iodine numbers of nylon-6 filter samples were 628 and 542g/kg for N6 30 and N6 35, respectively, where the iodine number decreased with an increase of fiber size. For the case of polymer blend nanofibers, the iodine numbers were much lower than those of nylon-6 fibers. Since there were very few disconnected ultrafine nanofibers in

the case of N6/CS 30/1 and N6/CS 30/1.5, the pore size inside the filter was governed by the size of the large fibers, thereby decreasing the iodine number to 187 and 90 g/kg, respectively. It was interesting, however, that for N6/CS 30/2, the iodine number increased to 254 g/kg. This result showed that if the continuous structures of the ultrafine nanofibers could be obtained, the total surface area of the nanofibers could be increased. Nonetheless, the effect of the large fibers was still dominant in this case, probably because of not all small pores were visited by iodine molecules due to the effect of surface tension of the solution. This kind of structures could be beneficial for separation of some molecules or particles in liquid phase which could be attached to the surface of the fibers while letting the liquid flow through easily.

3.4 Filtration of polystyrene particles

Figures (4)-(6) show SEM micrographs of polystyrene particles, whose average sizes were of 410, 200 and 90 nm, respectively, which were collected by different filters. As can be seen in Figures 4(a)-4(d) and Figures 5(a)-5(d), when 410-nm- and 200-nm-polystyrene particles were captured, few of them stuck onto the commercial nylon fabrics of both No. 80/55 and No. 150/35, whereas there were many particles were seen on the filter paper. A large number of polystyrene particles on N6 30 nanofibers were evidently seen because the average pore size of the structure was only 94 nm, which was smaller than the average particle sizes. Figures 6(a)-6(d) show that 90-nm polystyrene particles covered thoroughly on the nanofibers while the particles covered partly on the filter paper and very few on the commercial nylon fibers. The filtration efficiency of each filter was reported in Table 1.

In Table 1, it was indicated that the nanofibrous structures could capture polystyrene particles of all sizes unlike the filter paper and the commercial nylon fabrics. For No.1 filter paper, it could remove polystyrene particles with a size of 410 nm better than that of 200 nm but less than that of 90 nm. The higher efficiency was observed when filtering much smaller particles, which was attributable to particle self-aggregation due to high surface energy of fine particles. In addition, although the pore size of commercial nylon fabric No. 80/55 was larger than that of No. 150/35 but it was observed that the filtration efficiency of the former was higher than the latter. This may be because the commercial nylon fiber with No. 80/55 has also larger fiber size than that of No. 150/35 and the polystyrene particles may attach onto the fiber surface and then formed the filter layer or filter cake, thereby, increasing the efficiency.

Every sample of nanofiber filters, whose thickness were about 0.1 mm, showed 100% filtration efficiency for every particle size. Among the group of nanofibrous filters, it could be seen from the SEM figures that when filtering 90 nm-PS particles, the outlines of the fibrous structures were still observed for every filter medium except N6/CS 30/2, where all particles covered the filter surface. This was probably because particles could not move through the top layers because ultrafine fiber web could capture them all and generate the filter cake so that the fibrous outline could not be seen at all.

Separation of BSA from the aqueous solution was performed using nanofibrous filter media. The prepared concentration of BSA was as low as 10 ppm. It was found that N6 30 sample could remove proteins up to 37% and N6 35 could remove up to 41%. The increase in filtration efficiency was probably due to an increase in retention time when flowing inside the larger pores of N6 35, facilitating the attraction between nanofibers and proteins, even though there was less fiber surface area. The process involved adsorption of protein molecules on the surface of the nanofibers with attractive interaction between amino groups of proteins and amide groups of nylon-6 which could be enhanced if protein molecules have more time to travel to the fiber surface. Interestingly, for the sample of nylon-6/chitosan blends, the efficiencies of protein removals were higher than those of nylon-6 and the efficiency seemed not to depend on the chitosan content up to 2% of the amount of nylon. In the presence of chitosan, there would be more functional groups that could effectively attract protein molecules. It was reported that when BSA was dissolved in water, its molecule possessed negative charges (Wang et al., 2008), which favored the attraction with protonated chitosan molecules (protonated amino groups). It was possible that chitosan content was so small that chitosan molecules could not distribute uniformly on the fiber surface, thereby the effect of chitosan content was not seen clearly. This point deserves further investigation.

IV. Conclusions

In this work, nylon-6 and nylon-6/chitosan nanofibrous structures were used as filters for removals of polystyrene particles of different size and compared with commercial nylon fabrics and filter paper. It was found that kinematic viscosity of nylon-6 solutions and nylon-6/chitosan solutions increased with increasing polymer content, which in turn increased the size of the fibers as confirmed with SEM micrographs. The blend polymer solution generated untrafine fibers resulting in smaller average fiber diameters. The trends of the average fiber diameters of nanofibrous structures and their average pore size were found the same. In addition, the equation of Hagen-Poiseuille gave pore sizes consistent with SEM figures and the method of iodine adsorption could be used to investigate the available surface area for adsorption inside the nanofibrous structures.

In Filtration, the nanofiber filters could capture polystyrene particles much better than filter paper and the commercial nylon fabrics, No. 80/55 and No. 150/35. The nanofiber filters gave 100% of filtration efficiency while filter paper and commercial nylon fiber gave 8.27%-59.14% and 2.7%-14.50% of filtration efficiency, respectively. Interestingly, self-aggregation of fine particles played an important role on the filtration efficiency. Moreover, the adsorption of BSA proteins in a solution of 10 ppm could occur inside the nylon-6 nanostructures up to 41% and inside nylon6/chitosan nanostructures up to 53%. In conclusion, nanofibrous structures could successfully remove particles in a size range of 400 nm down to 90 nm from the suspension and could partly adsorb protein molecules as well, showing a potential use of these nanofibrous structures in separation of bioparticles and biomolecules.

Acknowledgements

This research was jointly funded by the Thailand Research Fund (TRF) and Thammasat University (Grant#DBG5380007). All assistances from the Faculty of Engineering are highly appreciated.

References

Aussawasathien, D., Teerawattananon, C., Vongachariya, A., 2008. Separation of micron to sub-micron particles from water: Electrospun nylon-6 nanofibrous membranes as prefilters. Journal of Membrane Science 315, 11-19.

Burkatovskaya, M., Tegos, G.P., Swietlik, E., Demidova. T.N., Castano, A.P., Hamblin, M.R., 2006. Use of chitosan bandage to prevent fatal infections developing from highly contaminated wounds in mice. Biomaterials 27, 4157-4164.

Chuachamsai, A., Lertviriyasawat, S., Danwanichakul, P., 2008. Spinnability and Defect Formation of Chitosan/Poly Vinyl Alcohol Electrospun Nanofibers. Thammasat International Journal of Science and Technology 13, 24-29.

Desai, K., Kit, K., Li, J., Michael Davidson, P., Zivanovic, S., Meyer, H., 2009. Nanofibrous chitosan non-wovens for filtration applications. Polymer 50, 3661-3669.

Geng, X., Kwon, O.-H., Jang, J., 2005. Electrospinning of chitosan dissolved in acetic acid. Biomaterials 26, 5427-5432.

Gopal, R., Kaur, S., Ma, Z., Chan, C., 2006 Ramakrishna, S., Matsuura, T. Electrospun nanofibrous filtration membrane. Journal of Membrane Science 281,581-586. Huang, Y., Onyeri, S., Siewe, M., Moshfeghian, A., Madihally, S.V., 2005. In vitro characterization of chitosan-gelatin scaffolds for tissue engineering. Biomaterials 26, 7616-7627.

Huang, Z.M., Zhang, Y.Z., Kotaki, M., Ramakrishna, S., 2003. A review on polymer nanofibers by electrospinning and their applications in nanocomposites. Composites Science and Technology 63, 2223-2253.

Hung, C.-H., Leung, W.W.-F., 2011. Filtration of nano-aerosol using nanofiber filter under low Peclet number and transitional flow regime. Separation and Purification Technology 79, 34-42.

Jiang, T., Abdel-Fattah, W.I., Laurencin, C.T. 2006. In vitro evaluation of chitosan/poly(lactic acid-glycolic acid) sintered microsphere scaffolds for bone tissue engineering. Biomaterials 27, 4894-4903.

Johnston, P.R., 2003. Fluid sterilization by filtration, third ed. Interpharm/CRC, Boca Raton.

Li, D., Xia, Y.N., 2004. Electrospinning of nanofibers: reinventing the wheel? Advanced Materials 16, 1151-1170.

Nirmala, R., Navamathavan, R., Kang, H.-S., El-Newehy, M.H., Kim, H.Y., 2010. Preparation of polyamide-6/chitosan composite nanofibers by a single solvent system via electrospinning for biomedical applications. Colloid and Surfaces B 83,173-178.

Wang, Y., Wang, X., Luo, G., Dai, Y., 2008. Adsorption of bovin serum albumin (BSA) onto the magnetic chitosan nanoparticles prepared by a microemulsion system. Bioresource Technology 99, 3881–3884.

Yoon, K., Hsiao, B.S., Chu, B., 2009. High flux ultrafiltration nanofibrous membranes based on polyacrylonitrile electrospun scaffolds and crosslinked polyvinyl alcohol coating. Journal of Membrane Science 338, 145-152.

Zhang, H., Li, S., Branford White, C.J., Ning, X., Nie, H., Zhu, L., 2009. Studies on electrospun nylon-6/chitosan complex nanofiber interactions. Electrochimica Acta 54, 5739-5745.

FIGURES

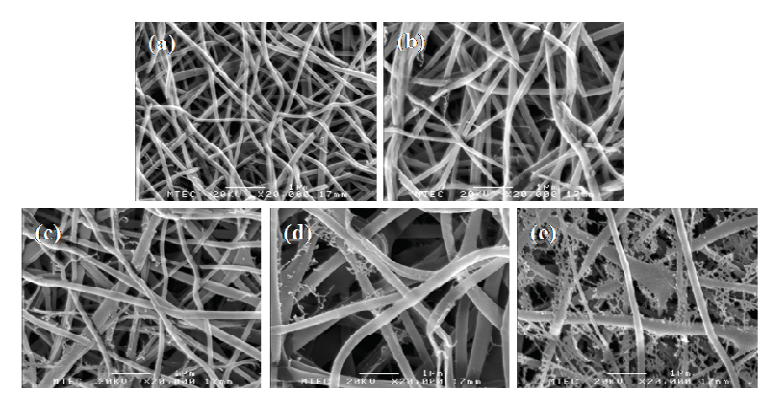


Figure 1: SEM micrographs of electrospun products from different polymer concentrations: (a) N6 30 (b) N6 35 (c) N6/CS 30/1 (d) N6/CS 30/1.5 and (e) N6/CS 30/2

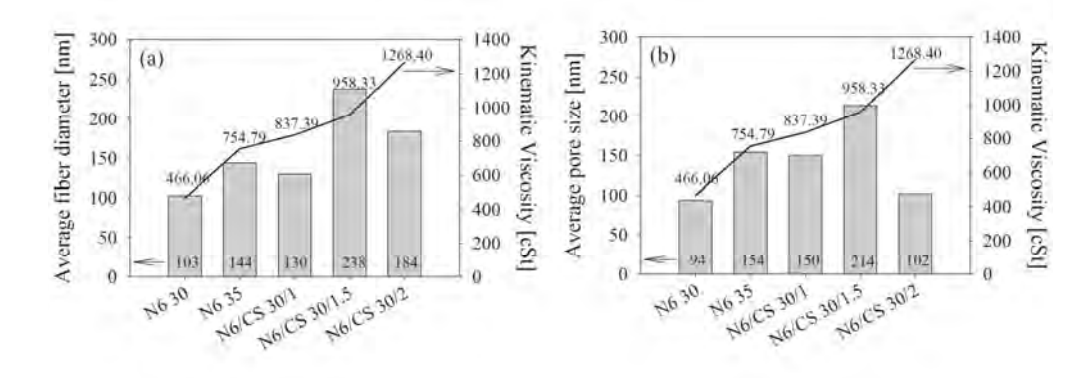


Figure 2: (a) the average nanofiber diameter and (b) the average apparent pore size of nanofibrous structures together with the kinematic viscosity of nylon-6 and nylon-6/chitosan solutions at various concentrations.

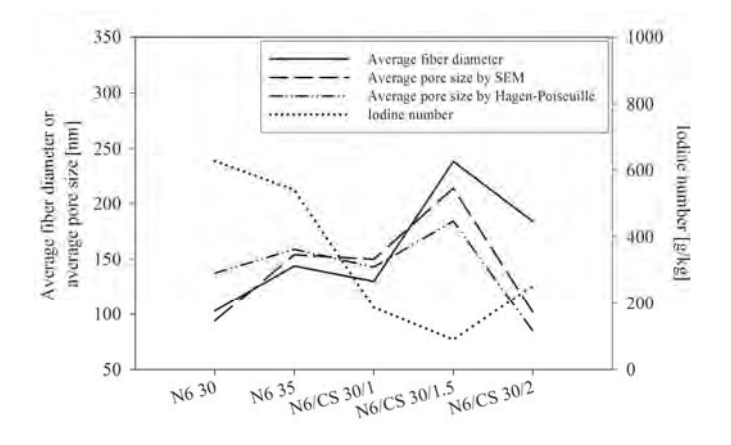


Figure 3: Comparison between the average nanofiber sizes and pore sizes determined from image analysis and Hagen-Poiseuille equation, together with the iodine number.

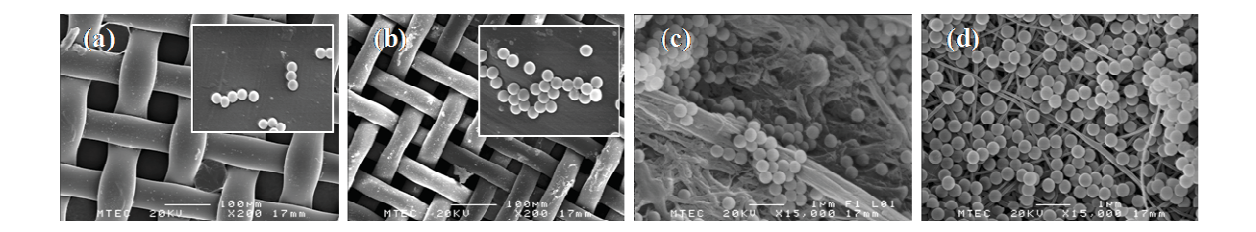


Figure 4: SEM micrographs of 410-nm polystyrene particles collected by different filters: (a) commercial nylon fabric, No. 80/55 with 200x magnification (b) commercial nylon fabric, No. 150/35 with 200x magnification (c) filter paper with 15,000x magnification and (d) nanofibers from N6 30, with 15,000x magnification.

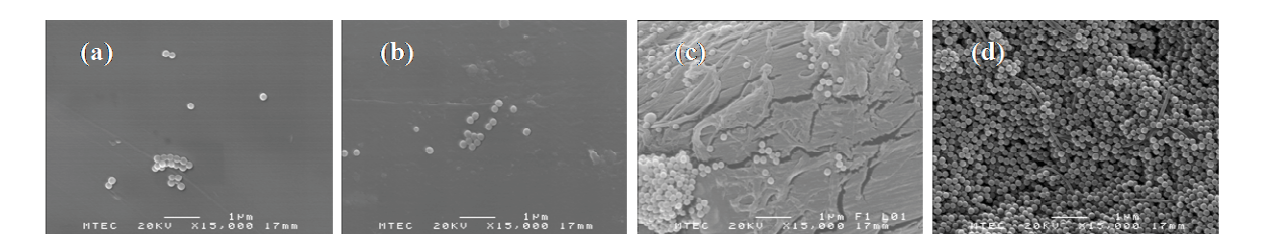


Figure 5: SEM micrographs of 200-nm polystyrene particles collected by different filters at 15,000x magnification: (a) commercial nylon fabric, No. 80/55 (b) commercial nylon fabric, No. 150/35 (c) filter paper and (d) nanofibers from N6 30

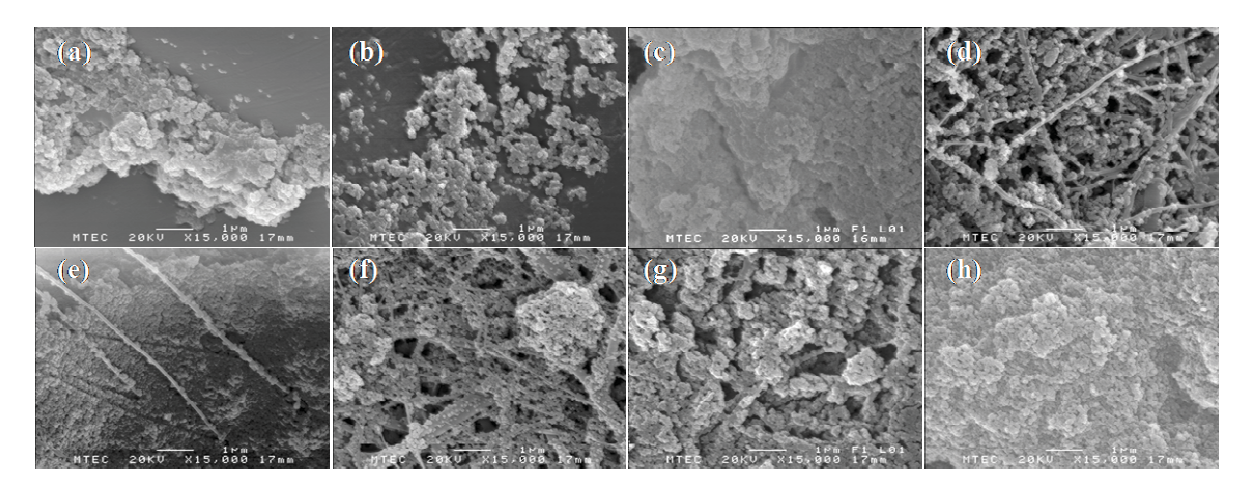


Figure 6: SEM micrographs of 90-nm polystyrene particles collected by different filters at 15,000x magnification: (a) commercial nylon fabric, No. 80/55 (b) commercial nylon fabric, No. 150/35 (c) filter paper (d) nanofibers from N6 30 (e) nanofibers from N6 35 (f) nanofibers from N6/CS 30/1 (g) nanofibers from N6/CS 30/1.5 and (h) nanofibers from N6/CS 30/2

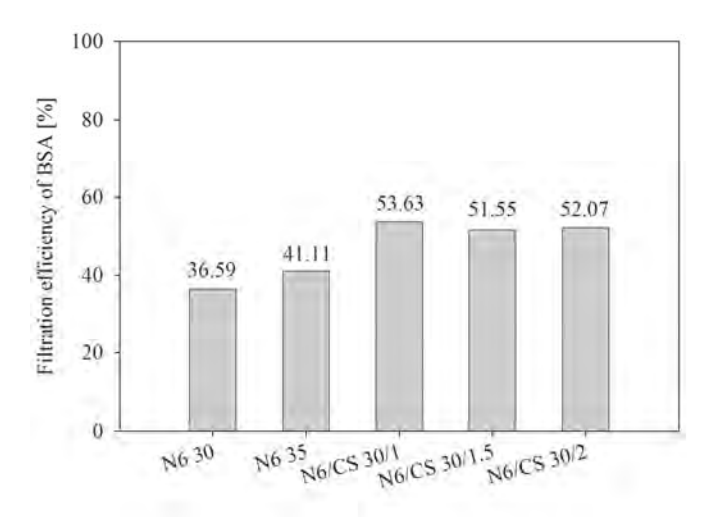


Figure 7: Filtration efficiency of BSA from 10 ppm solution using various nanofibrous filters.

Table 1: Filtration efficiency of different filters when applied to capture polystyrene particles with various sizes

	Filtration efficiency	(%)	
Filter type	PS particle size		
	410 nm	200 nm	90 nm
NC 80/55	7.79	4.93	14.50
NC150/35	4.96	2.93	2.71
Filter Paper	35.89	8.27	59.14
N6 30	100.00	100.00	100.00
N6 35	100.00	100.00	100.00
N6/CS 30/1	100.00	100.00	100.00
N6/CS 30/1.5	100.00	100.00	100.00
N6/CS 30/2	100.00	100.00	100.00

The Reduction of Electrical Resistivity of Poly(vinyl alcohol) Nanofibers by Filling with Acid-Treated-Carbon Fillers

Panu Danwanichakul, Sillawan Aschakulporn, and Totsapon Pattarapongdilok

Abstract

A family of poly(vilnyl alcohol) (PVA) nanofibers filled with carbon black particles and carbon nanotubes were investigated for their electrical properties. Carbon fillers were found to decrease the resistivity of the fiber mats linearly when detecting IPA vapor whose concentration increased from 1 to 8 ppm, confirming the possibility to be used as a gas sensor. Surface treatment with nitric acid could decrease the filler aggregate size and disperse the fillers more uniformly in the fibers, thereby, reducing the resistivity. The self-dispersible carbon black (SDCB) particles could decrease the resistivity of the PVA nanofibers better than untreated carbon nanotubes (CNT). Both SDCB and SDCNT samples could maintain the resistivity when the temperature increased, while the resistivity of CB and CNT samples decreased with temperature. In addition, the resistivity decreased along the dynamic increase in moisture content at 45°C. However, the presence of IPA could still be detected together with moisture.

Keywords: Carbon Black, Carbon Nanotube, Nanofiber, Poly(vinyl alcohol).

I. Introduction

The electrospinning technique has been investigated extensively in order to understand all parameters governing the morphology of the obtained nanofibers [1]. Due to its large surface area to volume ratio, the nanofibrous structure could be used in many applications related to surface activity of the fibers. For example, in catalysis lots of pores in nanofibrous structures yield higher rate of adsorption of reactants and higher reactivity due to a large number of active sites. In biomedical engineering, the nanostructures have been applied for drug release and promoting cell growth, each of which process needs large surface area to increase its rate and process continuity. Besides, gas sensing applications have also been studied since the initial steps of sensing, which are diffusion and adsorption of gas molecules into the material of fibers, required a large interfacial area between solid and liquid or gas phase. Such application is the focus of this research.

Polymers usually applied in electrospinning process should be easily fabricated from their solutions or melts. Poly(vinyl alcohol) (PVA) is one of the most used in film forming or fiber fabrication. Therefore, it has been used in all applications mentioned so far as a polymer matrix of nanofibers. The composite of PVA and other materials, which are also polymers or particulate fillers to enhance specific properties of the fibers, has been widely experimented. The mechanical properties of PVA nanofibers were enhanced

by adding carbon black particles in the fibers [2]. As expected, carbon black, which has been used as reinforcing filler in rubber tyre industries for a long time, could increase tensile strength of the nanofibers as the filler loading increased from 1 to 10% wt of PVA content. Multi-walled carbon nanotubes (MWCNT) were also reported to improve tensile strength of PVA fibers [3] since it could nucleate crystallization of PVA in the composite nanofibers. The composite nanofibers mats were later crosslinked with glutaraldehyde to improve its mechanical strength as a post-treatment.

Those carbon-filled PVA nanofibers were of interest for their mechanical properties. However, carbon nanotubes (CNT) were also well known for their electrical conductivity. Recently, the composite of PVA and CNT was prepared and studied as conductive nanofibers [4]. In that work, CNTs were dispersed homogeneously in N-methyl-2-pyrrolidone and mixed with PVA solution. It was found that the conductivity could increase upon increasing the CNT loading. Since gas sensing application is closely related to the electrical conductivity of the materials, the improvement of conductivity of PVA nanofibers by incorporating carbon nanotubes have attracted many research groups, one of which blended PVA, polyaniline and CNT together and electrospun the fibers in order to make a CO sensor and their product could detect CO in the range of 100-500 ppm [5].

The success of conductivity or mechanical properties improvement of PVA nanofibers not only lies in filling the fibers with conductive carbon particles but it also depends on how well the fillers are dispersed inside nanofibers. Ultrasound was applied to suspensions four times before electrospinning the PVA solution blended with carbon black particles [3]. Bang et al. [6] have currently treated the MWCNT with acids by varying the pH of the solution and they found that a lower pH gave smaller fiber diameter, thereby, increasing mechanical properties. Li and Sun [7] have applied the method of acid treatment before to carbon black particles in order to disperse them more homogeneously in suspension as a black dye in coloration of cotton fibers.

In this work, the nitric acid treatment [7] was adopted in order to produce self-dispersible carbon black (SDCB) particles to be filled in PVA nanofibers, which have not been reported before by other groups. The electrical properties were compared with those of carbon-black-filled-, carbon-nanotube-filled- and self-dispersible-carbon-nanotube-filled PVA nanofibers. The model gas to be detected in the study is isopropyl alcohol (IPA), which is usually used as a degreaser in electronic device productions. To test the sensitivity of nanofibrous structures, the concentration of IPA was varied lower than 8 ppm.

II. Material and Methodology

Material

Polyvinyl alcohol (PVA) used in this research was purchased from Sigma Aldrich. It is a cold water soluble type with molecular weight (Mw) of 40,000-70,000 and degree of hydrolysis of 98%. Carbon black (N-330, particle size about 33 nm) was supplied by Loxley Public Co., Ltd. Multi-walled carbon nanotube with carbon content

more than 95%, (O.D. x L equals 6-9 nm x 1 μm) was purchased from Sigma-Aldrich Co. LLC. Nitric acid and isopropyl alcohol (IPA) were supplied from Merck Ltd., Thailand.

Self-dispersible carbon black and self-dispersible carbon nanotube preparation

2 g carbon black or carbon nanotube was mixed with 150 ml. of 65% w/w nitric acid and then it was refluxed at 120°C for 2 hr. After that the mixture was heated at 130°C. To remove nitric oxide left on particle surfaces, particles were washed in water and then were precipitated by using centrifugal speed of 3000 for 15 min. The filtered precipitate was then added into distilled water and was centrifuged at the same condition again. The self-dispersible carbon black (SDCB) particles and self-dispersible carbon nanotubes (SDCNT) were received after drying the precipitate at 80°C for 24 hr. The size distributions before and after surface treatment of carbon black particles were analyzed by a centrifugal particle size analyzer (Shimadsu, model SA-CP3).

Spinning solution preparation

To obtain pure PVA solution, PVA powder was dissolved in distilled water to get PVA concentration of 25, 30 and 35%w/v. The spinning solution was prepared by firstly mixing 1 g of PVA with 10 ml of distilled water. After that the fillers which are CB, SDCB, CNT and SDCNT were added into PVA solution to obtain the ratio of PVA to filler of 100:4, 100:6 and 100:8.

Electrospinning of nanofibers

The spinning solution was poured into a 2 ml syringe with 0.8 mm-ID and 3.5 cm needle. The high voltage power supply (PS/MJ30PO400 Glassman) was connected to the end of the needle by a stainless steel electrode. Another electrode was connected to the stationary collector covered with 2 x 2 cm 2 copper plate. The electrospinning voltage was set at 18 kV and the distance between the needle tip and the collector was held constant at 7 cm. The spinning time was about 25 min.

Morphology of nanofibers

The morphology of nanofibers was observed with scanning electron microscope (SEM) (JEOL JSM-6310F) after gold coating by a gold sputtering coater for 100 seconds. The average fiber diameter was obtained with an image analyzer.

Resistivity of nanofibers

The nanofiber of unknown resistance was connected in series with the known resistance. The voltage of the known resistance and that of nanofiber were measured by using a multimeter as shown in Figure 1 for the experimental setup. The resistivity of nanofiber was calculated from (1). When R_{known} and R_{fiber} are resistivity of known and nanofiber, respectively while V_{supply} and V_{known} are the supply voltage and voltage measured from known resistance, respectively.

$$R_{fiber} = \frac{\left(V_{supply} - V_{known}\right)}{V_{known}} x R_{known} \tag{1}$$

The effect of IPA concentration on resistivity of fibers

The experiment was done at the condition of fixing the relative humidity at 40% and the temperature at 32°C. The concentration of IPA in the air was varied by adding liquid IPA drop by drop into the whole volume where the fibers were placed and the resistivity of the fibers was measured.

The effect of temperature on resistivity of fibers

The air in the closed vessel contained 67 ppm IPA. The relative humidity was fixed at 40% and the temperature was at 32°C. The whole system was heated to 40°C. The resistivity of the fibers was measured at various temperatures stepping up with an increment of 1°C.

The effect of relative humidity on resistivity of fibers

The experiment was done with 67 ppm IPA vapor in the air. The liquid water was placed inside this close system while maintain the constant temperature of 45°C so the relative humidity was changed from 45% to 80% upon continuing evaporation, during which time the resistivity of the fibers was measured. The results were also compared with those in the presence of only water vapor in the air.

III. Results and Discussion

Size distribution of carbon black particles

The size distributions of carbon black particles before and after surface treatment with nitric acid were shown in Figure 2. It was clearly seen that carbon black particles in suspension usually aggregated as a large particle, whose size was as large as 50 microns, whereas the self-dispersible carbon black particles were much smaller, whose size mostly fell in the range of 100 nm to 250 nm. This is due to the repulsive forces among the carboxylic groups generated upon oxidation with nitric acid on the treated particle surface that preclude the aggregation of particles [7].

Morphology of nanofibers

When mixing surface-treated and untreated carbon black particles into PVA solution and spinning electrically to obtain nanofibrous mats as shown in Figure 3, the structures looked similar to one another. The fibers filled with treated carbon nanotubes and untreated looked similar to other fibers as well. Nonetheless, the average size of the fibers of each sample was a little different. It seemed that adding self-dispersible fibers yielded slightly larger nanofibers. This may be attributable to more amount of fillers could be dispersed in the fibers since the particle dispersion was better, leading to a little higher viscosity, which in turn resulting in larger diameters. However, on the whole, they could be considered physically similar to one another. Therefore, incorporating each species of carbon filler of the same loading in the fibers did not affect the shape and size of fibers similar to what observed in [2].

Resistivity of nanofibers

The resistivity of nanofibers was shown in Figure 4. The concentration of IPA was varied in a very low range up to 8 ppm in order to observe the sensitivity of the nanofibers. It is clearly seen that for all types of fibers a decreasing trend of resistivity was seen when the IPA concentration increased because IPA is a polar substance that could conduct electricity. Therefore, these nanofibers could be applied as gas sensors for detecting polar molecules such as alcohols and quantifying their concentrations in ambient air.

When comparing all types of fibers, pure PVA nanofibers possessed highest Embodying the fibers with carbon fillers could linearly increase the conductivity as shown. Since all samples looked similar, the surface area per unit volume of them should also be similar. Thus, the decrease in resistivity should be resulted from the conductive filler loading. It was experimented earlier by our groups that upon increasing the filler loading up to 8% wt/vol in suspension, the resistivity was decreased. Therefore, in this work, we fixed the loading at 8% wt/vol in prepared suspension. Adding more filler beyond that resulted in particle aggregation which caused poor conductivity in the solid fiber mats. Surface treatment of particles is, thus, essential. As shown in the figure, the influence of self-dispersible carbon black particles was very interesting since it could decrease resistivity of the fibers to be lower than fibers filled with carbon nanotubes which are widely known as an excellent conductor. This finding implied that aggregation of carbon nanotubes occurred during the mixing process in PVA solution. As expected, the sample filled with self-dispersible carbon nanotubes was the best conductors among all. The surface treatment of particles could benefit an increase in conductivity of nanofibers since particles could be dispersed more uniformly in each fiber, yielding better percolation throughout the structures, which is the mechanism governing electrical conductivity of the membrane.

The effect of temperature on nanofiber resistivity

It is also intriguing to investigate the effect of temperature on the resistivity of nanofibers while absorbing IPA vapor which was fixed at 67 ppm. This effect is important when a sensor is applied at a temperature higher than room temperature. The results are shown in Figure 5. At first, the resistivity of PVA increased with temperature and then dropped. It is possible that when heated, PVA fibers initially relaxed and the whole nanostructures might slightly expand resulting in disconnected path of electrical conduction. However, when the temperature increased, both the diffusion rate of IPA molecules from the air to the nanofiber surface and the diffusion rate inside the solid fibers could increase, which are favorable for an increase in electrical conduction. Therefore, these two factors were competitive and the maximum of resistivity of PVA nanofibers was observed.

For other carbon-filled nanofibers, the results could be classified into two groups. The first group represents the trend of decreasing of resistivity and the second group represents the trend of almost constant resistivity. As shown Figure 5, PVA nanofibers with untreated fillers belong to the first group while PVA nanofibers with self-

dispersible fillers belong to the second group. These phenomena could also be explained with the same reason provided for pure PVA nanofibers. The carbon-filled nanofibers possessed much higher mechanical strength than pure PVA fibers [2] because PVA chains were more or less fixed in place with attractive interactions from carbon particles, which act as reinforcing filler in polymer matrix. The structures would be stronger if the filler particles were smaller and dispersed more uniformly inside each fiber, which is the case for self-dispersible carbon black particles and self-dispersible nanotubes. It is possible that the PVA/SDCB and PVA/SDCNT structures were strong enough to withstand thermal expansion so the diffusion of more IPA to the structures did not occur at higher temperatures. Unlike those two, the resistivity of PVA/CB and PVA/CNT decreased with temperature, which was likely due to a slight effect of thermal expansion of PVA matrix, which facilitated the diffusion of more IPA molecules inside the fibers. Interestingly, the change of resistivity of PVA/CB and PVA/CNT upon changing the temperatures implies that these two nanofibers could be applied as a temperature sensor while the PVA/SDCB and PVA/SDCNT could be used as a gas sensor at any temperature.

It should be noted that at lowest temperature of 33°C, the resistivity of nanofibers of the PVA was the highest, followed by PVA/CB, PVA/CNT which was close to PVA/SDCB and then PVA/SDCNT, whereas at highest temperature of 40°C, the order was rearranged to PVA, PVA/SDCB, PVA/SDCNT, PVA/CNT and PVA/CB. The trend at a high temperature was confirmed again in a separate experiment where the temperature was set at 45°C, as shown in Figure 6, which showed the comparison of resistivity of fibers when exposed to water vapor alone and when exposed to water vapor together with IPA vapor.

The effect of water vapor on fiber resistivity

Because there is always water vapor in the air, the effect of humidity on the detection of IPA vapor should also be studied. It is obvious that the PVA fibers were sensitive to water vapor in the air as they were sensitive to the IPA vapor. These fibers could be potentially applied as humidity sensors as well. As the relative humidity increased from 45% to 80% while the IPA concentration was fixed at 67 ppm in the air, the resistivity of the fibers absorbing both gasses decreased and it was closer to the resistivity of fibers absorbing water vapor alone. However, the separation between these two could be seen at a low humidity of 40% which is the ambient humidity when the experiment was done. When the differentiation between the resistivity of both systems was mainly considered, the sample PVA/SDCB shows the largest separation of the two numbers, followed by PVA/SDCNT.

III. Conclusion

This research showed the possibility of applying electrospun poly (vinyl alcohol) filled with self-dispersible carbon black (SDCB) and self-dispersible carbon nanotube (SDCNT) compared with the nanofibers filled with as-received fillers to be used as a gas sensor. The morphology of nanofibers, their electrical properties before and after the detection of isopropyl alcohol (IPA) vapor in the air, as well as the effect of moisture

content in the air were investigated in this work. The results showed that adding those fillers in the nanofibers decreased the resistivity of the structures at room temperature especially with SDCB and SDCNT particles, which were dispersed better in the structures because of charges from the surface treatment. The surface treatment was proved to be the essential step during incorporation of nanosized fillers in the polymer matrix. This actually benefit in the reduction of filler usage as well as the increase in performance of the nanofibers as was seen for the case of SDCB particles which could enhance the fiber conductivity comparable to CNTs.

When nanofibers were tested for both humidity and the presence of IPA vapor in the air, the resistivity was found decreasing along the dynamic increase in moisture content at 45°C. However, the presence of IPA could still be detected together with the effect of moisture. The SDCB-filled and SDCNT-filled PVA nanofibers could differentiate the presence of IPA and water more clearly than others. In addition, a dynamic increase in temperature was found to decrease the resistivity of nanofibrous structures embodied with CB and CNT while the ones with SDCB and SDCNT showed small degree of fluctuation around a constant resistivity, implying that the latter two were more appropriate for gas sensor application. More importantly, the nanostructures could detect the low concentration limit of IPA concentration ranging from 1-8 ppm. The linear relationship between the IPA concentration and the resistivity of the sensors were clearly observed.

All the results evidently indicated that these nanocomposites, especially SDCB composites should gain more attention in the field of sensors, provided that the degree of dispersion of carbon black particles is maximally enhanced.

Acknowledgment

This research was jointly funded by the Thailand Research Fund (TRF) (Grant number: DBG5380007) and Thammasat University. All assistances from the Faculty of Engineering are highly appreciated.

References

- [1] P. Danwanichakul, D. Dechojarassri, R. Werathirachot, "An Approximate Model Describing Electrospinning of Nanofibers: Process Parameter Investigation," International Journal of Electrospun Nanofibers and Applications, 2008, 2(2), pp. 103-114.
- [2] S. Chuangchote, A. Sirivat, P. Supaphol, "Mechanical and electro-rheological properties of electrospun poly(vinyl alcohol) nanofibre mats filled with carbon black nanoparticles," Nanotechnology, 2007, 18 (14), art. no. 145705.
- [3] M. Naebe, T. Lin, W. Tian, L. Dai, X. Wang, "Effects of MWNT nanofillers on structures and properties of PVA electrospun nanofibres," Nanotechnology, 2007, 18 (22), art. no. 225605

- [4] O. Koysuren, "Preparation and characterization of polyvinyl alcohol/carbon nanotube (PVA/CNT) conductive nanofibers," Journal of Polymer Engineering, 2012, 32 (6-7), pp. 407-413
- [5] Y. Wanna, S. Pratontep, A. Wisitsoraat, A. Tuantranont, "Development of nanofibers composite Polyaniline/CNT fabricated by Electro spinning Technique for CO Gas Sensor," Proceedings of IEEE Sensors, 2006, art. no. 4178628, pp. 342-345
- [6] H. Bang, M. Gopiraman, B.-S. Kim, S.-H. Kim, I.-S. Kim, "Effects of pH on electrospun PVA/acid-treated MWNT composite nanofibers," Colloids and Surfaces A: Physicochemical and Engineering Aspects, 2012, 409, pp. 112-117
- [7] D. Li, G. Sun, "Coloration of textiles with self-dispersible carbon black nanoparticles," Dyes and Pigments 2007, 72, pp. 144-149

FIGURES

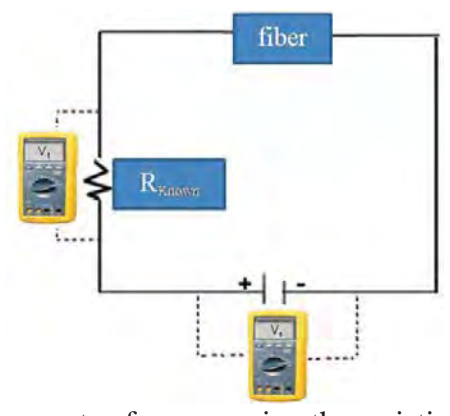


Fig. 1 The setup apparatus for measuring the resistivity of nanofibers.

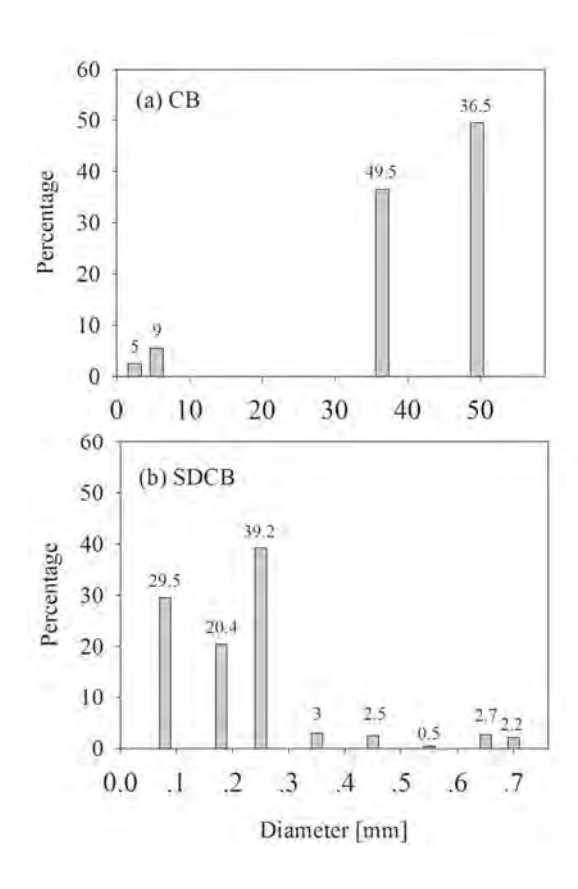


Fig. 2 Size distributions from centrifugal size analyzer of (a) carbon black particles (CB) and (b) self-dispersible carbon black particles (SDCB)

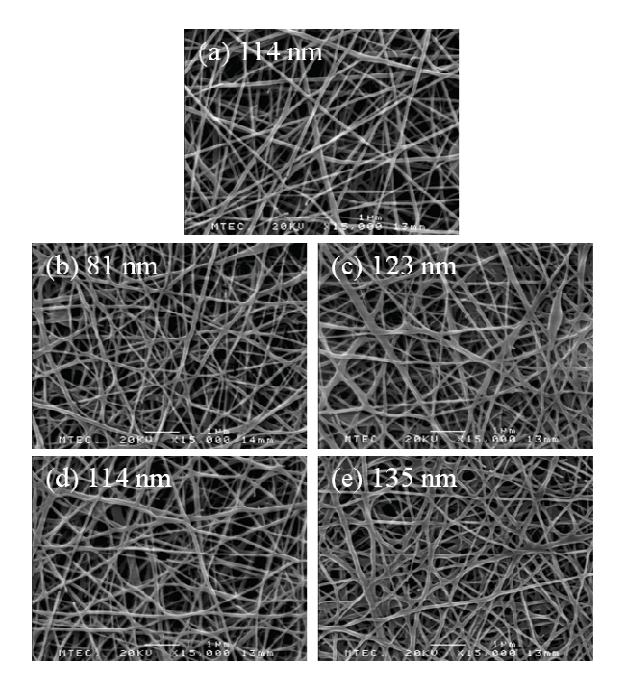


Fig. 3 SEM micrographs of (a) PVA nanofibers (b) PVA nanofibers filled with carbon black (PVA/CB) (c) PVA nanofibers filled with self-dispersible carbon black (PVA/SDCB) (d) PVA nanofibers filled with carbon nanotubes (PVA/CNT) (e) PVA

nanofibers filled with self-dispersible carbon nanotubes (PVA/SDCNT)

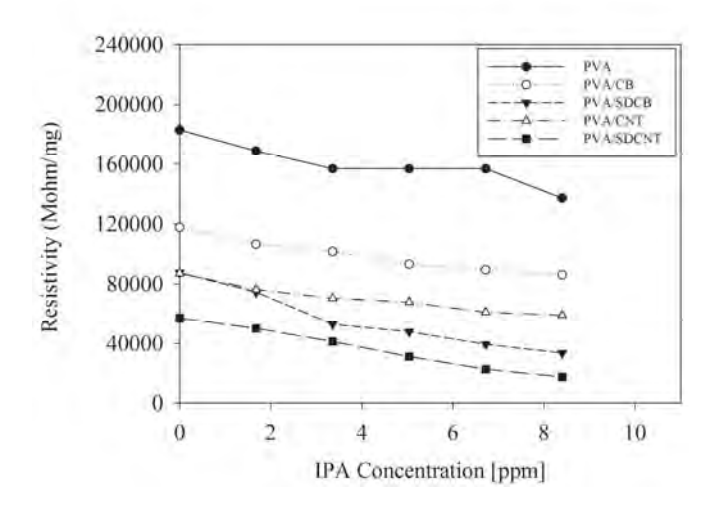


Fig. 4 The resistivity of various nanofibers at 32°C and 40%RH was shown decreasing with an increase in IPA concentration.

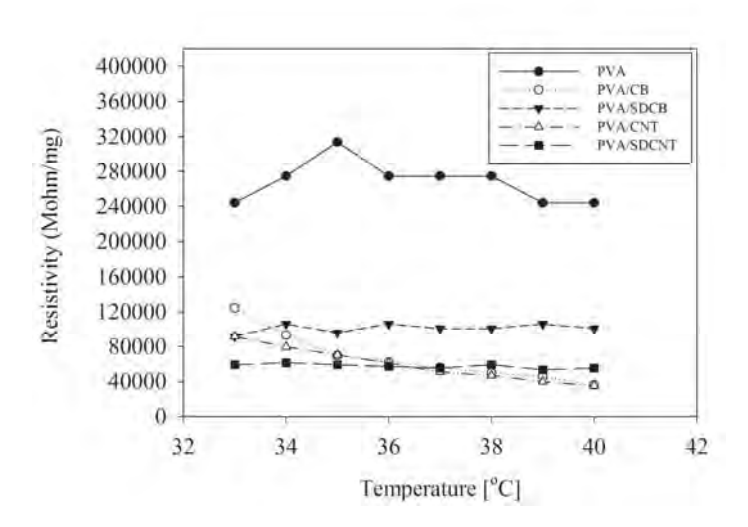


Fig. 5 The effect of temperature on resistivity of various nanofibers absorbing 67 ppm isopropyl alcohol (IPA) at 32°C and 40%RH. (a) PVA (b) PVA/CB (c) PVA/SDCB (d) PVA/CNT (e) PVA/SDCNT

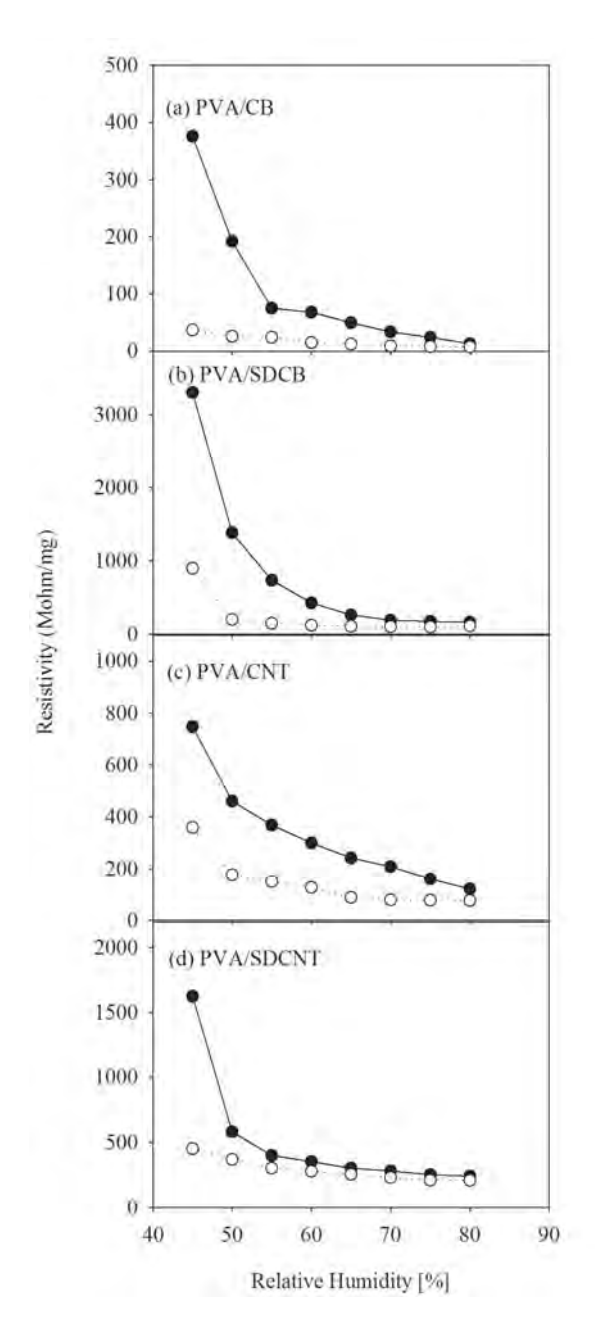


Fig. 6 The effect of relative humidity on resistivity of various fibers. The black dot refers to water vapor alone and the white dot refers to water and IPA vapors. (a) PVA (b) PVA/CB (c) PVA/SDCB (d) PVA/CNT (e) PVA/SDCNT

Two-Dimensional Simulation of Electrospun Nanofibrous Structures: Connection of Experimental and Simulated Results

Panu Danwanichakul*, Duangkamol Danwanichakul

Department of Chemical Engineering, Faculty of Engineering,
Thammasat University,
99 Moo 18, Paholyothin Rd, Khlong Nung,
Khlong Luang, Pathumthani 12120, THAILAND

Tel & Fax: (662) 5643001-9 ext. 3123 Email: dpanu@engr.tu.ac.th

ABSTRACT

This research aims to simulate the structures of nanofibers on a surface of a collector by electrospinning technique. Since the nanofibrous structures contain many tiny pores with size ranging from nanoscale to microscale, it is of interest to utilize such structures for processes involving surface activity. In this work, nylon-6 with concentrations of 30 and 35 wt% were electrospun to obtain the nanofibrous mats and they were tested for filtration of polystyrene particles in suspension. Some experimental results were compared with the simulated ones. In the simulation methods, the 2-dimensional connected structures of nanofibers were constructed by assuming a nanofiber as an ellipse with an aspect ratio of 100 deposited randomly one by one. In addition, the size of nanofiber is assumed polydisperse. It was found that the configurations generated via simulations resembled the real structures of nanofibers with polydisperse diameters. Fibers from higher solution concentration were larger, resulting in larger pore size, which was also confirmed with simulations. Varying the size distribution around the same average value did not make any difference to the coverage of fibers deposited on the surface but it affected 2D pore areas for the systems at low fiber density. In addition, the probability for a particle passing through the porous structure was less when the fiber number density was higher and the particle diameter was larger, which is consistent with the filtration test. Lastly, water flux measurement could be used to estimate the void volume fraction of the structures as well as the volume-averaged pore diameter, which was found greater than the 2D pore diameter measured from SEM micrographs by the quantity related to the fiber size.

Keyword: nanofiber, porous membrane, polydispersity, simulation, filtration

1. Introduction

Electrospinning technique is an easy method to produce nanofibers whose size are in submicron or nanometer range by applying the electrical force generated by the electric fields between the end of the metal needle and the ground collector. The liquid source may be a polymer melt or a polymer solution. Once the electrical force is greater than the surface tension of the hanging hemisphere liquid drop at the end of the needle, the liquid is pulled out of the needle and swirled onto the ground surface. Continuous fibers are produced in this manner while the solvent evaporates and the final nonwoven nanofibrous structure is solidified. A large number of literatures discussing the production of nanofibers from various polymer systems and their applications have been investigated [1-5]. The research on nanofibers is still receiving more and more attention since the benefit of large surface area to volume ratio of nanostructures has been proven to improve the performance in many aspects including higher mechanical strength, an increase in surface activity, and an increase in adsorption capacity. Therefore, nanofibers were widely studied for their uses as sensors [1], catalysts [2], drug delivery systems [3], tissue scaffolds [4] as well as filters [5]. The study on surface characterization and pore generation of nanofibrous membrane is, thus, of great interest.

There are many factors influencing the size of fibers produced via electrospinning. Those are voltage of power supply, distance between the needle tip and the ground, solution flow rate, viscosity, conductivity and surface tension of polymer solutions. Some of these process parameters were modeled by Danwanichakul et al. by using poly(vinyl alcohol) as a model polymer [6]. However, not only the fibers but also the pores generated by the overlap of fibers themselves are of importance. Park and Park found that pore size distribution in nanofibrous structures was narrow or sometimes considered as monodisperse pores [7]. The study was done experimentally and there was no explanation for that. The theoretical work could then fill the gap. Eichhorn and Sampson simulated the fibers by assuming that they are of cylindrical shape whose diameter is so much smaller than its length [8]. They found that if the mass of fibers per unit area was fixed, when the mass of the fibers increased, the average pore size increased. Maze et al. simulated the filter using nanofibers with a diameter of 200 nm and allowed the particles with diameters between 50-500 nm to pass through the pores. They found that the pressure drop was related to the pore size as could be predicted by the fluid mechanics [9]. In addition to 2D simulations, Hosseini et al. attempted to simulate 3D nanofibrous structures by building a rigid cylindrical fiber one by one on top of each other and used the computational fluid dynamics to study the collection of particles in the air when passing through these simulated filters [10]. Another attempt to create 3D nanofibrous structure was made by Sambaer et al. to simulate the filtration process via polyurethane nanofibers [11]. To construct the fiber mats, they used image of top layer of fibers as a template for creating the whole mate with multiple layers. This method proved successful in imitating the real behavior of the nanofibers in filtration process.

The success of 3D-simulation by Sambaer et al. [11] was based on the 2D structures of the nanofiber network so the knowledge of 2D structures is still important. All the work about simulation of electrospun nanofibers has dealt with the filtration of aerosol and all has assumed that the fiber size was monodisperse. In this work, the nylon-6 was selected as a model polymer for producing nanofibers by electrospinning and the

use in filtration of particles from liquid suspension was presented. The 2D simulation was performed to study the effect of fiber size polydispersity on the pore size of the structures as well as to connect the simulated results with the experimental results either qualitatively or quantitatively.

2. Material and Method

2.1 Materials

Nylon-6 was purchased from Sigma-Aldrich Co. LLC. Formic acid was supplied by Ajax Finechem Pty Ltd. The suspensions of polystyrene particles with average particle sizes of 90 nm (50-100 nm) and 200 nm (200-300 nm) were purchased from Spherotech, Inc. All chemicals were of analytical grade and used without further purification.

2.2 Electrospinning of Nylon-6 nanofibers

Nylon-6 was dissolved in 10 ml of 90%wt formic acid to obtain the spinning solutions with concentrations of 30 and 35 %wt/vol, namely N6-30 and N6-35, respectively. Each mixture was blended with a magnetic stirrer at room temperature for 2-4 hr until the solution was homogeneous. The spinning solution was poured into a 2 ml syringe with a needle with a diameter of 0.8 mm and a length of 4.2 cm. The high voltage power supply (Glassman PS/MJ30PO400) was connected to the end of the needle by a stainless steel electrode. Another electrode was connected to the stationary collector covered with 3.5 x 3.5 cm² copper plate. The electrospinning voltage was set at 21 kV and the distance between the needle tip and the collector was held constant at 9 cm. The spinning time was about 1.5-3 hr in order to obtain the nanofiber mats with 0.1±0.02 mm in thickness.

2.5 Morphology of nanofibers

The morphology of nanofibers was observed with scanning electron microscope (SEM) (JEOL JSM-6310F) after coating by a gold sputtering coater for 100 seconds. Each SEM figure was analyzed for the average fiber size as well as the apparent average pore size of the structure.

2.6 Water flux measurement

In this experiment, a syringe containing 5 ml water was vertically connected to a filter holder where the filter medium would be placed inside. A 0.5 kg piece of metal was then placed at the end of the syringe, pushing the water to pass through the circular filter medium whose diameter of 13 mm. The volumetric flow rate of water was measured. The flow is so slow that it could be considered a laminar flow and pores inside nanofibrous structure are usually interconnected, thus the structures resemble a bundle of tortuous tubes. With the relation of water flux and pressure drop across the membrane, the volume-averaged pore size could be determined.

2.7 Filtration of polystyrene particles

Firstly, the nanofiber filter was placed in the filter holder with a diameter of 13 mm and 5 ml of 200 ppm polystyrene particle suspension was pumped through the filter by a syringe pump at a fixed flow rate of 8 μ l/sec. The polystyrene (PS) colloidal particles were collected by the filter and the concentration of the filtrate was measured by using the calibration curve showing the linear relation between the concentration and absorbance

measured with UV-VIS spectrophotometer at 490 nm. The filtration efficiency is expressed as

Filtration efficiency (%) =
$$1 - \frac{C_{\text{filtrate}}}{C_{\text{initial}}} \times 100$$
 (1)

Here, C_{initial} and C_{filtrate} are the initial concentration of PS particles in suspension and the concentration in the filtrate coming out of the filter, respectively.

2.8 Computer simulation of nanofibrous structures

The computer programming was written in FORTRAN in this study. The deposition of fibers on a surface was performed by Monte Carlo simulations. First, the position on the 2D system and the size of fibers are randomly sampled one by one. Each "2D" fiber is modeled as an ellipse whose aspect ratio, i.e. the ratio of the long axis length to the short axis length, equals to 100. The length of short axis of the reference fiber is set at d_f which is scaled with a unit size d as 0.075d. The deposited area is scaled as $100d^2$, equivalent to the area of the width of 10d and the length of 10d. Therefore, if the size d is set as 500 nm, then the fiber size is 150 nm and the deposited square area is $5x5 \mu m^2$. Not the position of the fiber center but the angle of the fiber major axis respect to the x-axis is also sampled randomly on the surface.

To study the effect of fiber size, the size polydispersity of the fibers was varied according to the uniform size distribution to be $0.85d_{\rm f}$ - $1.15d_{\rm f}$, $0.75d_{\rm f}$ - $1.25d_{\rm f}$, $0.65d_{\rm f}$ - $1.35d_{\rm f}$, and $0.55d_{\rm f}$ - $1.45d_{\rm f}$, where $d_{\rm f}$ is the size of reference fiber which is 0.075d as described above. The simulated structures were analyzed for the surface coverage on the deposited area and the average pore size of the structures when more fibers were deposited.

To quantify how difficult the particles will pass through the 2D porous structures as in the filtration test, the number of attempts for the particle to deposit on the structure was measured until it could successfully pass the 2D pore. The number of attempts reflects the probability of capturing the particles inside the nanostructures. In this test, the particle diameter was varied as d, 0.75d and 0.40d and the fiber diameter was fixed at d_f.

3. Results and Discussion

3.1 Morphology of nanofibers

SEM micrographs of electrospun products from solutions of different nylon-6 concentrations were shown in Figure 1. The left-handed side represents the structures from 30 % wt nylon solution while the right-handed side from 35 wt% solution. The image analysis of SEM figures yielded the average diameters of fibers and pores of the structures, which are also shown in the figure. Upon increasing the concentration from 30 wt% to 35 wt%, the average diameter was increased from 103 to 144 nm because of an increase in solution viscosity [12]. It is clearly seen from the SEM figure and the size distribution of both fibers and pores that the larger fibers could form the structures with larger pores [13]. The average pore size was estimated to be 94 nm and 154 nm for N6-30 and N6-35, respectively.

3.2 The simulated 2D nanostructures

The number of deposited fibers on a unit area is defined as the number density of fibers. For instance, the system with number density of 0.1 contains 10 fibers on $100d^2$ area. The structures are shown in Figure 2 where the number density increases from 0.1 to 0.8 for the structures composed of the same fiber size of d_f . However, since the actual structure contains the fibers with disperse size as shown in Figure 1, the simulation was then done to obtain the structures of various size distributions as displayed in Figure 3.

In Figure 3, all samples are compared at the same fiber number density of 0.8. It could be seen that the fiber size could be differentiated from one another more easily as the size distribution is wider and this realization is similar to the SEM figures. The information that could be obtained from the simulated figures using the gray scale analysis is the surface coverage of the nanofibers at different number density. The knowledge of surface coverage is important in the applications of surface coating with nanofibers in order to modify the hydrophilicity or hydrophobicity of the original surfaces by using more hydrophilic or more hydrophobic nanofibers. For instance, the superhydrophobicity of the surface confirmed with water contact angle measurement was reported when coating fluorine-plasma-treated cellulose nanofibers on microfiber, which possessed large surface area [14]. Another example dealing with surface coverage is that the minimum amount of nanofibers was also deposited on top of the large fiber filter to increase the filtration efficiency [15].

3.3 The closeness of simulated structures and the real nanofibers

In order to compare the 2D nanofibrous structures with the simulated structures, the system of N6-35 was chosen. The average fiber size is 144 nm while the simulated average fiber size, $d_{\rm f}$, is 150 nm on 5 x 5 micron². As seen in Figure 1, the size distribution of the fibers ranges from 70 nm to 225 nm so the closest distribution for the simulated fibers to be chosen is $0.55d_{\rm f}$ -1.45 $d_{\rm f}$ corresponding to 82.5 nm to 217.5 nm. Lastly, the number density of fibers was chosen to be 0.3. The simulated structure and its pore size distribution were displayed in Figure 4.

The pore size distribution in Figure 4 shows that the range of pore size is similar to the real pore size ranging from small pores to around 670 nm. The average pore size of simulated structure is 165 nm which is close to 154 nm of the real structures. Therefore, it is possible to simulate the electrospun nanofibers in 2D to resemble the real structure. Usually, one could compare the nanofibrous structures containing different average size of fibers at the same solid volume fraction (SVF) or solidity which could be ranged from few to 13% [10]. The comparison of simulated structures is shown in Figure 5.

Figure 5 shows the structure of simulated nanofibers of the average size around 100 nm, which corresponds to N6-30, and the one whose average size around 150 nm, which corresponds to N6-35, at the same solid volume fraction. If the thickness of the membrane is assumed to be the same, the number density is then inversely proportional to fiber diameter squared. Therefore, to be compared, the number densities of the two systems are 0.45 and 0.2, respectively. It is evident that at the same solid volume fraction, the pore size of the structures containing large fiber is larger as previously seen in Figure 1.

3.4 The surface coverage of nanofibers and projected pore area

The surface coverage and the average pore size of the corresponding simulated structures in Figure 3 were illustrated in Figures 6 and 7, respectively. It should be noted that all uniform distributions applied in this work are around the same average size of d_f but their ranges are different. The ranges are $0.30d_f$, $0.50d_f$, $0.70d_f$, and $0.90d_f$ for the distributions of $0.85d_{f}$ - $1.15d_f$, $0.75d_{f}$ - $1.25d_f$, $0.65d_{f}$ - $1.35d_f$, and $0.55d_{f}$ - $1.45d_f$, respectively.

The gray scale analysis with Photoshop was applied in this study. Differentiation between the deposited area (gray area) and the available area or porous area (white area) could be done by the program. These monotonous results show that all samples had the same coverage area even though the fiber sizes could be differentiated. This happens probably because the chosen size distribution is still too close to each other and all distributions have the same average size which is $d_{\rm f}$. This may be considered as a confirmation that if the *average size* of nanofibers could be controlled to be equal for all samples, the surface coverage of the fibers could be pretty much the same, independent on the fiber size distribution with various size ranges studied here.

The effect of number density on the surface coverage is also clearly seen in Figure 6. The coverage certainly increases upon increasing the number density but the increase rate is slower at higher density due to higher chance of fiber overlaps as seen in two dimensions. However, upon adding more fibers, the projected pore sizes of the structures decrease as shown in Figure 7. In the figure, it is obvious that an increase in fiber density could decrease the pore size of nanostructures rapidly at low fiber density. The rate of decreasing the pore size is lower when the fiber density increases due to less probability for fibers to deposit on the vacant area. The transition is seen at density of 0.2 or it may be thought as a crossover of the pore generation mechanism. At a high fiber density on the surface, it could be seen that there are lots of small pores whose size is around 1-2 times the fiber size. Figure 7 also shows the similar results of the average pore areas when the size distribution was varied. The discussion was already given earlier. However, the difference was clearly seen at the low coverage of the fiber. It seems that for a low fiber density, the distribution that contains the larger size range results in smaller pore area. The 2D structure at a low density is important in simulation of nanofibers in 3 dimensions where the whole membrane is made of layers of thin 2D networks [11].

3.5 The probability of a particle passing through 2D pores

Since one of the applications of nanofibers is being used as a filter, with these simulated structures, it is possible to obtain the probability for a particle to successfully move through the pores perpendicular to the direction of the flow. In this test, particles are sampled one by one to be deposited in the pore as described by ballistic deposition model. The number of attempts made to successfully place the particle in the pore, i.e. the particle does not overlap with the fibers, is counted. Therefore, the reciprocal of this number is the probability of the particle passing through the filter without interception with the fibers. The results are shown in Figure 8, where the size of the particles is varied while the size of the fibers is fixed at $d_{\rm f}$.

It is found that at the same fiber number density, larger particles tend to stick more easily to the fibers than the smaller particles, yielding higher efficiency of the filtration [16]. However, in real situation there are some size ranges in which small

particles could aggregate because of their high surface energy which results in large agglomerates leading to a high efficiency in filtration. Therefore, there is the most probable size range for particles to easily get through the filter [9]. The topic of aggregation will be investigated more in the future. The number density in this case actually correlates with the thickness of the filter in 3D. As the number of fiber increases, the thickness of the membrane increases and this certainly increase the filtration efficiency with an expense of high pressure drop across the membrane [15].

The experimental study of filtration of small particles with nylon-6 nanofibers was also done. With the membrane whose thickness is around 0.1 mm, the N6-30 samples could completely remove all particles from the 200 ppm polustyrene particle suspension, i.e. the separation efficiency according to Equation (1) equals 100%. Figure 9 shows the fiter fronts where particles with diameters of 90 nm and 200 nm were captured. The outline of the nanofibers are still seen for the case of smaller particles while almost complete surface coverage is seen for the larger ones, implying higher probability for smaller particles to move inside the pores of nanofibrous structures as was seen in the simulations.

3.6 The void volume fraction and tortuosity of the structures

Based on the Kozeny-Carman relation, which could well describe the pressure drop of laminar flow through fibrous mats, the void volume fraction of the nanostructures could be estimated [17]. The equation was modified here to take into account the tortuosity of the structures and the actual velocity of the flow.

$$\frac{\Delta P}{\tau z} = \frac{16k\mu U_0}{d_f^2} \frac{\left(1 - \varepsilon\right)^2}{\varepsilon^4} \tag{2}$$

In the equation, U_o is the superficial velocity (m/s), μ is the viscosity of water at 30°C (Pa·s), z is the filter thickness (m), ΔP is pressure drop (Pa), ε is the void fraction, and τ is the tortuosity, k is the Kozeny constant, which is equal to 0.55 for nearly cylindrical fibers if void fraction (ε) varies from 0.6 to 0.8.

The tortuosity could be approximated by realization that the whole fibrous mat is composed of many layers of nanofiber networks. Each layer is very thin and the surface coverage is equal to θ . Thus, the probability of liquid to pass through each layer is $1-\theta$, which is equivalent to void fraction, ε . The thin layer of thickness dz is considered and the liquid is divided into N parts. If some parts of the liquid could pass directly through this layer then the traveling distance of these parts is $\varepsilon N dz$. The other parts are blocked by the fibers so the liquid has to move laterally for a distance $(1-\varepsilon)\varepsilon N 2 dz$, in case the available pore is located at the distance dz from the fiber. Still there are liquid parts that are blocked by the fibers and have to travel farther with a distance $(1-\varepsilon)\varepsilon^2 N 3 dz$. It is obvious that the probability for the liquid to find the pore depends on the void volume fraction. With this logic, one could write the equation of tortuosity which is defined as the actual distance for the liquid to travel to the thickness of the mat. The actual distance is the average of traveling distance of all liquid parts. Therefore,

$$\tau = \frac{D_{travel,ave}}{dz} = \frac{\varepsilon N + 2N(1-\varepsilon)\varepsilon + 3N(1-\varepsilon)^2\varepsilon + 4N(1-\varepsilon)^3\varepsilon + \dots}{N}$$
(3)

The number of terms in Equation (3) could reach infinity so tortuosity could be approximated as

$$\tau = \frac{1}{\varepsilon} \tag{4}$$

The fixed volume of water was fixed at 4.60×10^{-6} m³ and the weight pushing the water through the filter was also fixed at 6.42 N. The filtration time was recorded as shown in Table 1 and the void fractions of N6-30 and N6-35 mats can be calculated.

It is noted that as seen from the SEM images in Figure 1 and simulated images in Figure 5, the pore size is larger when the deposited fibers are larger and this could affect the void fraction as a whole so N6-35 had higher void fraction than N6-30. Based on this value, one could assume the first layer is the network with surface coverage equal to $1-\varepsilon$, which is 0.252 and 0.281 for N6-30 and N6-35, respectively. According to Figure 6, For N6-35 with the surface coverage about 0.3, the number density is a bit larger than 0.1. If the structure with density 0.1 is adopted for the structure of the first layer and the multiple layers could be built layer by layer to obtain the whole mat as previously done by Sambaer et al. [11]. Thus, using the connection of the experimental results and simulated results, one could have a guide to construct the structure of each layer.

3.7 The average pore size determination

Based on the water flux measurement as discussed in the previous section, the Hagen-Poiseille equation could be used to estimate the volume-averaged pore size [18].

$$\frac{d^2}{32} = \frac{U_o \mu \tau z}{\varepsilon \Delta P} \tag{5}$$

The equation was derived for the flow in circular pipe so in this work, the channel inside the structure is assumed to be little tortuous circular pipes with non-uniform cross-sectional area. The variables in the equation are defined in the same way as in Equation (2) and d is the volume-averaged pore diameter (m). With Equation (5), the volume-averaged pore size was obtained as shown in Table 2.

From Table 2, it is found that the volume-averaged pore size obtained from Hagen-Poiseille equation is larger than the pore size obtained from SEM figures. If the volume-averaged pore size is considered as 3D pore size and the average from SEM image as 2D pore size, it is possible to relate two quantities by

$$d_{2D}^2 + d_f^2 = d_{3D}^2 (6)$$

The Equation (6) was used to estimate the d_{3D} for N6-30 and N6-35 and it is found that d_{3D} 's are 139 nm and 210 nm, respectively, being compared with 181 and 216 nm. The

numbers imply that the pore size in vertical axis is at least equal to the fiber diameter as was assumed when 3D simulated structures were created by Hosseini et al. [10] and our example of 3D-structure of N6-35 is shown in Figure 10. The structures were built by adding one fiber at a time on top of the previously added, which means that the pore size in vertical axis equals to the fiber diameter.

4. Conclusions

The simulation of nanofibrous structures via Monte Carlo method in 2 dimensions was performed. The results confirmed that even though there are some variations in fiber size, if the average size of fiber could be controlled, the surface coverage of fibers randomly deposited during electrospinning process could be the same. However, at a low number density of fiber, the average pore size was different when the fiber size range was varied. This structure may be thought of the structure of initial layers that could be used to simulate the 3D structures by combining multiple thin 2D networks together as a whole mat.

The simulated structures resembled real SEM images of nanofibers closely since the fiber size distribution and the average size of the fibers were chosen to be close to the real systems, confirming efficiency of 2D simulations. Calculations of void fraction and tortuosity of the structures could be used to prove that vertical pore size is at least the size of the fibers deposited, providing the connection between 3D pore size and 2D pore size from the SEM figures or from the simulated 2D figures.

5. Acknowledgments

This research was jointly funded by the Thailand Research Fund (TRF) and Thammasat University (Grant# DBG5380007). All assistances from the Faculty of Engineering are highly appreciated.

6. Conflicts of Interest

The authors do not have any conflict of interest in this research work.

REFERENCES

- [1] S.-W. Choi, A. Katoch, G.-J. Sun, S.S. Kim, "Synthesis and Gas Sensing Performance of ZnO-SnO₂ Nanofiber-Nanowire Stem-Branch Heterostructure," *Sensors and Actuators, B: Chemical*, vol. 181, pp. 787-794, 2013
- [2] H.R. Pant, D.R. Pandeya, K.T. Nam, W.-I. Baek, S.T. Hong, H.Y. Kim, "Photocatalytic and Antibacterial Properties of a TiO₂/Nylon-6Electrospun Nanocomposite Mat Containing Silver Nanoparticles," *Journal of Hazardous Materials*, vol. 189, pp 465-471, 2011
- [3] D.-G. Yu, W. Chian, X. Wang, X.-Y. Li, Y. Li, Y.-Z. Liao, "Linear Drug Release Membrane Prepared by a Modified Coaxial Electrospinning Process," *Journal of Membrane Science*, vol. 428, pp. 150-156, 2013
- [4] R. Nirmala, R. Navamathavan, H.-S. Kang, M.H. El-Newehy, H.Y. Kim, "Preparation of Polyamide-6/Chitosan Composite Nanofibers by a Single Solvent System via

- Electrospinning for Biomedical Applications," *Colloid and Surfaces B*, vol 83, pp. 173-178, 2010
- [5] K. Desai, K. Kit, J. Li, P.M. Davidson, S. Zivanovic, H. Meyer, "Nanofibrous Chitosan Non-Wovens for Filtration Applications," *Polymer*, vol. 50, pp. 3661–3669, 2009
- [6] P. Danwanichakul, D. Dechojarassri, R. Werathirachot, "An Approximate Model Describing Electrospinning of Nanofibers: Process Parameter Investigation," *International Journal of Electrospun Nanofibers and Applications*, vol. 2, pp. 103-114, 2008
- [7] H. Park, Y.O. Park, "Filtration Properties of Electrospun Ultrafine Fiber Webs," Korean Journal of Chemical Engineering, vol. 22, pp. 165-172, 2005
- [8] S.J. Eichhorn, W.W. Sampson, "Statistical Geometry of Pores and Statistics of Porous Nanofibrous Assemblies," *Journal of the Royal Society Interface*, vol. 2, pp. 309-318, 2005
- [9] B. Maze, H.V. Tafreshi, Q. Wang, B.A. Pourdeyhimi, "Simulation of Unsteady-State Filtration via Nanofiber Media at Reduced Operating Pressures," *Aerosol Science*, vol. 38, pp. 550-571, 2007
- [10] S.A. Hosseini, H.V. Tafreshi, "3-D Simulation of Particle Filtration in Electrospun Nanofibrous Filters," *Powder Technology*, vol. 201, pp. 153-160, 2005
- [11] W. Sambaer, M. Zatloukal, D. Kimmer, "3D Modeling of Filtration Process via Polyurethane Nanofiber Based Nonwoven Filters Prepared by Electrospinning Process," *Chemical Engineering Science*, vol. 66, pp. 613-623, 2011
- [12] S. Zhang, W.S. Shim, J. Kim, "Design of Ultra-fine Nonwovens via Electrospinning of Nylon-6: Spinning Parameters and Filtration Efficiency," *Materials and Design*, vol. 30, pp. 3659-3666, 2009
- [13] D. Hussain, F. Loyal, A. Greiner, J.H. Wendorff, "Structure Property Correlations for Electrospun Nanofiber Nonwovens," *Polymer*, vol. 51, pp. 3989-3997, 2010
- [14] A. Thorvaldsson, P. Edvinsson, A. Glantz, K. Rodriguez, P. Walkenström, P. Gatenholm, "Superhydrophobic Behaviour of Plasma Modified Electrospun Cellulose Nanofiber-Coated Microfibers," *Cellulose*, vol. 19, pp. 1743-1748, 2012
- [15] J. Wang, S.C. Kim, D.Y.H. Pui, "Investigation of the Figure of Merit for Filters with a Single Nanofiber Layer on a Substrate," *Aerosol Science*, vol. 39, pp. 323-334, 2008
- [16] D. Aussawasathien, C. Teerawattananon, A. Vongachariya, "Separation of Micron to Sub-micron Particles from Water: Electrospun Nylon-6 Nanofibrous Membranes as Pre-filters," *Journal of Membrane Science*, vol. 315, pp. 11–19, 2008
- [17] E. Mauret, M. Renaud, "Transport Phenomena in Multi-Particle Systems I. Limits of Applicability of Capillary Model in High Voidage Beds Application to Fixed Beds of Fibers and Fluidized Beds of Spheres," *Chemical Engineering Science*, vol. 52, pp. 1807-1817, 1997

[18] P. Johnson, "Fluid Sterilization by Filtration," Interpharm/CRC, Third Edition, New York, 2003

FIGURE CAPTIONS

- Figure 1: SEM figures of nylon-6 nanofibers electrospun from solutions of 30 wt% (left) and 35 wt% (right) along with the fiber and pore size distributions.
- Figure 2: The simulated structures of nanofibers with monodisperse size of d_f when the number density of fibers are (a) 0.1 (b) 0.2 (c) 0.3 (d) 0.4 (e) 0.5 (f) 0.6 (g) 0.7 and (h) 0.8
- Figure 3: Nanofibrous structures with various size polydispersity (a) monodisperse size of d_f (b) $0.85d_f$ - $1.15d_f$ (c) $0.75d_f$ - $1.25d_f$ (d) $0.65d_f$ - $1.35d_f$ (e) $0.55d_f$ - $1.45d_f$
- Figure 4: The simulated N6-35 nanofibrous structures and its pore size distribution to be compared with Figure 1.
- Figure 5: The comparison of simulated structures for N6-30 (size around 100 nm) and N6-35 (size around 150 nm) at the same solid volume fraction.
- Figure 6: Surface coverage of nanofibers at various number density for various size distribution
- Figure 7: The average projected pore areas in squared micron (as seen in 2D) at different fiber number density. The comparison is for all distributions.
- Figure 8: The probability for a particle with different size to successfully move through the 2D pore in the structures made of various fiber densities.
- Figure 9: SEM images of polystyrene particles with different diameters, 90 nm (left) and 200 nm (right), on the filter fronts.
- Figure 10: An example of 3D structures of nanofibers

TABLE CAPTION

- Table 1: The void fraction of the nylon nanofibrous structures
- Table 2: The pore sizes from Hagen-Poiseille equation and from SEM images

FIGURES

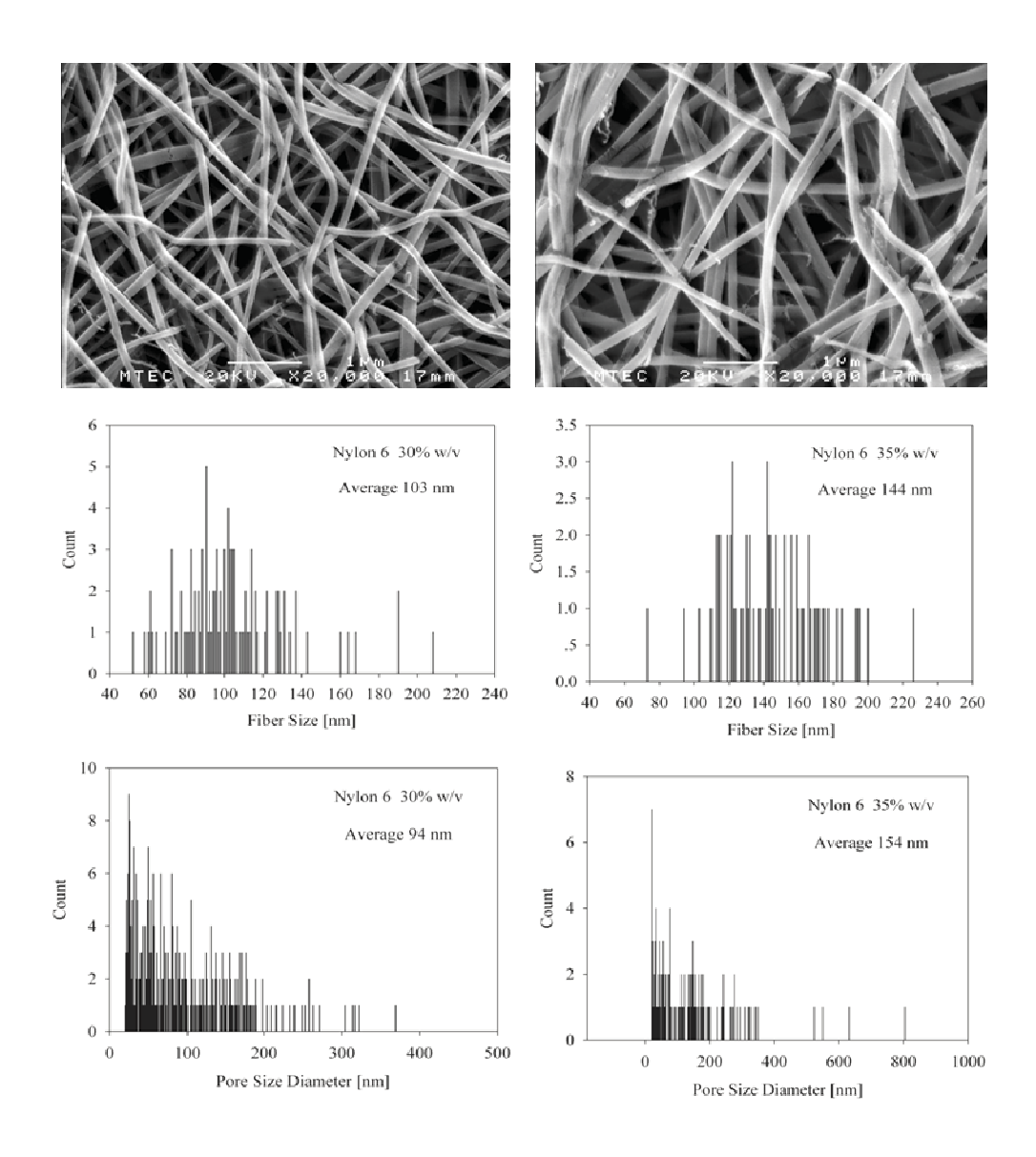


Figure 1: SEM figures of nylon-6 nanofibers electrospun from solutions of 30 wt% (left) and 35 wt% (right) along with the fiber and pore size distributions.

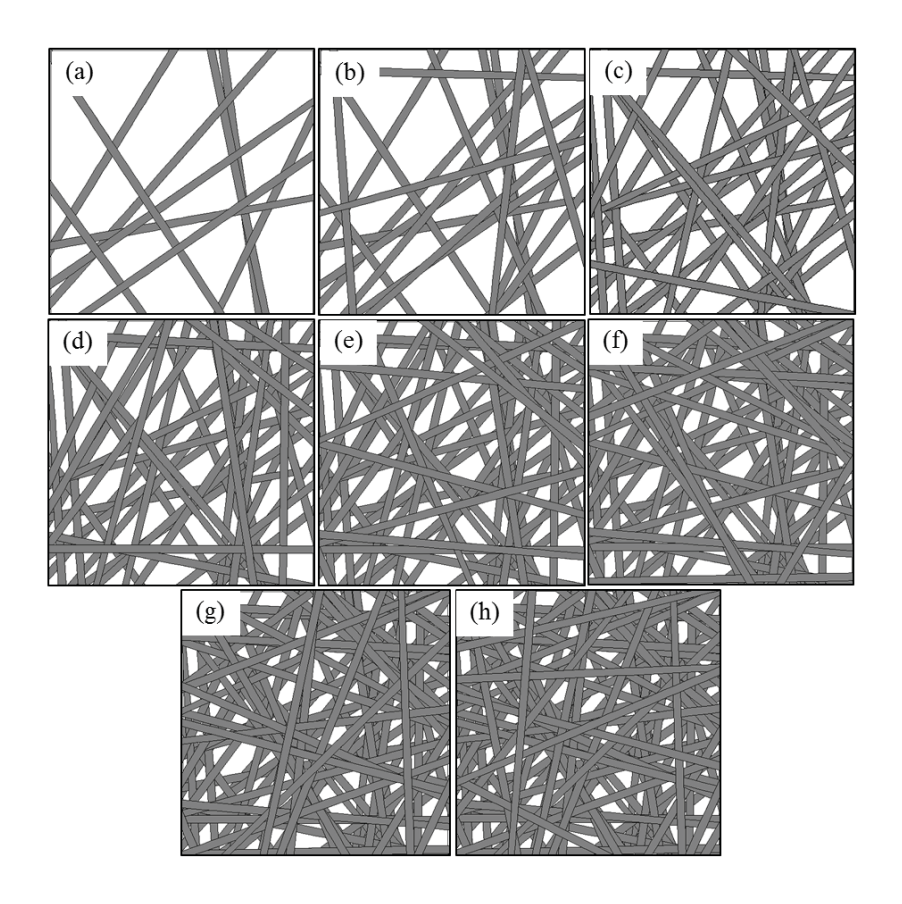


Figure 2: The simulated structures of nanofibers with monodisperse size of $d_{\rm f}$ when the number density of fibers are (a) 0.1 (b) 0.2 (c) 0.3 (d) 0.4 (e) 0.5 (f) 0.6 (g) 0.7 and (h) 0.8

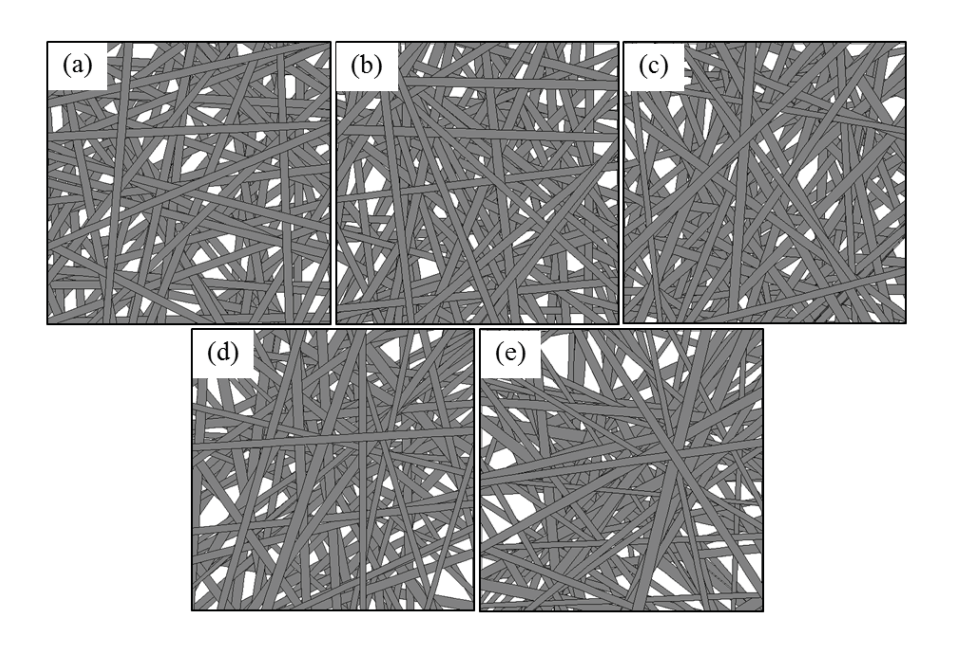


Figure 3: Nanofibrous structures with various size polydispersity (a) monodisperse size of $d_{\rm f}$ (b) $0.85d_{\rm f}$ - $1.15d_{\rm f}$ (c) $0.75d_{\rm f}$ - $1.25d_{\rm f}$ (d) $0.65d_{\rm f}$ - $1.35d_{\rm f}$ (e) $0.55d_{\rm f}$ - $1.45d_{\rm f}$

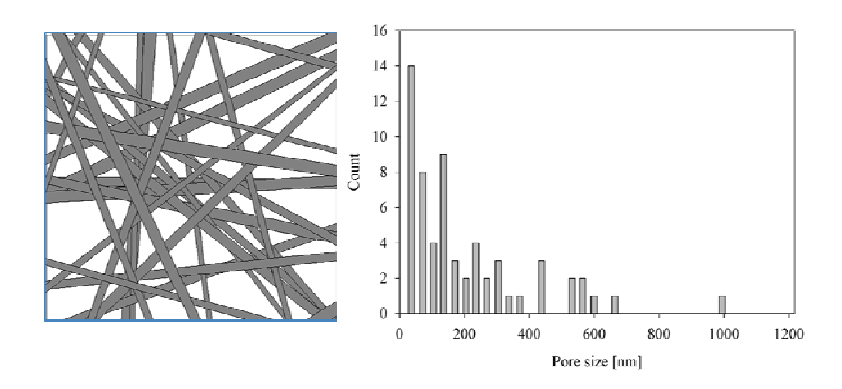


Figure 4: The simulated N6-35 nanofibrous structures and its pore size distribution to be compared with Figure 1.

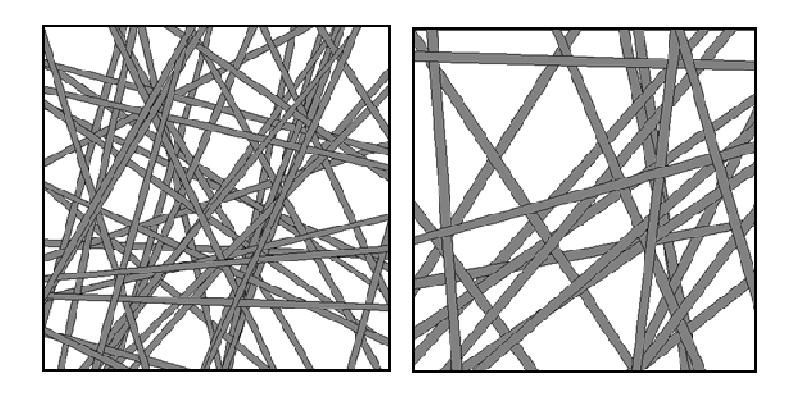


Figure 5: The comparison of simulated structures for N6-30 (size around 100 nm) and N6-35 (size around 150 nm) at the same solid volume fraction.

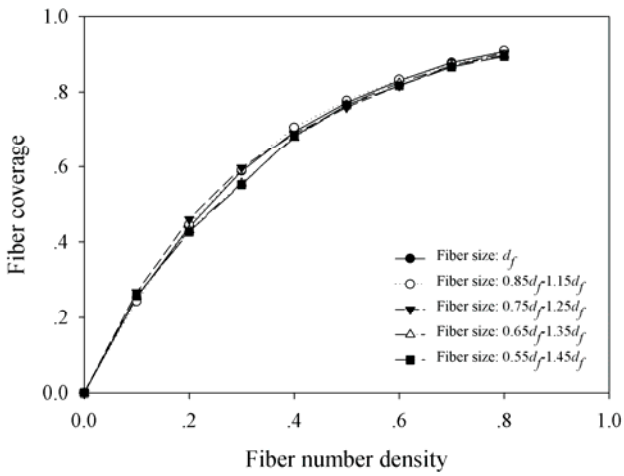


Figure 6: Surface coverage of nanofibers at various number density for various size distribution.

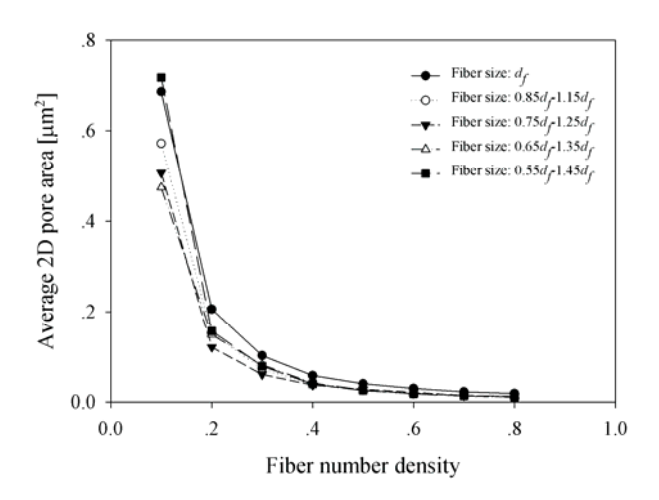


Figure 7: The average projected pore areas in squared micron (as seen in 2D) at different fiber number density. The comparison is for all distributions.

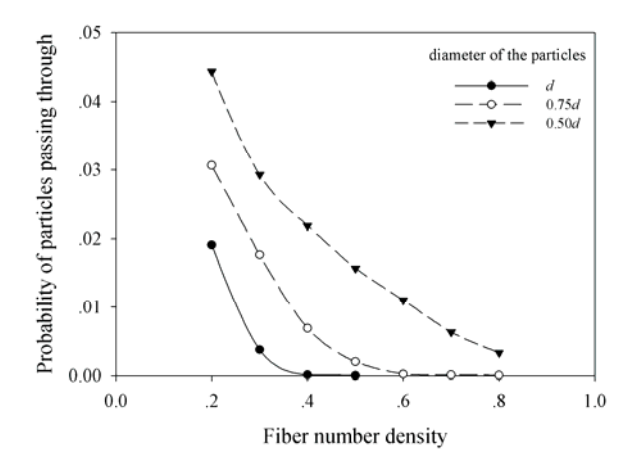


Figure 8: The probability for a particle with different size to successfully move through the 2D pore in the structures made of various fiber densities.

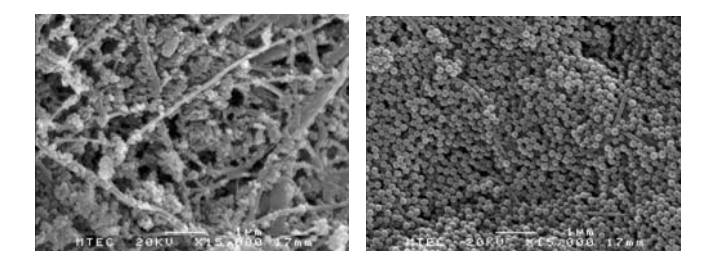


Figure 9: SEM images of polystyrene particles with different diameters, 90 nm (left) and 200 nm (right), on the filter fronts.

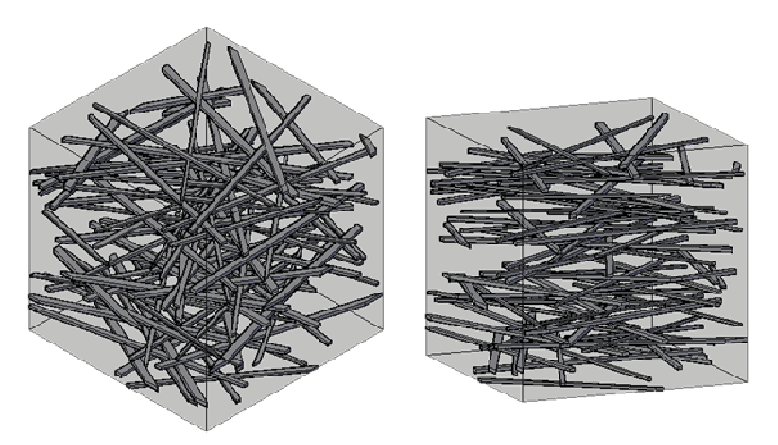


Figure 10: An example of 3D structures of nanofibers

TABLES

Table 1: The void fraction of the nylon nanofibrous structures

Sample	Thickness (m)	time (s)	void fraction	Tortuosity
N6-30	1.04E-04	112.34	0.748	1.34
N6-35	1.16E-04	93.66	0.719	1.39

Table 2: The pore sizes from Hagen-Poiseille equation and from SEM images

	Pore size from	Pore size from SEM	Fiber diameter
Sample	Hagen-Poiseille (nm)	(nm)	(nm)
N6-30	181	94	103
N6-35	216	154	144